UiT
THE ARCTIC UNIVERSITY OF NORWAY

Faculty of Science and Technology
Department of Geosciences

Identifying the Controlling Factors on Variable Glacial Modification of Bedrock Dominated Areas in Kongsfjorden, Svalbard

Mikis van Boeckel
GEO-3900 Master's thesis in Geology
July 2018

NORWEGIAN POLAR INSTITUTE
UNIVERSITY OF TROMSØ

Identifying the Controlling Factors on Variable Glacial Modification of Bedrock Dominated Areas in Kongsfjorden, Svalbard

Mikis van Boeckel

60 ECTS thesis, submitted in partial fulfillment of a
Magister Scientiarum degree in Geology

Advisors
Anders Schomacker
Per Inge Myhre

Faculty of Science and Technology
Department of Geosciences
UiT the Arctic University of Tromsø
Tromsø, July 2018

Identifying the Controlling Factors on Variable Glacial Modification of Bedrock Dominated Areas in Kongsfjorden, Svalbard

60 ECTS thesis submitted in partial fulfilment of a *Magister Scientiarum* degree in Geology

Faculty of Science and Technology
Department of Geosciences
UiT the Arctic University of Norway
Dramsveien 201
N-9037 Tromsø
Norway

Bibliographic information:
Mikis van Boeckel, 2018, *Identifying the Controlling Factors on Variable Glacial Modification of Bedrock Dominated Areas in Kongsfjorden, Svalbard*, Master's thesis, Faculty of Science and Technology, UiT the Arctic University of Norway.

Abstract

This thesis aims to better understand the variability of glacial erosion along glacial troughs located in high latitude settings, through a case study of Kongsfjorden, Svalbard. Kongsfjorden is one of the major glacial troughs in northwest Svalbard and acted as a paleo-ice stream tributary, draining large amount of ice towards the continental margin over the Quaternary. The inner part of Kongsfjorden hosts several bedrock dominated islands covering a varied geological configuration, including several tectono-structural geological units bound by major tectonic contacts, which allows for a broad variety of bedrock parameters to asses.

The research question of this thesis is to identify the controlling factors on variable glacial modification of the bedrock dominated areas in Kongsfjorden. Fieldwork was conducted to analyze bedrock structures and glacio-erosional landforms of outcrops on islands distributed within Kongsfjorden. These findings were compared with regional patterns using available Digital Elevation Model's (DEMs) of the surface, subglacial and bathymetrical topography.

The identified factors controlling variable glacial modification included variation in bedrock mechanical properties, linear fracture zones, and changes in glacio-erosional processes. The bedrock mechanical properties show that the rocks located at Lovénøyane, around the center part of the fjord, have a lower erosion resistance compared to the rocks located at the nunataks, at the innermost part of the fjord. The assessment of the linear fracture zones show that the main structures of the area are N-S and NW-SE oriented. These structures relate with overdeepended linear valleys within the fjord and are suggested to have formed by differential glacial erosion of the weak brecciated rocks within the fracture zones. The geomorphology on outcrops shows that the glacio-erosional processes acted upon the bedrock varied between abrasion to plucking dominated surfaces for different lithologies. The geomorphology on the regional scale shows that streamlining of landforms are unevenly distributed within the fjord floor, with more streamlined and elongated landforms distributed towards the outer fjord.

The implications of the findings suggest a modest amount of glacial erosion took place at the Lovénøyane ridge, at the center part of the fjord, relative to the outer fjord. Evidence suggesting modest glacial erosion comes from the weak bedrock mechanical properties standing out of the water and the low elongation ratio of landforms. This study suggests that the ice dynamical behavior at the Lovénøyane ridge was lower relative to the overdeepened channel down-ice towards the outer fjord. This change in paleo-ice flow dynamics could represent a zone of acceleration of the Kongsfjorden paleo-ice stream tributary.

Table of contents

List of Tables

List of Figures

Acknowledgements

First and foremost, I would like to express my deep gratitude to my two supervisors, Anders Shomacker and Per Inge Myhre. Through his invitation to be part of this project, Per Inge Myhre, was instrumental in enabling me to do research in Kongsfjorden, Svalbard and to write this resulting thesis. I am grateful for his supervision of both my activities in the field and the compilation of this study. I am also thankful to Anders Shomacker who also supervised me on compilation of my thesis and has been the main contact person at the university with whom I could share my thoughts. I appreciated that during my research both of my supervisors have given me much freedom to make my own choices, while always being willing to help me out and to answer my questions.

I am grateful to Synnøve Elvevold, Tamer S. Abu-Ablam and Per Terje Osmundsen with whom I worked in the field. Fieldwork would have been hard without Wojtek Moskal and Johnny Schneider who took care of the logistics involved in taking us around in Kongsfjorden.

This thesis would not have been possible without the generous assistance of the Norwegian Polar Institute (NPI) and the Norwegian Hydrographic Service (NHS). The NPI made it possible for me to travel to Ny-Ålesund and to use the datasets necessary for conducting this study. Over the years, NHS has collected rich sets of data that proved highly relevant to this research project. I could freely use these and they were an invaluable source to me.

Winfried Dallman has contributed much to my work through his extensive experience of working with the geology of Svalbard. He provided important literature on the Kongsfjorden area that was invaluable to my study area. Many thanks to Maarten Krabbendam who inspired me to work with glacio-erosional landforms and for his suggestions of ways to tackle some of the challenges brought forth when conducting fieldwork.

My family has been of great support. My parents, Jan and Ceciel, have given me great support in writing my thesis and helped me to improve the manuscript through their comments. My brother Tayo was always available when I needed to share my thoughts with someone and to develop new ideas. My sister Luca and her partner Fokke gave me just the right boost of energy at the final stages of the writing process. And of course there is Willeke, who has encouraged me throughout this whole research project with an endless amount of energy and an uplifting spirit.

Finally, I would like to thank Sindre Holten Natvig for being a great office partner and Håvard Lytskjold Haukenes for several stimulating and fruitful discussions.

1 Introduction

Glacial troughs are among the most impressive landforms formed by glaciers. Landscape evolution at high latitude locations is characterized by its specific tectonic setting, the glacial modification of repeated glaciations and interglacial erosional processes (Sugden, 1974). Glacial troughs, i.e. large linear U-shaped features carved into bedrock, mark the areas with most dramatic glacial modification (Sugden, 1978; Glasser & Bennett, 2004; Benn & Evans, 2010). Within ice sheets these glacial troughs are commonly occupied by channeled and relatively fast flowing ice confined by topography which often comprises of ice streams or ice-stream tributaries. The distribution of these glacial troughs is primarily controlled through the pre-glacial topographic settings, such as drainage pattern and tectonic grabens, in parts of the high latitude locations, such as in Norway (Nesje & Whillans, 1994), in Greenland (Swift et al., 2008; Peulvast et al., 2011), in Canada (England, 1987) and in South America (Glasser & Ghiglione, 2009). Subsequent widening and deepening of the pre-existing topography, due to extensive glacial modification (which took place during repeated glaciations of fast flowing ice), have led to the characteristic fjord landscapes at high latitudes (Sugden, 1978). Positive relationships have been established between glacial valley size and ice drainage (Brook et al., 2003). Larger stresses and velocities of the ice caused larger erosion rates and these in turn further increased the cross-sectional profile of the valley (Hirano & Aniya, 1989). However, there is also a relation between glacial valley morphology and bedrock properties. Glacial valleys consisting of weak rock tend to be broader and shallower in size, whereas glacial valleys consisting of strong resistant rock tend to be narrower and deeper (Augustinus, 1992, 1995; Harbor, 1995; Brook et al., 2004; Swift et al., 2008).

The area of Svalbard has been repeatedly glaciated during the Quaternary. This created a glacial landscape of rugged mountains, coastal plains and fjords. Recent studies have found that the alpine regions and some low-lying areas of north-western Svalbard have only experienced minimal erosion during the late Quaternary (Houmark-Nielsen & Funder, 1999; Gjermundsen et al., 2015). During the late Quaternary, cold-based ice preserved large parts of the landscape, including the alpine uplands and some strandflats. Recent research suggests that the occurrence of significant erosion was constricted to the central axes of fjords and valleys, related with the paleo-ice stream activity (Hormes et al., 2011; Gjermundsen et al., 2015).

Kongsfjordrenna was one of the major paleo-ice streams in north-western Svalbard, conveying large amounts of ice towards the continental margin, and was fed on its turn by two paleo-ice stream tributaries: Krossfjorden and Kongsfjorden (Ottesen et al., 2007). Recent studies of the

reconstruction of the Kongsfjorden paleo-ice stream tributary activity have primarily focused on: (i) bathymetrical mapping and marine stratigraphy (Howe et al., 2003; Landvik et al., 2005, 2014, Ottesen et al., 2005, 2007; Jessen et al., 2010; Maclachlan et al., 2010; Ingólfsson & Landvik, 2013; Streuff et al., 2015); (ii) cosmogenic dating of erratics (Hormes et al., 2011; Gjermundsen et al., 2013; Landvik et al., 2013; Henriksen et al., 2014; Grant, 2016); and (iii) terrestrial sedimentology and geomorphology (Miller, 1982; Lehman & Forman, 1992; Houmark-Nielsen & Funder, 1999; Miccadei et al., 2016). However, no studies have been performed thus far that have focused on the geomorphic signatures of the bedrock dominated areas of the paleo-ice stream tributary within Kongsfjorden.

The innermost part of Kongsfjorden, which is exposed at the surface, is bedrock dominated. These bedrock-dominated areas are characterized by areas with net erosion. The study of bedrock-dominated areas is important for the following reasons:

1) Research of the characteristics of these bedrock-dominated areas may contribute to an increased understanding of paleo-ice stream activity on basis of its glacio-erosional signature. The bedrock-dominated areas provide the sediments downstream that contribute to fast flowing ice-streams through soft sediment deformation (Bradwell, 2013; Livingstone et al., 2013). Furthermore, the transition from slow sheet flow to fast streaming flow – also called *onset zones* of ice streams and their tributaries –typically occurs within these bedrock-dominated areas (Bradwell, 2013; Margold et al., 2015). These onset zones mark an ice flow acceleration from <10 to >400 m/a, sometimes within a range of 10 km (Rignot et al., 2011). The mapping of glacio-erosional landforms in bedrock-dominated areas has been used to locate such paleo-onset zones, e.g. the topographically-controlled onset zone of a paleo-ice stream tributary in NW Scotland (Bradwell, 2013). Such zones of acceleration have never specifically been mapped for the Kongsfjorden paleo ice-stream tributary in Svalbard.
2) Studying bedrock-dominated areas may contribute to an increased understanding of variable glacial modification of landscapes covered by repeated glaciations. In turn, this could improve our understanding of present day glacial erosional processes at the bed of ice-sheets. The main controlling factors of variable glacial modification in those bedrock-dominated landscapes are changes in glacio-erosional processes and bedrock properties (Glasser & Bennett, 2004; Swift et al., 2008; Benn & Evans, 2010; Krabbendam & Glasser,

2011). Increased glacial modification due to glacio-erosional processes can be recognized by establishing the presence of a smoother and more streamlined landscape compared to the shape of landscape structures in surrounding areas (Phillips et al., 2010; Bradwell, 2013). Increased glacial modification due to bedrock properties can be recognized by relating bedrock mechanical properties with glacio-erosional landforms, such as overdeepened rock basins and streamlined landforms (Roberts & Long, 2005; Krabbendam & Bradwell, 2014). The main factors controlling the variable glacial modification of the Kongsfjorden area have previously not been identified.

The Kongsfjorden paleo-ice stream tributary is a suitable place to study the variable glacial modification of bedrock-dominated areas of glacial troughs and this is for the following three main reasons: (i) Kongsfjorden is one of the areas of Svalbard that is most intensively studied. This implies a broad availability of geological maps and datasets, such as surface, bathymetry and subglacial Digital Elevation Models (Norwegian Mapping Authority Hydrographic Service, 2014; Norwegian Polar Institute, 2014a; Lindbäck et al., 2018); (ii) The geological setting of Kongsfjorden is varied, comprising of several tectono-structural geological units that are bound along major tectonic contacts (Hjelle et al., 1999). This implies that many geological parameters can be analyzed to evaluate the relative erosion resistance of the bedrock; (iii) Many bedrock outcrops are exposed on islands at the central axis of the glacial trough, and these are locations where the glacial erosion related to the ice activity is highest (Hormes et al., 2011; Gjermundsen et al., 2015).

1.1 Research Question

This thesis aims to address the variable glacial modification of bedrock-dominated areas by combining the pre-quaternary geological elements with the present landscape morphology in the Kongsfjorden paleo-ice stream tributary in north-west Svalbard.

The research question guiding this study is as follows: What are the factors that control the variability in glacial modification of the bedrock-dominated areas in the Kongsfjorden paleo-ice stream tributary? In order to answer this, the main research question is broken down into the following three sub-questions:

i) What are the main bedrock characteristics outcropping within the Kongsfjorden area?
ii) What are the main geomorphological characteristics of the Kongsfjorden area?
iii) To what extent are outcropping bedrock structures related to linear morphological features occurring at the fjord floor?

To be able to answer the first sub-question, detailed field analysis of the mechanical and structural properties of the different lithologies within the study area needed to be conducted. This was undertaken between the 16th and 27th of August 2017.

For answering the second sub-question, glacio-erosional landforms were identified and classified on outcrops that were visited in the field. Linking the observed glacio-erosional landforms to findings that were retrievable from the existing literature made it possible to infer the glacial-erosional process that formed them. However, observations of glacio-erosional landforms in the field provides us only individual observations of various glacial-erosional processes that act upon the bedrock and yields no information about features related to glacial origin spatially. This thesis aims to overcome this shortcoming by using the elongation ratio of landforms which allows for spatial evaluation of the distribution of streamlined landforms.

For being able to address the third sub-question, the implementation of remote sensing techniques was required. Such techniques allow to compare linear morphological features at the fjord floor with structural weak zones as found in the field. These features can then be identified as geological lineaments and be linked to overdeepend linear valleys that have evolved through differential glacial erosion (Krabbendam & Bradwell, 2014).

2. Study area

2.1 Geographical setting

Kongsfjorden is located between 78.9 N and 79.1 N, and 11.2 E to 11.4 E in the northwest part of Spitsbergen (Figure 1), the largest island of the Svalbard archipelago. Currently, about 60 percent of the land area of Svalbard is covered with glaciers.

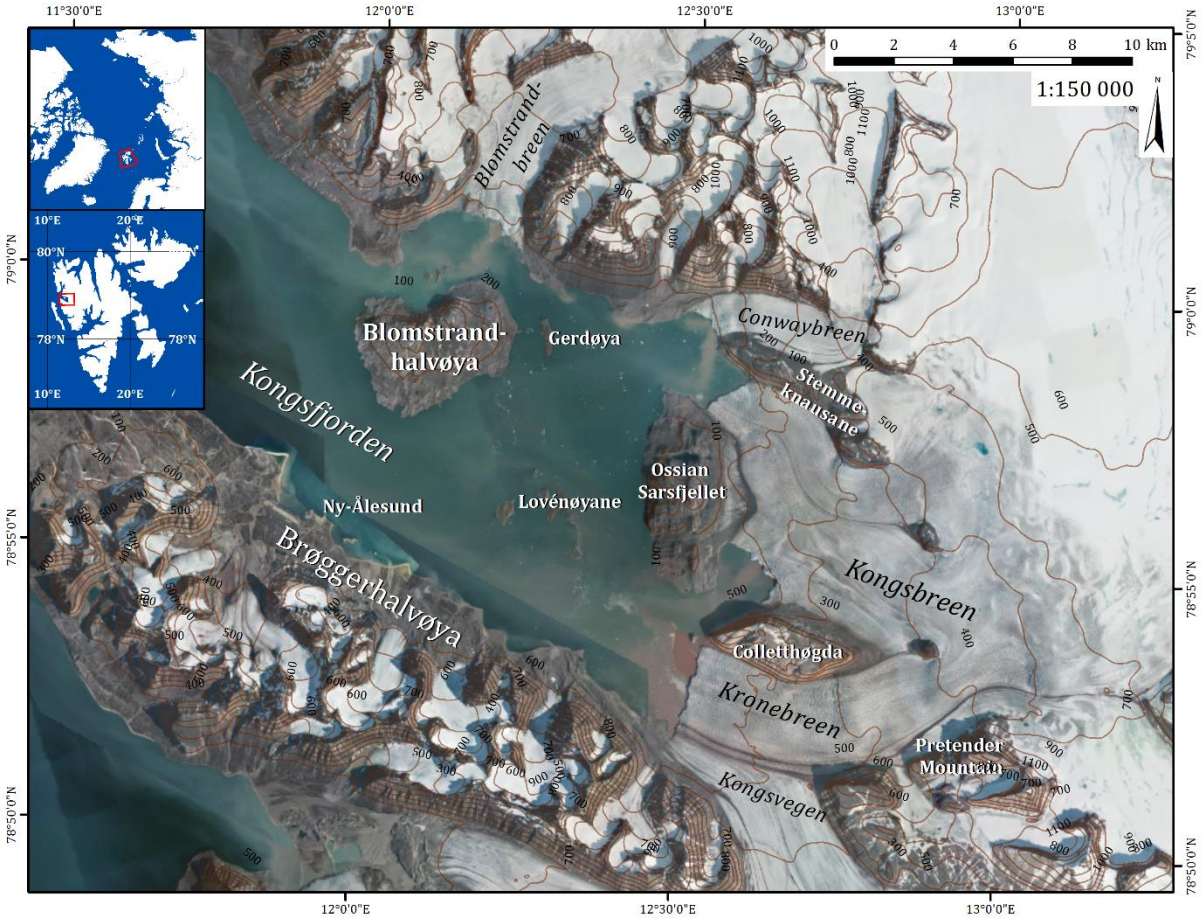

Figure 1: Overview of study site indicating main islands and nunataks. Background image is an orthophoto of the study area for which aerial photographs made in 2009 were used. The contour lines have a 100m interval and are made from a Digital Elevation Mode (DEM) available at Norwegian Polar Institute (2014b).

Kongsfjorden is characterized by an Arctic climate with a mean annual temperature of -3.4 °C and mean annual precipitation of <400 mm. Summer temperatures rarely exceed 10 °C (Svendsen et al., 2002; Cisek et al., 2017). These climatic conditions suggest the rocks only experiences slight chemical weathering.

The present landscape of the Kongsfjorden area is characterized by glaciers, islands, coastal plains and steep mountains. Elevation of the mountains surrounding the fjord reach up to 1000m

a.s.l (Figure 1). Between the mountain peaks, numerous cirque glaciers terminate on the coastal plains along with five tidewater glaciers terminating within Kongsfjorden. The tidewater glaciers are called, from south to north; Kongsvegen, Kronebreen, Kongsbreen, Conwaybreen and Blomstrandsbreen. The tidewater outlet glaciers towards the east are separated by three major nunataks; Colletthøgda (611m a.s.l), Ossian Sarsfjellet (364m a.s.l) and Stemmeknausane (579m a.s.l). Blomstranhalvøya is the largest island (385m a.s.l), it represents the last island before Kongsfjorden slowly opens up towards the open sea in the west.

The NW-SE trending Kongsfjorden is about 20km long and 4 to 10km wide. Towards the NW, Kongsfjorden merges with Krossfjorden at Kapp Guissez into a large submarine trough, Kongsfjordrenna, which runs out towards the shelf-edge.

The bathymetry of Kongsfjorden consists of an inner and an outer basin separated by an N-S trending threshold, north and south of Lovénøyane. This threshold is also referred to as the Lovenøyane ridge. It plays a significant role within Kongsfjorden for the following reasons: (i) the ridge acts as a barrier for oceanic circulation. The outer basin is up to 375m deep and has direct communication with North Atlantic seawater. The inner basin, however, is about 100m deep and contains a large freshwater input of glacial meltwater during the summer season. This variability of the freshwater input between summers and winters controls the sediment discharge into the fjord and the stability of the stratification within the water column (Svendsen et al., 2002; Aliani et al., 2016); (ii) The ridge traps the high sediment load from the glacial meltwater of the surrounding tidewater outlet glaciers, with Kronebreen as the main sediment contributor (Elverhøi et al., 1980). The sediment accumulation rate within the inner basin at the margin of Kronebreen is about 20.000 g m^{-2} yr^{-1} and drops sharply to about 2500 g m^{-2} yr^{-1} at the threshold around Lovénøyane and again towards the outer basin north of Ny Ålesund. In the latter case the rate drops to about 200 g m^{-2} yr^{-1} (Svendsen et al., 2002). Dominant deposition of sediments within Kongsfjorden includes suspension settling from meltwater plumes and ice rafting (Elverhøi et al., 1980). The outer basin is bedrock-dominated draped with a thin (< 10m) sediment cover (Howe et al., 2003). The inner basin is characterized by sediment deposits with a thickness of up to 20m (Streuff et al., 2015); (iii) The Lovénøyane ridge marks the maximum advance during the 1869 surge of Kongsbreen (Elverhøi et al., 1980; Liestøl, 1988; Streuff et al., 2015) and could represent a topographic barrier streaming the surge flow towards the north.

2.2 Geological setting

2.2.1 Regional geological setting

The geology of Svalbard resembles the geology of the adjacent Barents Sea and northern Greenland and in many respects the Kongsfjorden area exemplifies and reflects the key development of Svalbard as a whole. Kongsfjorden is located on the tectonic boundaries between the Northwestern Basement Province (NWBP) to the north, the Post-Caledonian sedimentary deposits in the east and the West Spitsbergen Fold-and-thrust Belt (WFSB) in the south (Hjelle, 1993), Figure 2. Contact between the Northwestern Basement Province and the Post-Caledonian sediments is characterized by fault-controlled basins within the Basement Province and with an angular unconformity towards the east, exposed at Pretender Mountain (Hjelle et al., 1999). The contact between the WFSB and the two previously mentioned structures is marked by a NW-SE trending frontal thrust fault zone that runs through the southern part of Kongsfjorden (Figure 3). Each of these features mark an important geological event that contributed to the present geological and geomorphological setting of Svalbard and will be described separately below.

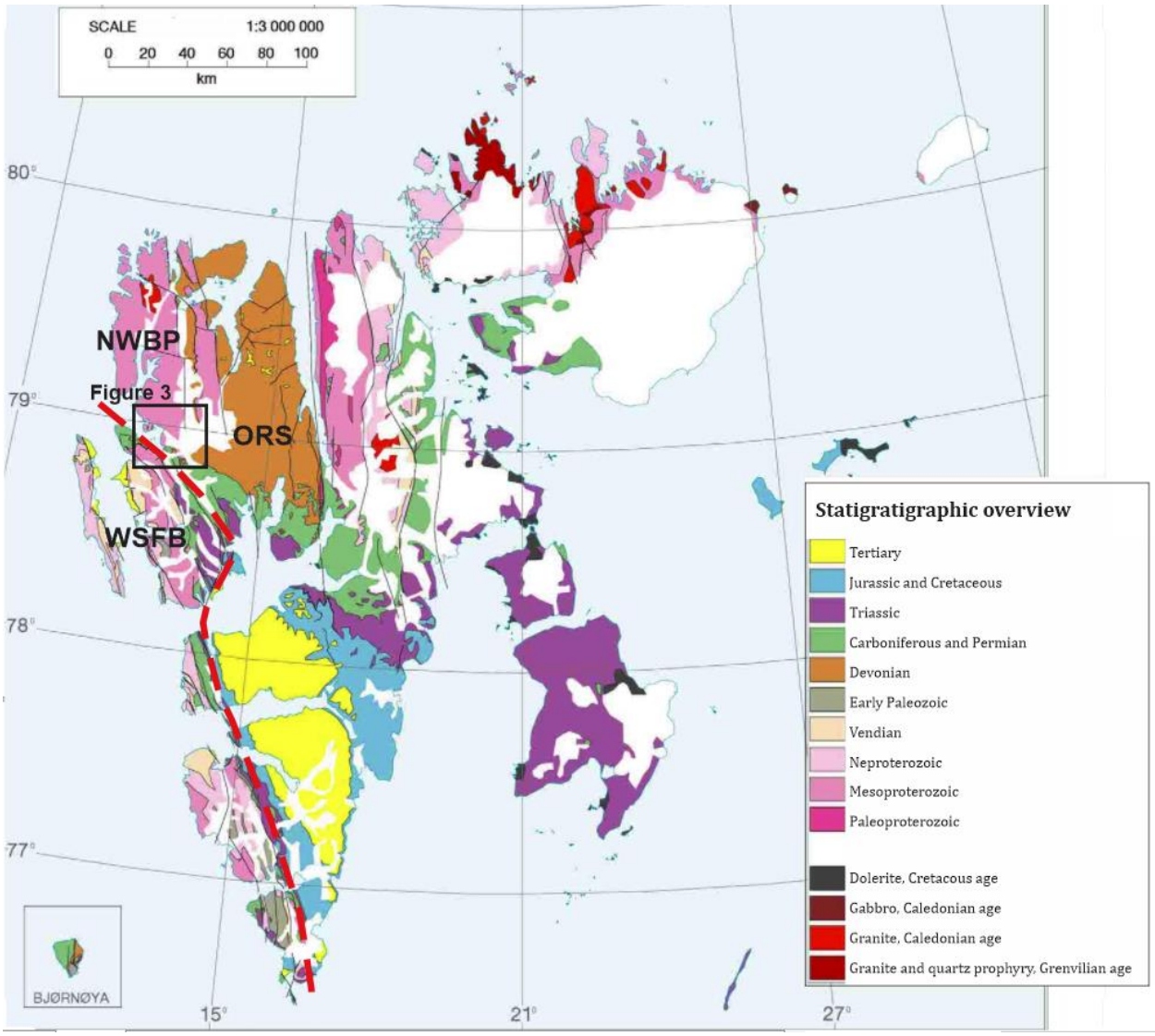

Figure 2: Geological map of Svalbard modified from Hjelle (1993). The black box indicates the location of Figure 3. Note the tectonic boundaries in Kongsfjorden between the Northwestern Basement Province (NWBP), the Post-Caledonian sediments, including Carboniferous strata together with the Old Red Sandstone (ORS), and the West Spitsbergen Fold-and-thrust Belt (WSFB).

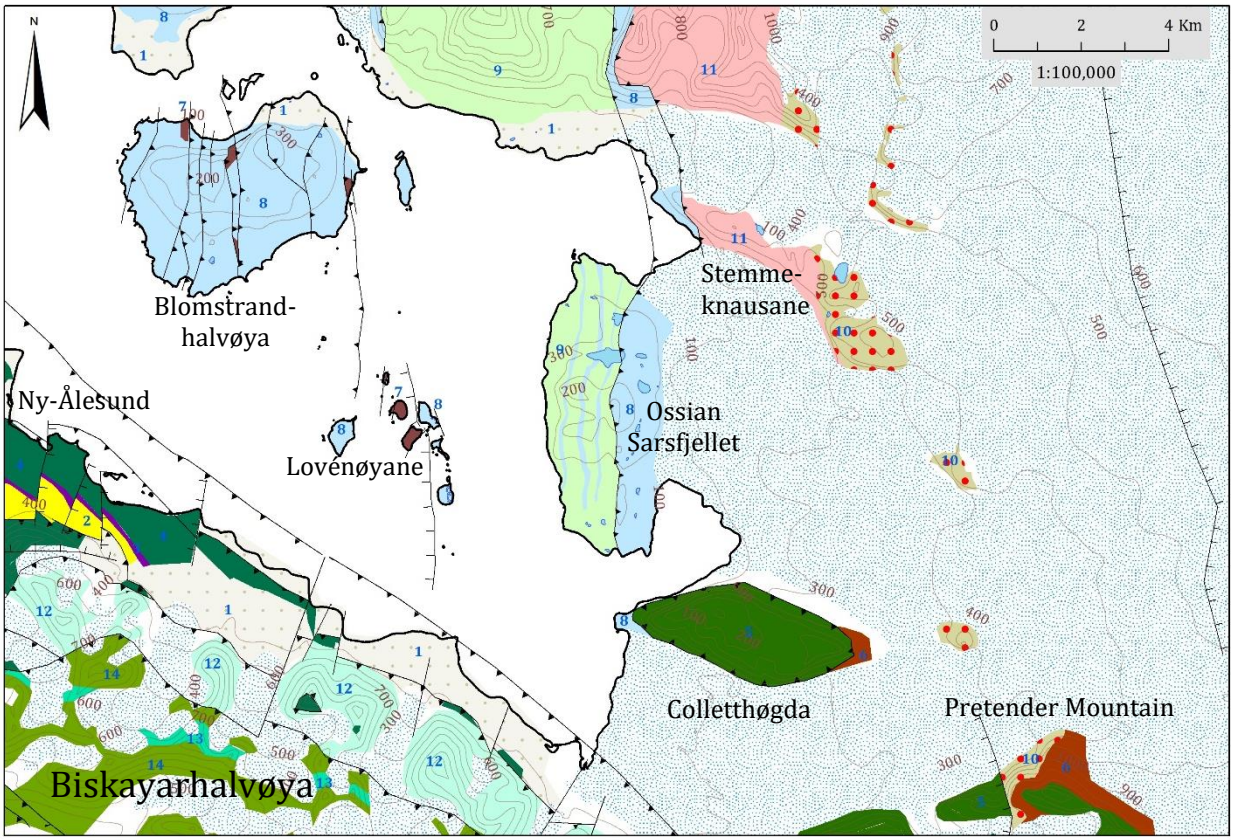

Legend

- Normal fault
- Fault
- Thrust fault
- Water
- Glacier
- 1 Unconsolidated material

WEST SPITSBERGEN FOLD-AND-THRUST BELT

- 2 Sandstone, siltstone and conglomerate
- 3 Black shale and siltstone
- 4 Carbonate rocks
- 12 Phyllite and quartzite
- 13 Marble
- 14 (Garnet-)mica schist

DEVONIAN AND LOWER CARBONIFEROUS SEDIMENTARY UNITS

- 5 Dolomite, limest., anhydrite/gypsum, carb. breccia
- 6 Sandstone, siltstone and shale
- 7 Red sandstone and conglomerate

NORTHWESTERN BASEMENT PROVINCE

- 8 Marble
- 9 Mica schist
- 10 Garnet mica schist
- 11 Migmatite

Figure 3: Regional geological map of Kongsfjorden area indicating the different lithological units within Kongsfjorden along with structural data (based on Hjelle, 1993 and Dallmann, 2015). Contour lines represent surface topography with 100m intervals (Norwegian Polar Institute, 2014b). The shore line is obtained from the Norwegian Polar Institute (2014c) and modified through use of a smoothening filter. Note the frontal thrust of the WSFB running through the southern margin of Kongsfjorden and the Kongsvegen glacier.

The Northwestern Basement Province (NWBP)

The NWBP of Svalbard is structurally the lowermost and oldest feature within the Kongsfjorden area. The NWBP is one out of three major basement blocks that are suggested to be juxtaposed during the Caledonian orogeny. This process was accommodated by large-scale transcurrent faults with predominantly sinistral strike-slip kinematics (Gee & Tebenkov, 2004). The NWBP around Kongsfjorden consists of three litho-tectonic units (Hjelle et al., 1999; Dallmann et al., 2006; Ohta et al., 2008; Dallmann, 2012, 2015); metasedimentary rocks (belonging to the Middle Proterozoic to Neoproterozioc, also referred to as the Krossfjorden Group); granitoids of early Tonian age (around 970 Ma); and granites of Caledonian origin. The Krossfjorden group is estimated to be around 7.5 km thick and consists of metapelitic schist and quartzite in the lower part (Signehamna formation) and marbles in the upper part (Generalfjella formation). It was then intruded by granotoids during the early Tonian age (around 970 Ma), followed by a phase of migmatization along with partial melting, during the Caledonian Orogen about 444 to 419 Ma (Myhre et al., 2009). The granotoids and migmatites are also referred to as the Smeerenburgfjorden complex. Throughout the entire succession, folds can be traced with a fold axis trending N-S, a wavelength of 15 – 20 km and an amplitude of 2 - 3 km (McCann, 2000). The main foliation present within the NWBP is N-S oriented. Locally N-S oriented L-tectonites are dominating over foliation planes, measured further up north at Liefdefjorden (Braathen et al., 2017). The presence of L-tectonites suggests substantial extension along the L-tectonite lineation (Fossen, 2010).

2.2.2 Post-Caledonian sedimentary deposits

The Post-Caledonian sedimentary rocks at Kongsfjorden unconformably overlie the Northwestern Basement Province. The lower part is interpreted as an intra-montane basin infill in the Caledonian mountain chain which occurred after the tectonic collapse during the Late Silurian? to Middle Devonian, also referred to as the Old Red Sandstone (Gjelsvik, 1974; Friend et al., 1997; McCann, 2000). The basin was then tectonically inverted by the Svalbardian Event (Piepjohn, 2000). The upper part unconformably overlies the Devonian sediments and marks a renewed extensional phase which took place after the Svalbardian Event associated with platform sedimentation during the Carboniferous to Mesozoic (McCann & Dallmann, 1996). The Post-Caledonian sedimentary deposits at Kongsfjorden can be subdivided into clastic Old Red Sandstones (ORS) that were deposited terrestrially during the Late Silurian? to Middle Devonian (Gjelsvik, 1974; McCann, 2000), and Permian and Mesozoic clastic and carbonate sediments deposited on a shallow marine environment (Dallmann et al., 1999).

Old Red Sandstone (ORS)

The ORS in Kongsfjorden comprise the stratigraphically lowermost clastic sedimentary rocks deposited terrestrially after the Caledonian orogeny (Friend, 1961; Gjelsvik, 1974). The ORS deposits are characterized by their red colors, which indicate extensive hematite oxidation by sub-aerial weathering during deposition (Gjelsvik, 1974). Two different formations can be recognized within the Kongsfjorden area: the stratigraphically lowermost Red Bay Group located in fault-bounded basins within the NWBP (Gjelsvik, 1974; Thiedig & Manby, 1992), and the uppermost Wood Bay formation (Piepjohn, 2000; Dallmann, 2015).

The Red Bay Group is characterized by a syn-tectonic fluvial basin infill including boulder sized clasts from the basement which is generally fining upwards, but also fining northwards (Friend 1961, McCann 2000). The Red Bay Group directly overlies deeply weathered and brecciated marbles from the basement, also referred to as the Viggobreen formation (Thiedig & Manby, 1992; Piepjohn, 1997, 2000). The depositional environment of the Red Bay Group at Kongsfjorden area is interpreted to be the first deposition of clastic material in braided rivers and alluvial fans within narrow grabens (Gjelsvik, 1974) and corresponds with the Wulffberg member described as a 100m thick marble conglomerate at the base of the Red Bay Group at Liefdefjorden area, northwestern Spitsbergen (Friend et al., 1997). The Red Bay Group within Kongsfjorden is only exposed on Blomstrandhalvøya and on Lovenøyane (Figure 3). The tectonic setting of Svalbard during deposition of the Red Bay Group is still under dispute. Gjelsvik (1974) suggests that sedimentation in tectonically bounded grabens was displaced by strike-slip faulting, whereas Friend et al. (1997) and McCann (2000) maintain that deposition in fault blocks within pull-apart basins was accommodated by large-scale sinistral strike-slip faulting during the Monacobreen deformation phase (Early Devonian). Braathen et al. (2017), however, have recently put the tectonic setting of Svalbard into new light arguing that deposition of the ORS is due to a top-to-north extensional detachment with associated exhumation of a metamorphic core complex throughout the Late Silurian to Mid-Late Devonian. After deposition the Red Bay Group at Blomstrandhalvøya and Lovénøyane were emplaced on top of the marbles by thick-skinned thrusting and back-thrusting due to orthogonal compression during the Svalbardian orogeny (Piepjohn, 2000).

The overlying Wood Bay formation has a much thicker sequence, and it extends much more laterally towards the Billefjorden Fault Zone and is characterized by finer sediments deposited during subsidence in an extensional tectonic setting (McCann & Dallmann, 1996; McCann, 2000). The Wood Bay formation within the Kongsfjorden region is only exposed at Colletthøgda and

Pretender Mountain where the latter unconformably is situated between the NWBP and overlying Carboniferous-Mesozoic platform strata (Piepjohn, 2000; Dallmann, 2015).

2.2.3 West Spitsbergen Fold-and-thrust Belt (WSFB)

The WSFB is spanning from Kongsfjorden all the way down to the southern tip of Spitsbergen (Bergh et al., 2000; Piepjohn et al., 2015). The structures at the WSFB are similar to the structures in northern Greenland and Ellesmere Islands and are attributed to the Eurekan orogeny. The latter is characterized by an intraplate compressional activity, prior to the opening of the Greenland Sea, when Svalbard was located along the northern margin of Greenland (about 56 – 45 Ma; Dallmann, 2015).

The deformation event within the Kongsfjorden area is exposed on Brøggerhalvøya and has been described by Bergh et al. (2000) as a three-phase deformation event. This event comprises of an early stage of coupled dextral transpression, a mid-phase of decoupled transpression and a late phase of transtensional extension associated with dextral strike-slip faulting. The transpressional stresses, during the early and mid-phase deformation event of the WSFB, seem to derive from a rotational movement of Greenland due to active sea-floor spreading at the Labrador, Baffin Bay and North Atlantic sea (Dallmann, 2015). The late-phase extensional regime associated with dextral strike-slip characterizes the final stage of the Eurekan orogeny (after 45 Ma) and marks the onset of the separation between the Barents-shelf and northern Greenland which was concentrated along the De Geer Fracture Zone (Bergh et al., 2000; Piepjohn et al., 2015).

That part of the eastern margin of the WSFB that is located within the study area is marked by a major thrust fault running parallel to the NW-SE trend of Brøggerhalvøya along the southern margin of Kongsfjorden (Figure 3). Svendsen et al. (2002) proposed that the glacier Kongsvegen, and its deglaciated prolongation along Kongsfjorden, has probably been formed in a morphological depression due to structural weaknesses paralleling the major thrust front of the WSFB. The main orientation of the thrust belt is deflected from a NW-SE trend within Kongsfjorden to a more N-S trend south of Kongsvegen (Piepjohn et al., 2013), Figure 2. As part of this current study no measurements were taken from the WSFB, as the major thrust zone is not exposed at the surface and the bedrock only covers a very minor part at the southern part of Kongsfjorden.

2.3 Glaciological setting

During the Pleistocene, Svalbard has repeatedly been glaciated. The initiation of glaciations at the Svalbard Barents-sea Ice Sheet (SBIS) was marked by an increased deposition of Ice-Rafted Debris (IRD) in marine sediments between 3.5 and 2.4 Ma (Knies et al., 2009). The SBIS did not reach the shelf-edge at western Spitsbergen before 1.3 Ma (Rebesco et al., 2014). Although, only within the last 0.7 Ma ice drainage was facilitated through topographically bounded ice streams at western Svalbard, with dynamically active warm-based ice within the troughs bounded by cold-based ice on the adjacent banks (Patton et al., 2015). An overview of shelf-edge glaciations of the SBIS during the Pleistocene is presented in Figure 4.

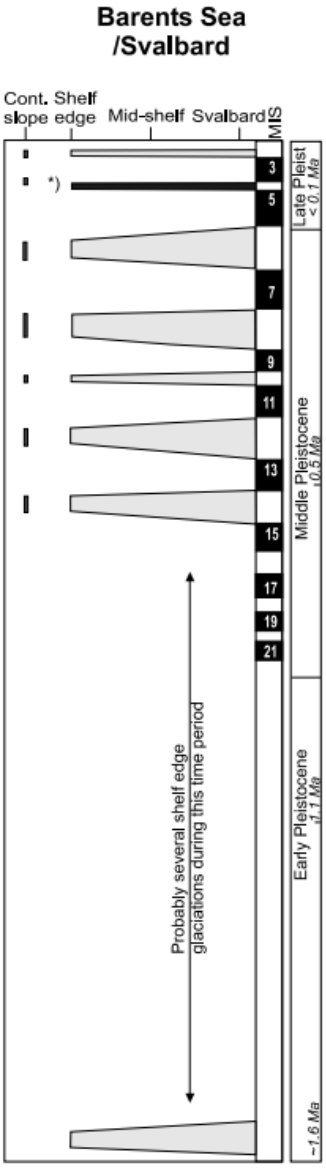

Figure 4: Glacial curves of the Barents Sea/Svalbard margin indicating shelf edge glaciation (Sejrup et al., 2005).

Unlike many other places in Svalbard, Kongsfjorden shows evidence, based on sedimentary records, of multiple glaciation events (Landvik et al., 2014) reaching back to the early Pleistocene glaciation (Miller, 1982; Houmark-Nielsen & Funder, 1999). The most important glacial events of the Kongsfjorden area since the last glaciation will be discussed below.

2.3.1 Last glaciation and deglaciation

The ice sheet at western Svalbard reached shelf-edge glaciation during the Late Weichselian around 24 cal ka BP (Jessen et al., 2010), marked by a terminal moraine at the shelf break (Ottesen et al., 2007), Figure 5 and Figure 6. Geomorphological evidence, such as mega-scale lineation, lateral moraines and grounding zone wedges found in the Kongsfjordrenna trough, suggests drainage of dynamically active warm-based ice through ice streams bounded by cold-based dynamically non-active ice (Landvik et al., 2005, 2013; Ingólfsson & Landvik, 2013), Figure 6. Throughout the last glaciation, Kongsfjorden and Krossfjorden together drained substantial amounts of ice from the NW Spitsbergen ice fields towards one of the main ice streams of western Svalbard, Kongsfjordrenna (Landvik et al., 2005; Ottesen et al., 2007).

Figure 5: Reconstruction of the ice flow regime during the Late Wechselian of the Svalbard-Barents Sea Ice Sheet, modified from Ottensen et al. (2007). Note the various ice streams at the western and northern margins of Spitsbergen.

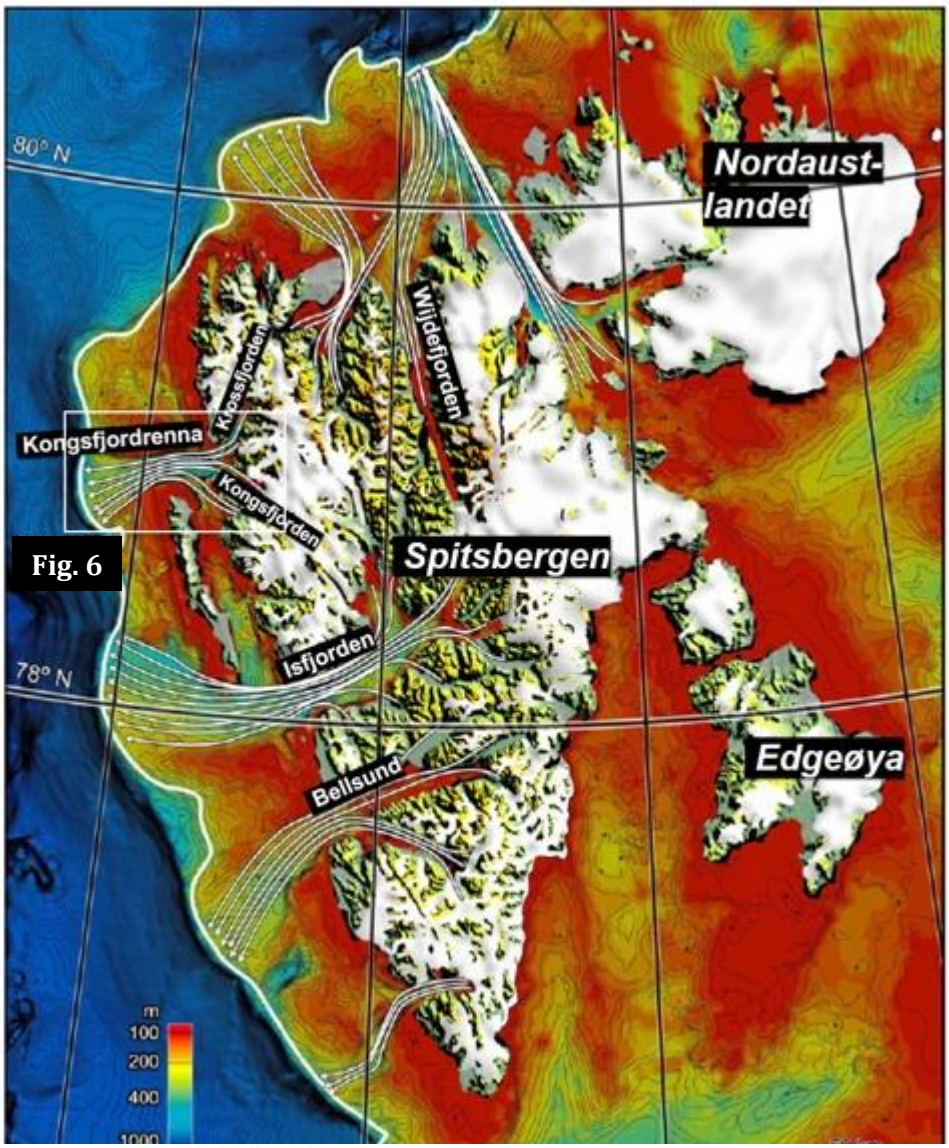

Figure 6: Compilation of submarine landforms of the Kongsfjordrenna trough and Kongsfjorden area described in literature, from Streuff (2013).

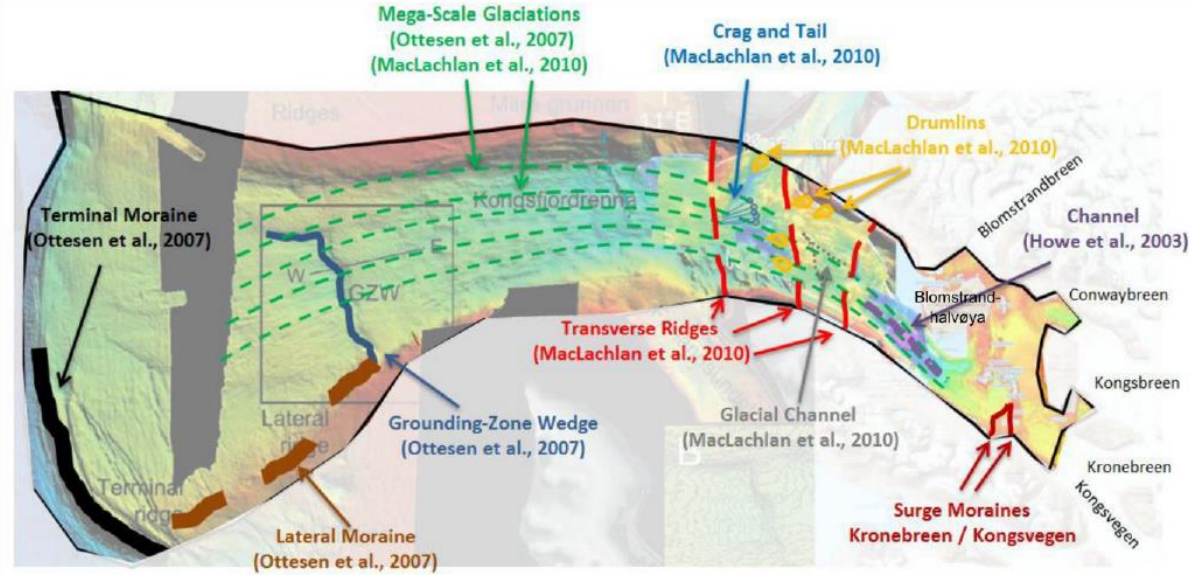

Reconstructions using cosmogenic dating of the ice sheet cover over Svalbard during the last glaciation have revealed a multi-dome arrangement (Hormes et al., 2011; Gjermundsen et al., 2013). Gjermundsen et al. (2015) found that cold-based ice in alpine topography of northwest Spitsbergen caused minimal erosion during the Late Weichselian and arguably erosion was concentrated within dynamically more active glacial troughs between the mountain summits. The occurrence of this erosional ice restricted in troughs during the Late Weichselian is supported by findings of Hormes et al. (2011). This study found, by analyzing exposure dates of erratic boulders in Nordaustlandet, that plateaus were covered with cold-based non-erosive ice and that the dynamically active erosional ice was restricted in lowlands and fjords below 230m a.s.l.

Deglaciation started with an initial thinning of the interior ice-sheet of northwest Spitsbergen around 25 -20 ka (Gjermundsen et al., 2013; Hormes et al., 2013; Henriksen et al., 2014). The thinning of the interior of the ice sheet was followed by ice marginal retreat around 20.5 ka, which was dated by a peak in IRD in marine sediments at the shelf-edge (Jessen et al., 2010). The minimum ice surface elevation in Kongsfjorden is estimated to be >450m a.s.l. during the Late Weichselian (20 - 17 ka; Henriksen et al., 2014). The ice-sheet retreated from the shelf-edge and reached the fjord mouth of Kongsfjorden around 16.6 ka (Landvik et al., 2005; Henriksen et al., 2014). Marine records from the Kongsfjordrenna trough suggest an ice proximal environment with low sedimentation rates and restricted ice-rafting, reflecting limited calving due to a low ice flux, between 16.5 and 15.2 ka (Landvik et al., 2005; Henriksen et al., 2014). This low ice flux does not support fast flowing ice streaming within Kongsfjorden and therefore it is suggested by the same authors that this indicates a major reduction in glacial dynamic activity. Henriksen et al. (2014) and Landvik et al. (2014) further suggested that the ice dynamical behavior of Kongsfjorden has changed from an active ice-stream to a less active outlet glacier around 16.6 ka.

Through use of geomorphological data (Maclachlan et al., 2010), cosmogenic dating of glacial erratics (Henriksen et al., 2014) and through ^{14}C dating on marine organic materials in raised beaches (Lehman & Forman, 1992), it has been documented that the recession of the outlet glacier from the fjord mouth of Kongsfjorden occurred in multiple stages. The earliest ice-free conditions in Kongsfjorden are estimated to have occurred around 9000 cal yr BP, on basis of ^{14}C dating on mollusk fragments on top of striated bedrock at Ossian Sarsfjellet (Lehman & Forman, 1992). Since the Late Weichselien (about 14 ka) Kongsfjorden has been uplifted about 44m a.s.l, a level that has been estimated on basis of exposed beach ridges at the northern shore of Kongsfjorden, due to glacio-isostatic rebound (Lehman & Forman, 1992).

2.3.2 Little Ice Age (LIA)

The LIA in Kongsfjorden, which ended at the end of the 19th century, marks the maximum Holocene advance of glaciers since the ice-free conditions after the LGM (Liestøl, 1988). Evidence from depositional glacial landforms indicates the occurrence of glacier margins extending up to 5 km beyond their present margins (Streuff et al., 2015). Surge activity has been identified on some of the tidewater glaciers draining into Kongsfjorden, namely Kongsvegen, Kongsbreen, Blomstrandbreen and Conwaybreen (Liestøl, 1988; Streuff et al., 2015; Farnsworth et al., 2016). The tidewater outlet glaciers are presently retreating and thinning, resulting in the exposure of new bedrock outcrops that have not yet been described.

Glacial landforms within Kongsfjorden produced before the Holocene are located in the outer and central part of the fjord and include: drumlins, flutes (Howe et al., 2003), crag-and-tails and transverse ridges (Ottesen et al., 2005; Maclachlan et al., 2010; Forwick et al., 2016). The landforms within the fjord are reworked by bottom currents and/or draped with a thin sedimentary cover (<10m) caused by suspension fallout and mass failures after the LGM (Howe et al., 2003). The outer and central fjord also consist of two deeper basins filled with at least 30m of sediments. However, the draped sediment cover is usually too thin to obscure landforms produced by the last full glacial and deglaciation period (Forwick et al., 2016). The inner fjord consists mainly of glacial landforms produced by the glacial advance during the LIA and these are described in detail by Streuff et al. (2015).

3. Theoretical framework

Observations of glacial erosional landforms within bedrock dominated areas can inform us about the glacio-erosional processes acting on the bedrock which were involved in the formation of those landforms. Information about glacio-erosional processes, in turn, can be used to infer paleo-ice flow dynamics (Glasser & Bennett, 2004; Benn & Evans, 2010; Bradwell, 2013).

3.1 Glacio-erosional processes

Glaciers underlain by bedrock-dominated areas ('hard beds') can be subjected to three different processes of erosion (Benn & Evans, 2010), namely: by *abrasion,* when rock particles scour on top of the bedrock surface; by *quarrying*, when large blocks of rock are being removed by failure of joints; and by *glacial meltwater*, when mechanically and/or chemically weathered rocks are removed by water. These three processes operate at different scales but combined they create an assemblage of different glacial landforms. Each process will be discussed below.

3.1.1 Abrasion

Bedrock surfaces eroded by *abrasion* is caused by two processes: scouring and polishing. Scouring results in the formation of linear grooves (striations) and polishing results in the reduction of the bedrock surface roughness (Benn & Evans, 2010). Striations are formed by localized stress concentrations of rock particles (usually larger than 1 cm) that are incorporated into the ice and then dragged over the rock surface. When this happens, they leave a linear groove behind them. These grooves are the result of the cumulative effect of small brittle fractures, caused by the localized stress concentrations of the rock particles, and the subsequent removal of the loose material. Polishing of rock surfaces is the result of the removal of small irregularities within the rock surface.

Controlling factors of erosion favored by abrasion include effective basal pressure greater than 1 MPa, high velocity of particles in the ice, high concentration of particles in the basal ice and relative rock strength between particles and bedrock (Boulton, 1974; Hallet, 1979; Iverson, 1991a; Benn & Evans, 2010; Krabbendam & Bradwell, 2011). Abrasion rates are inversely related to rock strength, therefore quantifying rock strength could be a tool to determine abrasion resistance (Boulton, 1979; Krabbendam & Glasser, 2011).

3.1.2 Quarrying

Bedrock erosion by *quarrying*, also known as plucking, describes the process of the separation of rock fragments from the host rock (Benn & Evans, 2010). Quarrying is fundamentally the same process as *abrasion*, although taking place at a different scale. Localized cumulating stress concentrations enlarges fractures within the bedrock which on its turn leads to separation of rock fragments from the host rock (Benn & Evans, 2010). It has been suggested that ideal conditions of rock fractures occur at rock steps were large stress gradients can develop as a result of fluctuating water pressures at lee-side cavities (Iverson, 1991b). If water pressure drops within lee-side cavity, fractures propagate downwards parallel to the lee face of the rock step, isolating large fragments (Iverson, 1991b; Cohen et al., 2006). These fragments will then be removed by the tensile deviatoric stresses in the direction of the ice flow, as the compressive stresses within the bedrock generally are vertically oriented (Benn & Evans, 2010). For this reason, the distribution and orientation of pre-existing joints within the bedrock have a strong influence on erosion by quarrying.

Controlling factors of erosion favored by quarrying include strong water pressure fluctuations, low-effective basal pressure (0.1 - 1 MPa), high sliding velocities, low porosity and presence of joints within the host rock (Iverson, 1991b; Hallet, 1996; Cohen et al., 2006; Benn & Evans, 2010; Dühnforth et al., 2010; Krabbendam & Bradwell, 2011). Several field studies have shown that joints effectively control whether quarrying occurs or not (Gordon, 1981; Dühnforth et al., 2010; Krabbendam & Glasser, 2011; Hooyer et al., 2012). Cavity formation is favored at the lee-side of landforms that are characterized by structural weaknesses, such as bedding, joints, foliation trends and fracture zones (Glasser et al., 1998; Krabbendam & Bradwell, 2014). Important is also the orientation of these structural weaknesses in respect to ice flow. It is of consequence if bedding and foliation of the bedrock strike parallel or transverse to ice flow (Gordon, 1981; Glasser et al., 1998; Krabbendam et al., 2016). For example, Glasser et al. (1998) found that quarried rock faces of metamorphic rock slabs located at the innermost Kongsfjorden are particularly well developed where former ice flow was (sub-)parallel to the dominant bedrock foliation. The same authors also found that the formation of cavities is suppressed where the former ice flow was normal to the trend of the dominant bedrock foliation. However, rocks without joints could possibly fracture sub-glacially, but such events seem to be exceptional (Hooyer et al., 2012).

3.1.3 Glacial meltwater erosion

Glacial meltwater erosion involves the removal of mechanically and/or chemically weathered particles. Glacier meltwater erosion is controlled by bedrock structure and strength; discharge regime (including water velocity and turbulence); and the amount of sediment transport within the meltwater (Glasser & Bennett, 2004).

3.2 Glacial erosional landforms

Glacial erosion can be distinguished from fluvial, coastal and/or aeolian erosion by recognition of glacial modified landforms. According to Glasser and Bennett (2004), erosional forms modified by glaciers can be grouped into three different scales: micro-scale, meso-scale and macro-scale landforms. More detailed descriptions and definitions of these glacial erosional landforms can be found in Sugden and John (1976); Glasser and Bennett (2004) and Benn and Evans (2010).

3.2.1 Micro-scale landforms

Micro-scale landforms are erosional forms smaller than 1m in size, often ornamenting larger landforms. In this study, micro-scale landforms are referred to as *striae* and *micro-crag and tails*.

Striae are linear grooves incised into bedrock, usually only a few millimeters deep and up to several meters long. They are produced through the process of glacial abrasion. Striae are formed parallel to local ice movement on flat surfaces and can therefore be used as a basis for paleo-ice flow orientation. The presence of striae, reflecting glacial abrasion, suggests warm-based subglacial conditions with basal debris, basal sliding and a moderate level of effective normal pressure (Glasser & Bennett, 2004). Striae are associated with areas of polished surfaces which comprise of numerous micro-striation (<10μm) (Benn & Evans, 2010).

Micro-crag and tails are small streamlined features consisting of a resistant bedrock crag at the stoss-side and a tapering tail at the lee-side of less resistant rock. The bedrock at the tail is preferentially protected from glacial abrasion at the lee-side of more resistant features on the surface of the rock. Presence of micro-crag and tails can be used to determine paleo-ice flow direction. The occurrence of such features indicates that abrasion processes are operating, and this reflects similar glacial conditions as the formation of *striae* (Glasser & Bennett, 2004).

3.2.2 Meso-scale landforms

Meso-scale landforms are between 1m and 1km in size and include landforms such as *whalebacks*, *roches moutonnées* and *megalineation*s.

Whalebacks are characterized as rounded, often streamlined bedrock bumps elongated in the ice flow direction with a relative low height to length ratio. Streamlining of the landform occurs through striation and polishing of all the bedrock surfaces by glacial abrasion. It is assumed that the absence of quarried lee faces on whalebacks implies that low-pressure cavity formation has been suppressed (Glasser & Bennett, 2004). Areas where cavity formation has been suppressed is proposed to occur below thick ice with high ice-overburden pressure. It has been further suggested that these conditions are present in two different subglacial settings: (i) below thick and slow-sliding ice with low basal meltwater pressures (Glasser & Bennett, 2004); and (ii) below thick, fast-sliding ice with stable meltwater pressures (Evans, 1996; Roberts & Long, 2005; Bradwell, 2013).

Roches moutonnées are partly streamlined asymmetrical bedrock bumps with abraded stoss-faces and quarried lee-faces along ice flow direction. However, joints and bedding within the bedrock have a strong control on the final shape of roches moutonnées once plucking is initiated (Gordon, 1981). Roches mountonées are typically formed where ice overburden pressure is high at stoss surfaces and sufficiently low at lee surfaces to allow for cavity formation. Cavity formation, together with rapid cavity pressure fluctuations, promote quarrying. These conditions are thought to take place beneath relatively thin, fast-flowing ice with rapid cavity pressure fluctuations. The fluctuations of pressure in cavities are in response to changes in meltwater input, which is derived from transport of surface meltwater through crevasses to the bed or by basal meltwater (Iverson, 1991b; Evans, 1996; Hallet, 1996; Glasser & Bennett, 2004).

Megalineations is a collective term for highly elongate positive and negative bedrock landforms larger than 100m and with an elongation ratio larger than 1:10 (Benn & Evans, 2010; Krabbendam et al., 2016). Megalineations are also referred to as *megaridges* or *megagrooves* if the landform is recognized as a positive or negative feature, respectively. Megalineations are related with fast flowing ice and have been used to map paleo-ice streams on bedrock dominated surfaces (Krabbendam et al., 2016). Bedrock surfaces with bedding striking parallel to ice flow generate more developed megalineations rather than bedrock surfaces with bedding transverse to strike (Krabbendam et al., 2016).

3.2.3 Macro-scale landforms

Glacially eroded macro-scale landforms are landscape features with dimensions larger than 1 km. These landscape features may be ornamented with such smaller landforms as mentioned above. The macro-scale landforms referred to in this study include: *glacial troughs* and *overdeepenings*.

Glacial troughs are deep linear U-shaped features carved into bedrock, probably developed over repeated glaciations of pre-glacial fluvial landscapes resulting in topographic channeling of ice flow into the glacial trough (Nesje & Whillans, 1994; Egholm et al., 2017). The transition of the shape of a fluvial valley into a glacial trough is thought to have developed after 200 000 years of glacial modification (Kirkbride & Matthews, 1997). Erosion of the bedrock within glacial troughs occurs through the combined effect of glacial abrasion, quarrying and glacial meltwater erosion. Zones of weaker bedrock, such as fracture zones paralleling the glacial trough, could lead to enhanced erosion and the development of locally deeper glacial channels than the overall U-shaped trough (Harbor, 1995). The formation of glacial troughs or channeling of ice in areas of low elevation is essential for flow focusing. This process leads to a positive feedback of dynamically more active ice with higher erosive power. Increased erosion leads to larger cross-sectional areas accommodating larger ice volume drainage through the glacial trough (Brook et al., 2003; Bradwell, 2013; Egholm et al., 2017). However, cross-profile morphology of glacial valleys is strongly related to bedrock properties such as rock mass strength, with soft and weak rocks usually having a wider and shallower cross-profile valley morphology (Augustinus, 1992; Brook et al., 2004; Swift et al., 2008).

Overdeepenings, represent basins eroded into bedrock within the floors of glacial troughs. Development of these basins is controlled by both glaciological variables such as thermal regime, ice velocity and ice thickness, and bedrock properties such as lithology and structural weak zones (Gonzales & Aydin, 2008; Benn & Evans, 2010; Cook & Swift, 2012). Overdeepened sections often develop in areas with increased ice drainage, such as downstream of merging tributary valleys or at narrow corridors within the glacial troughs (Shoemaker, 1986). However, overdeepened linear valleys can also develop at structural weak zones. Selective glacial erosion of the fractured rock could increase the vertical component of linear valleys resulting in overdeepened linear valleys (Krabbendam & Bradwell, 2014).

4. Methods and datasets

In this research project, fieldwork is used combined with available aerial photographs and Digital Elevation Models (DEM's) to assess the bedrock geology and geomorphology by comparing detailed outcrop observations with regional patterns within the study area.

4.1 Datasets

The available datasets used in this study include a geological map of the area and three different DEM's. These different DEM's cover the bathymetrical, subglacial and surface topography. An example of the bathymetrical DEM is presented in Figure 7. Details of each DEM are shown in Table 1 and will be described separately below.

Datasets

Type	Bathymetrical DEM	Subglacial DEM	Surface DEM	Geological map
Method	Swath-bathymetry data	Ice Penetrating Radar	Stereo aerial photographs	Mapping
Resolution	5 m	150 m	5 m	1:100.000
Accuracy	?	?	2 - 5 m	
Year	2010	2014-2016	2009	1999 - 2012
Source	Norwegian Hydrographic Service (2014)	Lindbäck et al. (in review)	NPI	NPI

Table 1: Datasets used in the study

4.1.1 Bathymetry DEM

The bathymetrical DEM with a 5 m resolution was compiled by the Norwegian Mapping Authority Hydrographic Service (2014). The high-resolution swath-bathymetry data used for compiling the DEM were captured in 2000, 2007, 2010 and 2011. In 2000, an EM 1002 multi-beam echo sounder was used for capturing data; in 2007, 2010 and 2011, an EM 3002 multi-beam echo sounder was used for the same purpose.

In this study, the bathymetrical data have been processed to produce a slope map, a hillshade map and an aspect map of the fjord floor. They were also used to draw transverse surface profiles, with the aim to relate the glacial landforms with the cross-valley morphology.

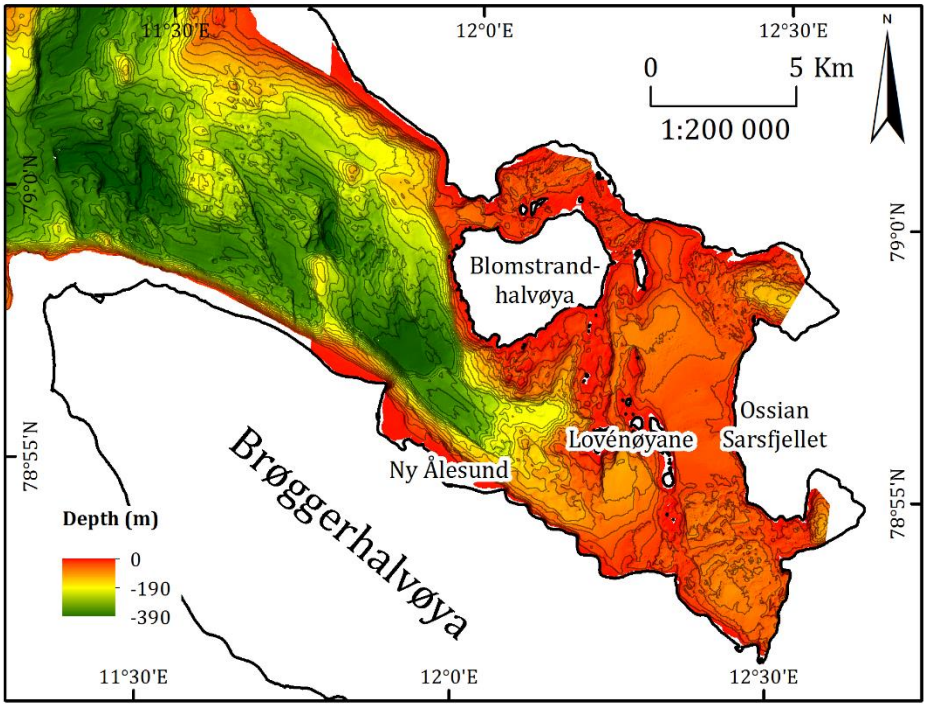

Figure 7 : Example of one of the Digital Elevation Models (DEM's) used in this study. This is the Bathymetrical DEM (Norwegian Mapping Authority Hydrographic Service, 2014) with 20m spaced contour lines. The shore line is obtained from the Norwegian Polar Institute (2014c) and modified through use of a smoothening filter. Note the high roughness around the Lovénøyane archipelago and the overdeepend channel between Ny-Ålesund and Blomstrandhalvøya.

4.1.2 Subglacial DEM

A subglacial topography DEM of the tidewater outlet glaciers; Conwaybreen, Kongsbreen, Kronebreen and Kongsvegen, was provided by the courtesy of the Norwegian Polar Institute. The subglacial topography data that were used to create the DEM were collected by Lindbäck et al. (in review), using radio-echo sounding radar profiles either mounted on a helicopter (in crevassed areas) or towed behind a snowmobile during expeditions executed in the spring of 2014, 2015 and 2016. These data, covering in total about 1300 km of common-offset radar profiles, were then supplemented with older radar profiles collected by the Norwegian Polar Institute during earlier expeditions. All the radar profiles were calibrated by determining the misfit in bed elevation at crossover points of different radar profiles. The resulting DEM has a resolution of 150 m.

In this study, the subglacial DEM was used to draw transverse surface profiles along Kongsfjorden, with the aim to highlight geomorphological features.

4.1.3 Surface DEM

Both a surface topography map and an orthophoto of the Kongsfjorden area are available online (Norwegian Polar Institute, 2014a). The surface DEM and the orthophoto were created using stereo aerial photographs of 2009 and 2010. The DEM has a resolution of 5m and an accuracy of 2 to 5m. It covers the whole Kongsfjorden area.

In this study, the orthophoto and surface DEM were used with the aim to map and interpret the morphological features of the islands within Kongsfjorden. The surface DEM was also used to draw transverse surface profiles of Kongsfjorden.

4.1.4 Geological maps

Four different geological map sheets with scale 1:100.000 were provided by courtesy of the Norwegian Polar Institute. The maps included Norsk Polarinstitutt Temakart numbers 30, 39, 42 and 49 (Hjelle et al., 1999; Dallmann et al., 2006; Ohta et al., 2008; Dallmann, 2012).

In this study, the geological maps were used to supplement the collected field data. Through that it was possible to extrapolate individual observations of outcrops to the study area at large.

4.2 Acquiring field data

In the field, priority was given to acquiring an overview of the variable bedrock characteristics and geomorphological characteristics for each different lithology within the study area. For this, 9 daytrips were made to various sites throughout Kongsfjorden to study the different lithologies. These daytrips were carried out between 18 and 27 August 2017, using a boat provided by the nearby research station in Ny-Ålesund. The locations visited are shown in Figure 8 (respectively A, B and C). Only the lithologies located north of Brøggerhalvøya, i.e. north of the West Spitsbergen Fold-and-thrust Belt (WSFB), were described.

Descriptions of the bedrock characteristics include lithology, structural data, bedrock mechanical properties and degree of alternation. The structural data that were noted comprise of strike, dip, lineations and slip kinematics of fault planes. The declination for the study site was 7° (derived from the World Magnetic Model acquired from http://www.ngdc.noaa). The assessment of the bedrock mechanical properties included measurements of intact rock strength and rock mass strength for each lithology, and will be described in more detail in sections 4.2.1 and 4.2.2.

The geomorphological characteristics were analyzed by identifying and classifying the glacial erosional landforms on the visited outcrops. The classification of glacial erosional landforms

was based on Glasser & Bennett (2004). On basis of striations on outcrops the paleo-ice flow direction at that particular locality could be approximated.

Finally, the characteristics of fracture zones were also closely examined as there are strong indicators that these exerted a major influence on differential erosion (Gonzales & Aydin, 2008; Krabbendam & Bradwell, 2014). Most of the fracture zones were poorly exposed, except the ones at Juttaholmen. For this reason, the findings of the central fracture zone at Juttaholmen (location 010) were extended to similar structures around the Lovénøyane archipelago. The assessment at Juttaholmen included descriptions of the fracture zone describing its lithology, texture, type of brecciation, bedrock mechanical properties and degree of alternation.

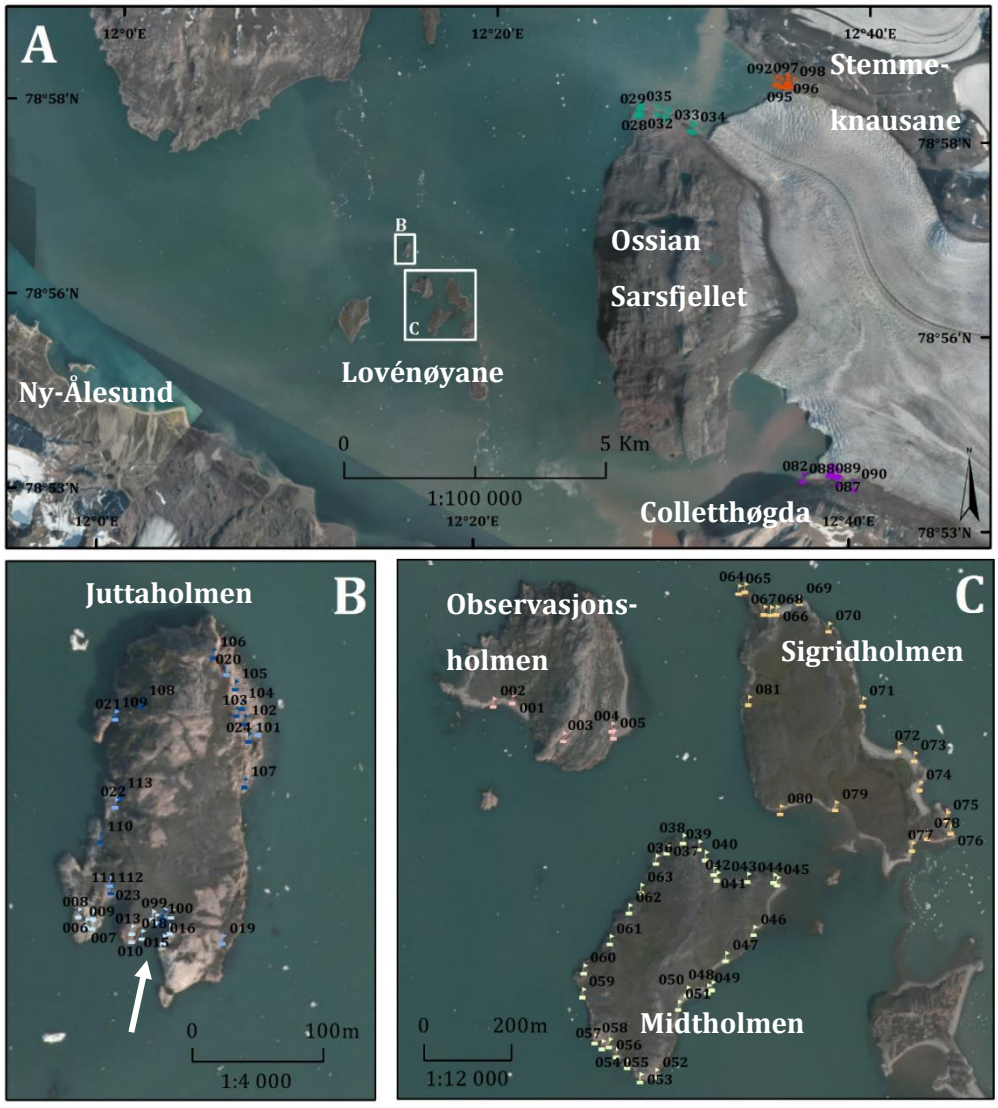

Figure 8: Locations visited by the author during fieldwork, as referred to in the text. Maps A, B and C display sites that were visited to determine the main bedrock and geomorphological characteristics. The white arrow indicates the location of the fracture zone assessment on Juttaholmen. The background image is an orthophoto of the study area provided by the Norwegian Polar Institute.

4.2.1 Intact Rock Strength (IRS)

In the literature, Intact Rock Strength (IRS) is mostly defined as the strength of rock material between discontinuities and this determines the hardness of the intact rock block material (Hack & Huisman, 2002). Diverse studies have shown that abrasion resistance is dependent on the absolute hardness of the bedrock, as well as on the relative hardness between basal debris particles and bedrock (Boulton, 1979; Iverson, 1991a; Sklar, 2001). The Schmidt Hammer rebound values have previously been used as a method to give a reliable approximation of the absolute hardness of the bedrock and can therefore satisfactorily be used as a proxy for IRS and abrasion resistance (Sachpazis, 1990; Augustinus, 1992; Brook et al., 2004; Aydin & Basu, 2005; Krabbendam & Glasser, 2011; Viles et al., 2011; Krabbendam & Bradwell, 2014). This method was chosen because the Schmidt Hammer is easily portable, quick-in-use, non-destructive and performs at low-cost. Through this, data could be gathered at many different localities and lithologies.

For this study, a 'BN' type electronic Schmidt Hammer (named SilverSchmidt) was used (made by Proceq). The 'BN' type SilverSchmidt collects indirect rebound values (Q-values) by calculating the difference of the velocity during impact and rebound at different outcrops. In the literature, studies tend to refer to an older version of Schmidt Hammer (called Original Schmidt) which measures direct rebound values (R-values). The R-values are calculated by measuring the fractional rebound distance during impact. R-values can be converted into Q-values by a conversion factor in the order of +9.6 - 10.1 units (Winkler et al., 2014). The SilverSchmidt provides measurements which are independent of the impact direction and it uses an impact energy of 2.207 Nm with a compressive strength of 10 - 100 MPa (Viles et al., 2011). However, the mechanical anisotropy within rocks influences Q-values. A mechanical anisotropy within rocks comprises of non-uniform and non-regular geometries of discontinuities, such as joints and fractures (Noorian Bidgoli & Jing, 2014). A strong mechanical anisotropy can contribute to a reduction in Schmidt Hammer rebound values and should be taken into account (Viles et al., 2011).

In the present study, the method described by Gupta et al. (2009) was employed for collecting the Schmidt Hammer hardness measurements. This method includes 50 single rebound measurements per site on a smooth flat surface, separated by at least a piston width (~2 cm). All measurements were taken at a distance of at least 10 cm from the edge of the outcrop, to minimize edge effects. The upper and lower 10 values were then discarded to reduce variability when calculating summary statistics. This method was chosen as it tends to minimize outlier values, which are common on bedrock surfaces due to local weathering remnants or minor discontinuities.

An effort was made to select outcrops with minimal weathering signatures and discontinuities within the rock, to reduce the influence of mechanical anisotropy of the Q-values.

4.2.2 Rock Mass Strength (RMS)

The Rock Mass Strength method, developed by Selby (1982), can be used in the field to determine the control of jointing in the rock strength of an outcrop. This method has been applied widely, e.g. to assess bedrock control in glacial valley development (Augustinus, 1992; Brook et al., 2004); to study overdeepened glacial erosion (Gonzales & Aydin, 2008; Dühnforth et al., 2010); and to research glacio-erosional landform formation (Krabbendam & Glasser, 2011; Krabbendam & Bradwell, 2014).

In this study, fracture spacing was used as a proxy for RMS (Krabbendam & Glasser, 2011). The fracture spacing values were obtained through application of the 'circle inventory method', as described by Davis & Raynolds (1996). This method aims to measure all the fractures within a predefined circle on a selected outcrop. The fracture spacing is then calculated by dividing the total length of all fractures by the area of the circle. This method was applied by making photos of outcrops visited in the field, using a 1 m measuring stick for scale. The photos could later be imported into *ArcGIS* 10.5 and referenced to the appropriate scale using a meter-stick. All visible fractures on the outcrops were digitally drawn in the photograph, within the predefined circle. The fracture spacing of the outcrop concerned would then be calculated by dividing the cumulative length of all drawn polylines by the area of the circle. Outcrops with background jointing were chosen to determine the fracture spacing value of a specific lithology to avoid bias from fracture zones. For the purpose of this study, structures were subdivided into joints and fracture zones. Fracture zones are linear zones of dense fracturing and joints are individual fractures without displacement (Davis & Raynolds, 1996).

4.3 Data analysis

After returning from the field the different types of data were analyzed separately. The collected data were divided to be able to tackle the three sub-questions separately, following a one-to-one comparison, and will be described separately below. A summary of the used datasets, type of analysis and products of the study is shown in Figure 9.

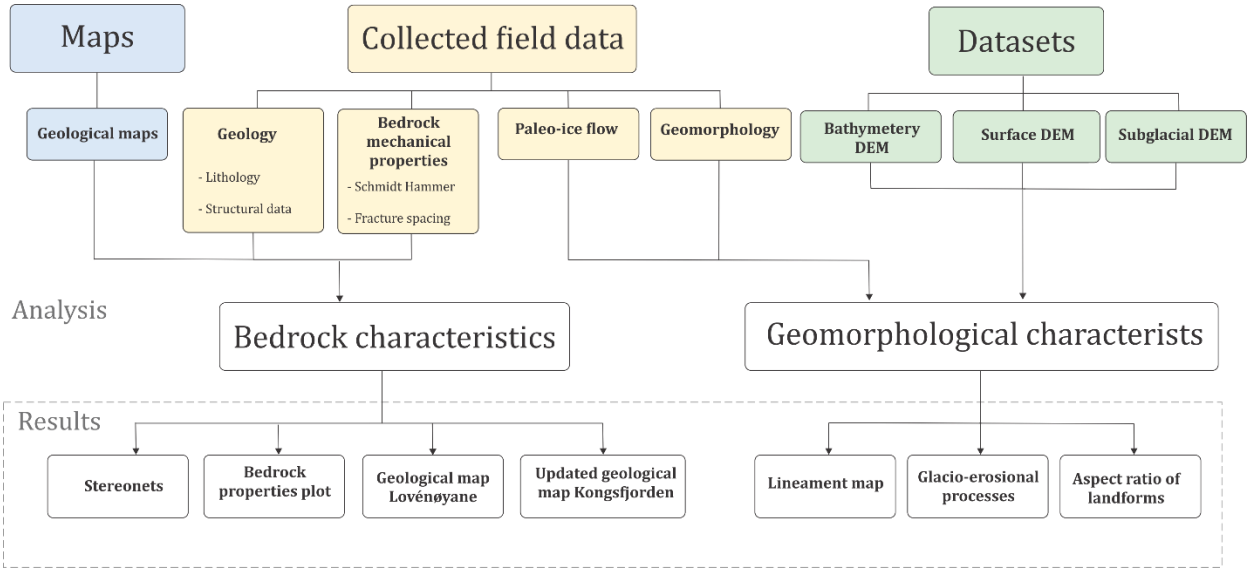

Figure 9: Summary of used datasets, type of analysis and results of the study. Arrows indicate the datasets that were used to obtain the final results (within the dashed grey box).

4.3.1 Main bedrock characteristics

The main bedrock characteristics were analyzed on basis of three different sub-sections:

i) A simple updated geological map of the Kongsfjorden area (1:100 000) was produced, using *ArcMap*, in which the spatial distribution of the different lithologies and fracture zones of the study area were highlighted. In addition, a detailed geological map of the Lovénøyane archipelago (1: 8 000) was produced highlighting the spatial variations in texture of lithologies and the distribution of fracture zones in this region. Sketches of outcrops were made for visualizing the geological configuration, using *CorelDRAW 2017*.

ii) Schmidt Hammer hardness measurements were plotted against fracture spacing to evaluate the bedrock mechanical properties of each lithology, according to Krabbendam & Glasser (2011) and Krabbendam & Bradwell (2014). A rock type with large fracture spacing and high rock hardness suggests a higher resistance to glacial erosion.

iii) Measurements of fault-slip planes, bedding and foliation of outcrops in the field were plotted and analyzed in Schmidt nets (equal area projections), using *Stereonet*. The

Schmidt net diagrams were used to differentiate fault populations within the fracture zone in Juttaholmen. This was done by first plotting all measured structural data, including fault planes and lineations, from the fracture zone into a Schmidt net. Then, clustering of fault planes and lineations were extracted and analyzed separately.

4.3.2 Main geomorphological characteristics

The main geomorphological characteristics were analyzed into two different sub-sections:

i) The classified glacio-erosional landforms described in the field were analyzed separately for each different lithology.

ii) Positive geomorphological landforms were manually digitized within the Kongsfjorden area and stored as polygon datasets. The elongation ratio for each landform was then calculated and analyzed according to their distribution. A modified version of the elongate landform method was applied, described by Phillips et al. (2010). In this study, the manually digitized landforms were stored as polygon datasets instead of line datasets to avoid geometry bias of the landforms. Therefore, the minimum bounding geometry tool from *ArcMap 10.5* was used to calculate the elongation ratio of the landforms.

iii) Four different transverse profiles were produced along Kongsfjorden. This allowed a detailed comparison to be made between the distribution of elongate landforms and underlying bedrock geology with the cross-valley morphology; in particular, the effect of topographic focusing on the elongation ratio of landforms and the effect of large-scale tectonic structures on the changes in cross-valley morphology.

The elongation ratios of the positive landforms were derived by first digitizing the foot of the landforms using a hillshade and a slope map of the Bathymetry DEM and Surface DEM. The hillshade and slope map were created in *ArcMap 10.5.* Only the landforms within Kongsfjorden beyond the LIA maximum extent were digitized to avoid bias from recent glacial activity that might have modified or covered the glacial landforms formed during the LIA. The elongation ratios of the mapped landforms were calculated using the minimum bounding geometry tool in *ArcMap 10.5*. This tool created a new shape file that is comprised of rectangles that represent the minimum geometry that fits the polygon of the landform, Figure 10. The long axis of the rectangle corresponds to the widest diameter of the polygon. The short axis corresponds to the widest diameter perpendicular to the long axis. The new shape file contained the orientation, the length

(long axis) and the width (short axis) of the minimum rectangle that fits the polygon. This information was used to calculate the elongation ratio of the landforms by dividing the length and width of the rectangle relative to paleo-ice flow. The paleo-ice flow was determined on basis of measured striations collected in the field at Lovénøyane. The mapped landforms were then divided into different assemblage zones which shared similar characteristics. The landforms of each assemblage zone were plotted in frequency diagrams according to their aspect ratio and plotted in rose diagrams according to the orientation of the long axis, relative to the course of the paleo-ice flow, using *Stereonet*.

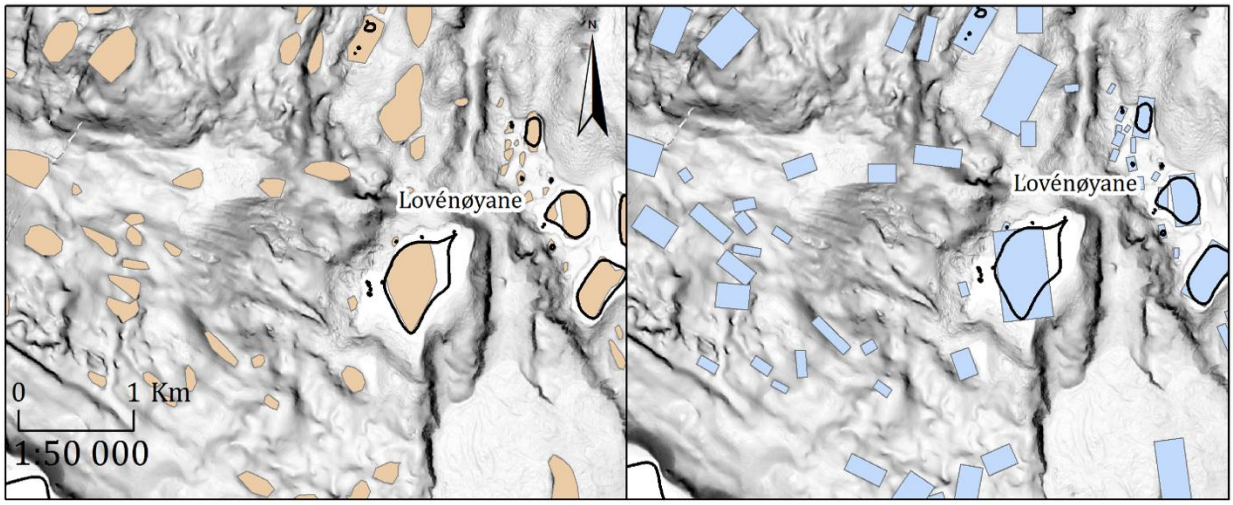

Figure 10: The map on the left indicates the digitized positive landforms (orange polygons). The map to the right presents the minimum rectangular geometry that fits the polygon (blue boxes). The attribute table of the rectangles includes length, width and orientation of each landform. Background image is a slope map of the bathymetrical DEM (Norwegian Mapping Authority Hydrographic Service, 2014). The shore line is obtained from Norwegian Polar Institute (2014b) and modified by a smoothening filter.

The transverse surface profiles were made by drawing transects for each DEM at the same location, using *ArcMap 10.5.* The parts that did not describe the surface topography, i.e. the glacier surface and the water surface, were clipped out. The elevation of the bathymetrical DEM close to shore lines or outlet glaciers are missing or unreliable due to challenges in collecting reliable data. This shortcoming of information was considered to be of minor importance considering the circumstance that transverse profiles can have a length up to 20 km long. The surface roughness was calculated by dividing the ground surface distance by the projected grid distance of each profile.

4.3.3 Linear morphological features

Distinct linear morphological features were digitized at the fjord bottom of Kongsfjorden and for this an aspect map of slopes steeper than 30° was used. The aspect map was created using the bathymetrical DEM in *ArcMap 10.5*. This method of digitizing linear morphological features is based on Indrevær and Bergh (2014), but differs from it in minor aspects. In this study, only slopes steeper than 30° were used rather than those of 5° to avoid bias from sub-glacial landforms that were formed during the LIA maximum extent, such as moraine ridges or crevasse squeeze ridges (Streuff et al., 2015). The aspect map was produced using the aspect tool in *ArcMap*, which calculates the downslope direction of each data point based on neighboring data points in a 3 x 3 (pixel) window. The linear morphological features were then identified and mapped according to this aspect map. A length weighted rose diagram was produced on basis of the mapped features. Through that the main orientations of the linear features could be determined by first assessing the geographical starting point (x1, y1) and end point (x2, y2) of each drawn polyline in an UTM grid. The angle between the two points was then calculated in the field calculator, using the following formula:

$$tan^{-1}\left((x2 - x1), (y2 - y1)\right) \times \frac{180}{\pi}. \quad (1)$$

In the attribute table the angle of each drawn polyline relative to north was obtained. By inserting the length of each polyline into the attribute table it was possible to plot the data into a length weighted rose diagram, using *MATLAB* script as developed by Puszta (2017).

5. Results

As a result, this study was able to identify (1) the main bedrock characteristics of the outcropping lithologies in the Kongsfjorden area; (2) the main geomorphological characteristics of the Kongsfjorden area; and (3) the linear morphological features at the fjord bottom of Kongsfjorden.

5.1 The main bedrock characteristics

Descriptions of the main bedrock characteristics of Kongsfjorden include:(i) the distribution of its lithologies; (ii) the mechanical properties of these lithologies; and (iii) the fracture zones cutting through these lithologies.

5.1.1 Lithologies of Kongsfjorden

The geological map of the study area, including the interpreted subsurface continuation of these lithologies, is shown in Figure 11. A profile of the bedrock geology along Kongsfjorden is shown in Figure 12. The lithologies that were visited can be subdivided into two zones: (i) Nunataks in the east-bearing basement rocks that were recently exposed, and (ii) the Lovénøyane archipelago in the west where fractured and altered marbles and red sedimentary rocks predominate. A detailed geological map of the visited field localities on Lovénøyane is presented in Figure 13.

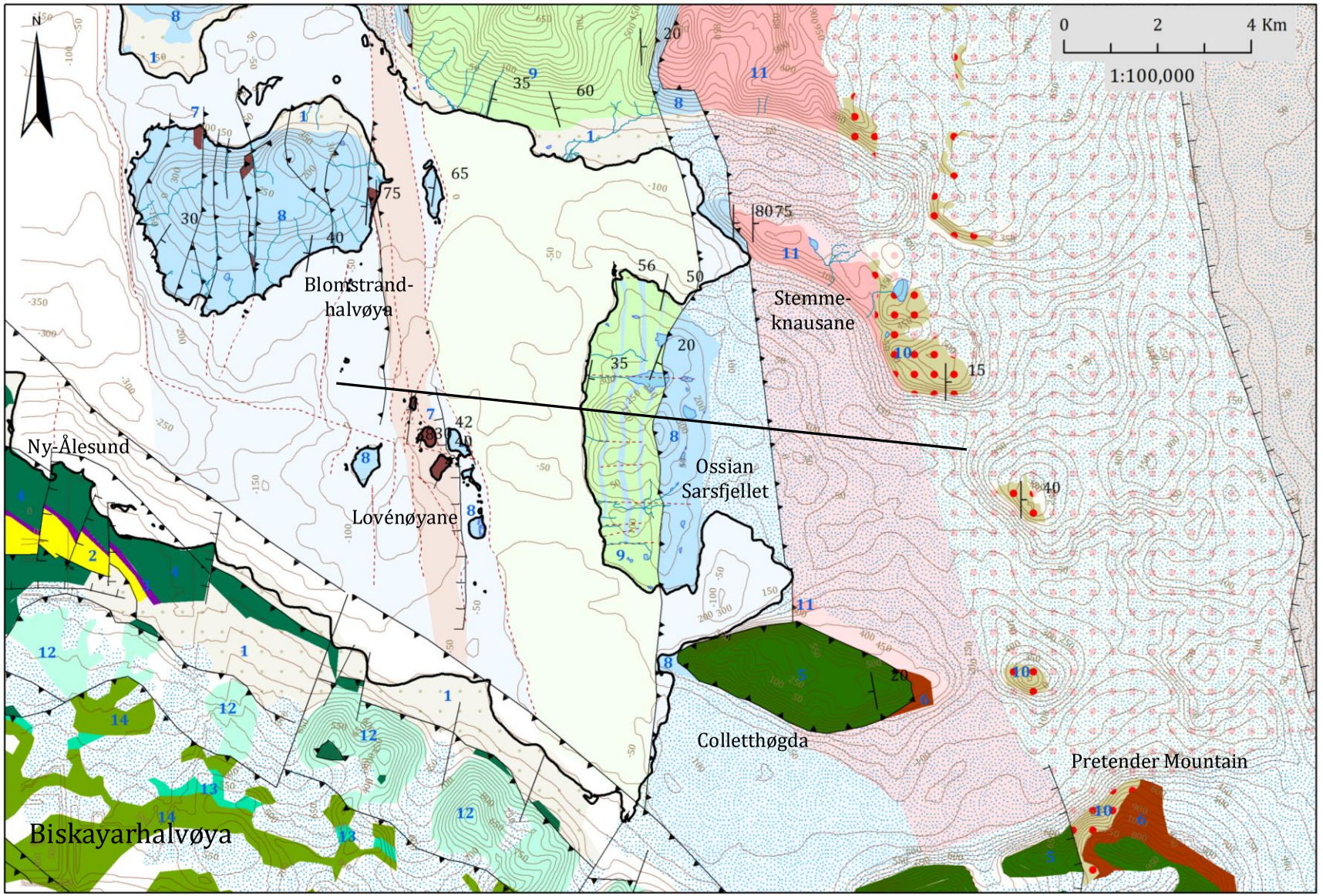
N
0
2
4 Km
1:100,000
Blomstrand-
halvøya
Stemme-
knausane
Ny-Ålesund
Ossian
Sarsfjellet
Lovénøyane
Colletthøgda
Pretender Mountain
Biskayarhalvøya

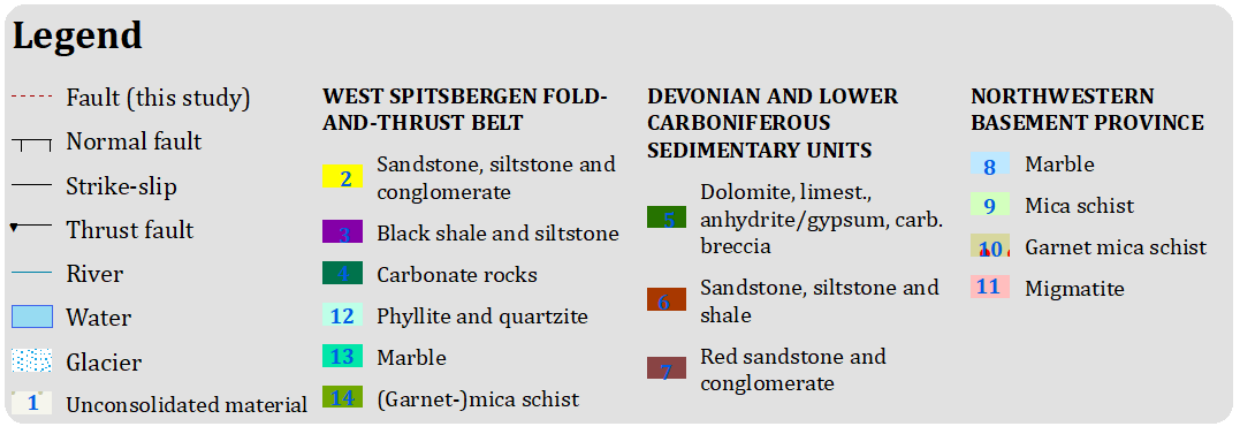

Figure 11: Updated geological map from Kongsfjorden modified on basis of Dallmann (2015). Faults (red dashed lines) and subsurface geology that are interpreted on basis of this study are added onto this geological map. Contour lines represent surface, bathymetrical and subglacial topography with 50m intervals. Transect of geological profile (Figure 12) is indicated with black line.

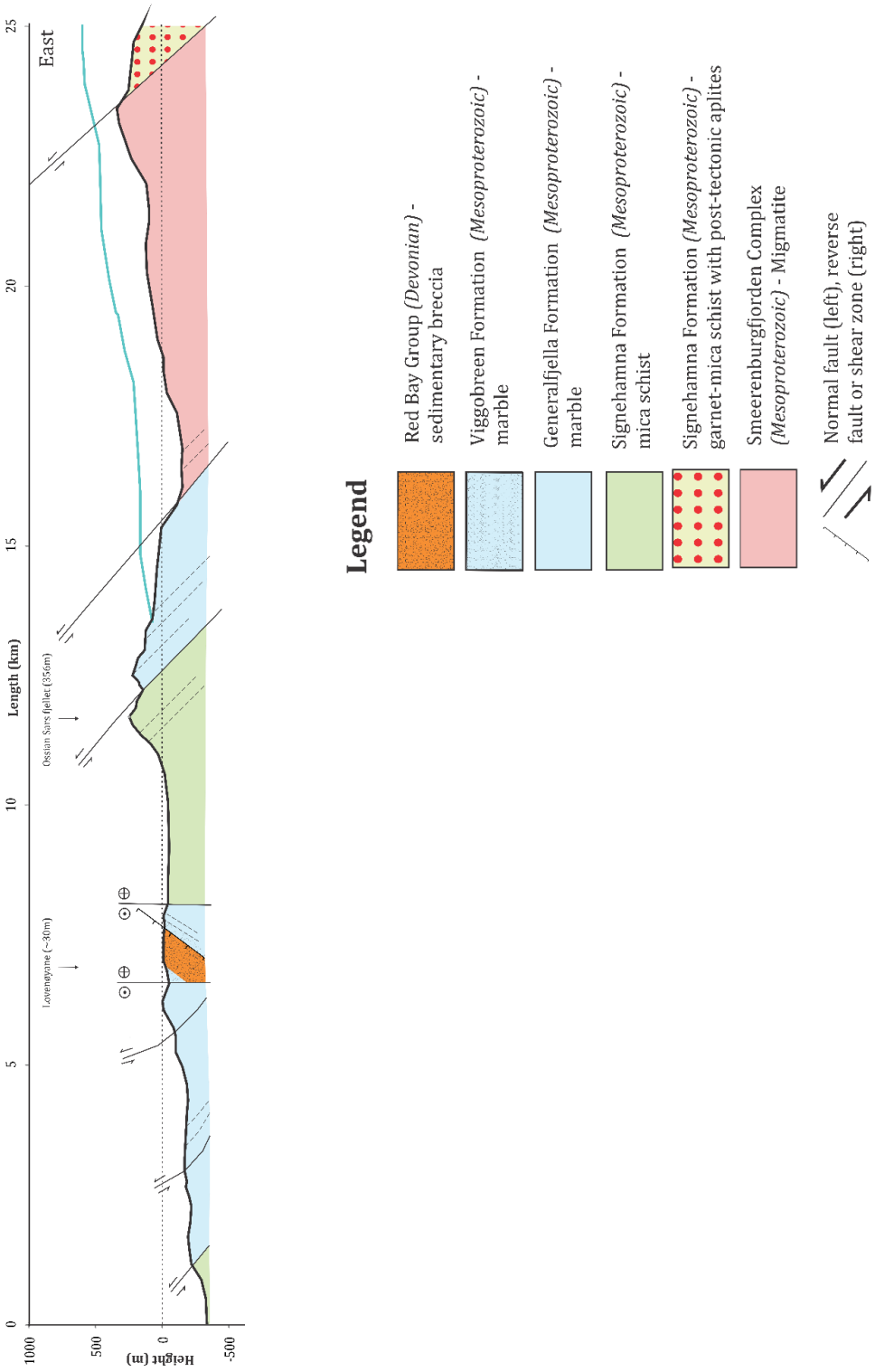

Figure 12: Profile of the bedrock geology along Kongsfjorden. geological map (Figure 11) for transect of the cross-section. Elevation is 2x vertically exaggerated.

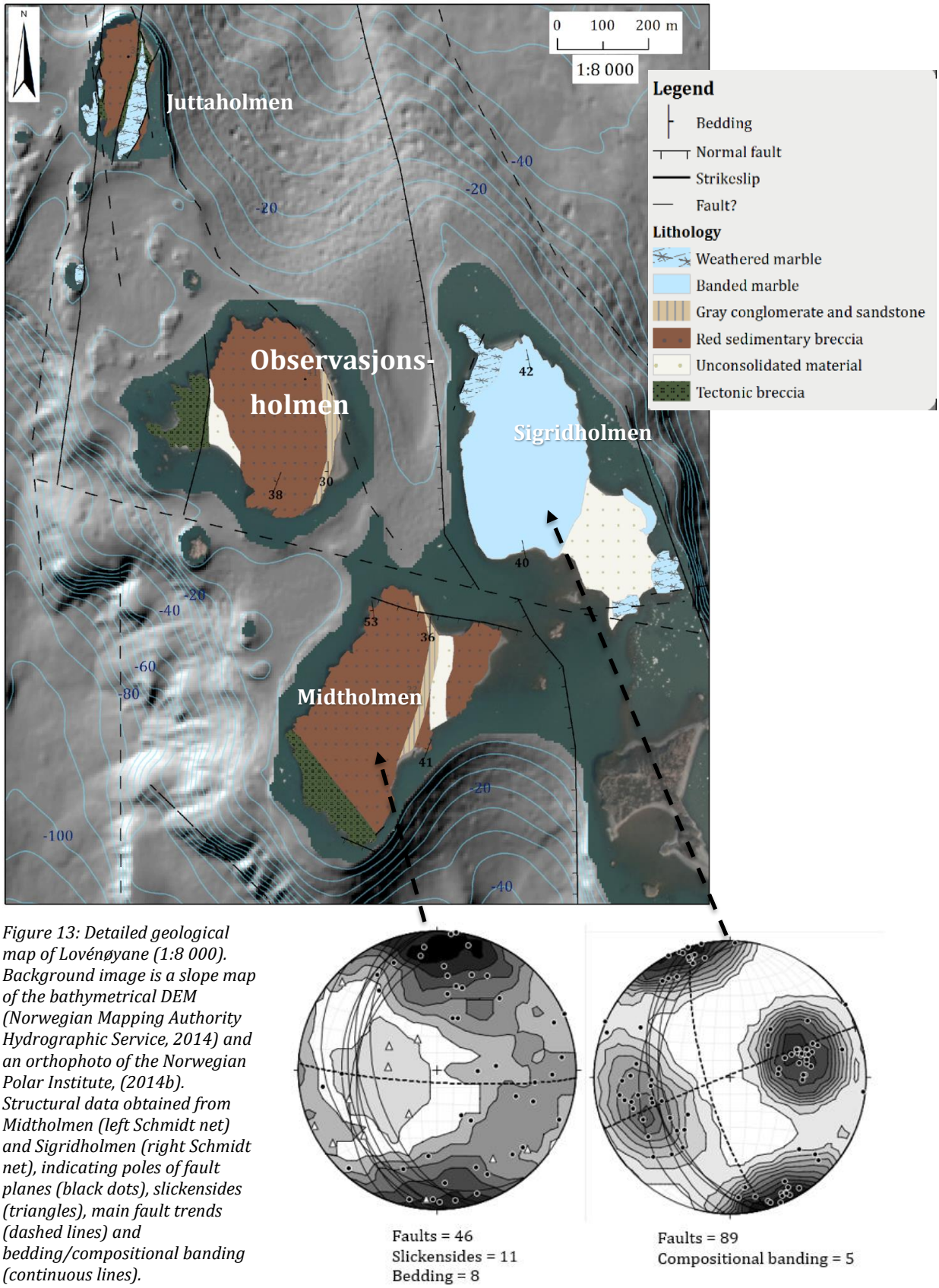

Figure 13: Detailed geological map of Lovénøyane (1:8 000). Background image is a slope map of the bathymetrical DEM (Norwegian Mapping Authority Hydrographic Service, 2014) and an orthophoto of the Norwegian Polar Institute, (2014b). Structural data obtained from Midtholmen (left Schmidt net) and Sigridholmen (right Schmidt net), indicating poles of fault planes (black dots), slickensides (triangles), main fault trends (dashed lines) and bedding/compositional banding (continuous lines).

Red sedimentary rocks

The red sedimentary rocks from the Red Bay Group (Old Red Sandstones) were described at different locations in the Lovénøyane archipelago, such as on the islands Juttaholmen, Observasjonsholmen and Midtholmen. Such sedimentary rocks are typically bedded and consist predominantly of 20m thick layers of clast-supported breccia, altered by thin sandy layers (<0.5m), Figure 14A. The bedding is dipping about 40° towards the west, Figure 13. The breccia has a silty to sandy reddish-brown matrix with angular marble clasts (and sporadically phyllite clasts). The size of the clasts ranges between 0.2cm and 20cm and the majority of them are of a size of about 5cm. Within the breccia layer, pressure solution stylolites can be found, located parallel to the bedding, Figure 14B. The sandy layers are remarkably red with grain size ranging from silt to coarse sand, Figure 14A. The base of the sedimentary sequence on Observasjonsholmen consists of a 15m thick sequence of m scale bedded grey-yellowish conglomerate, sandstone and silt (cf., Figure 14C and Figure 15). The gray conglomerate is composed of predominantly rounded marble clasts of up to 5cm in length. The sequence is coarsening upwards, whereas the individual layers *within* this sequence are fining upwards. Some of the layers contained trough cross-bedding dipping towards the north, indicating that the stratigraphy is not inverted (Figure 14D). At several locations calcite veins of about 1cm in width and up to 20cm in length could be found cross-cutting the red sedimentary breccia striking E-W, Figure 14D.

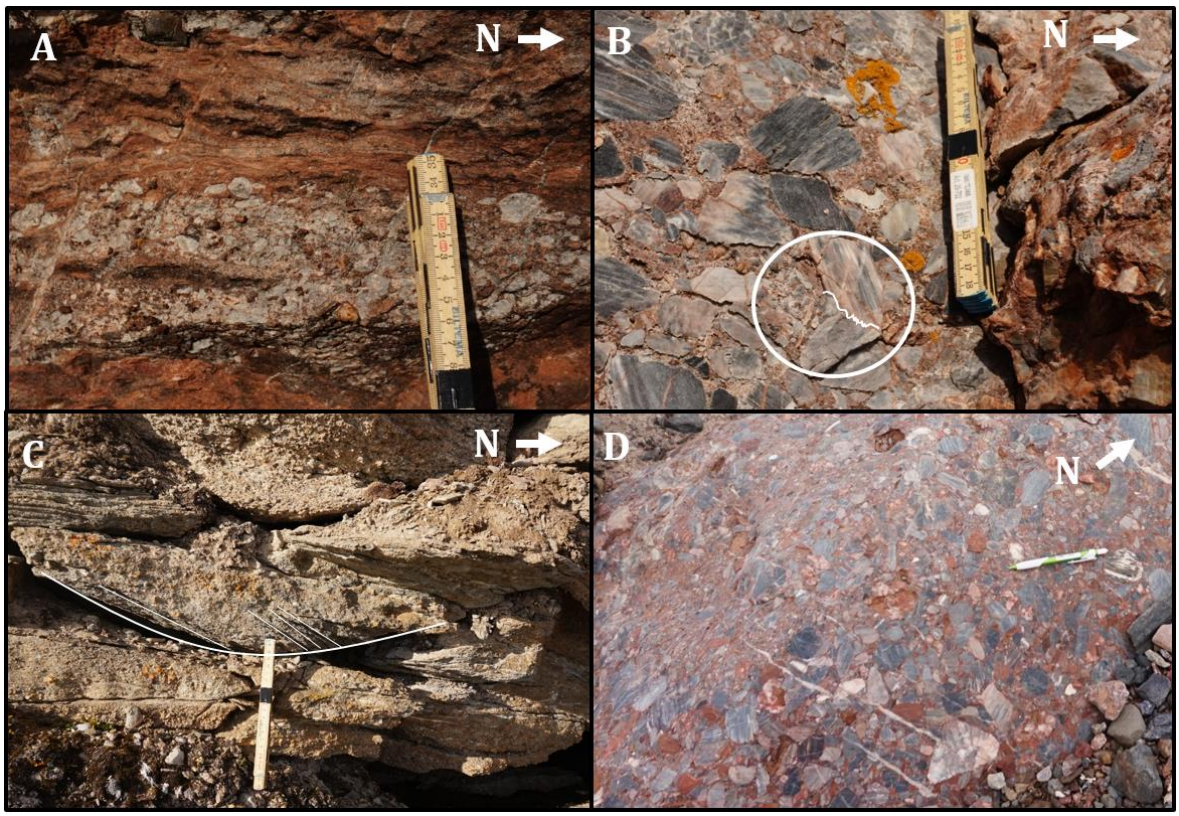

Figure 14 : (A) Red silt to coarse sandy layer altering with clast supported breccia. (B) Sedimentary breccia with stylolites parallel to bedding. Note the angularity of the marble clasts. (C) Trough cross-bedding in the grey-yellowish conglomerate and sandstones. (D) E-W striking calcite veins on a polished surface at Midtholmen.

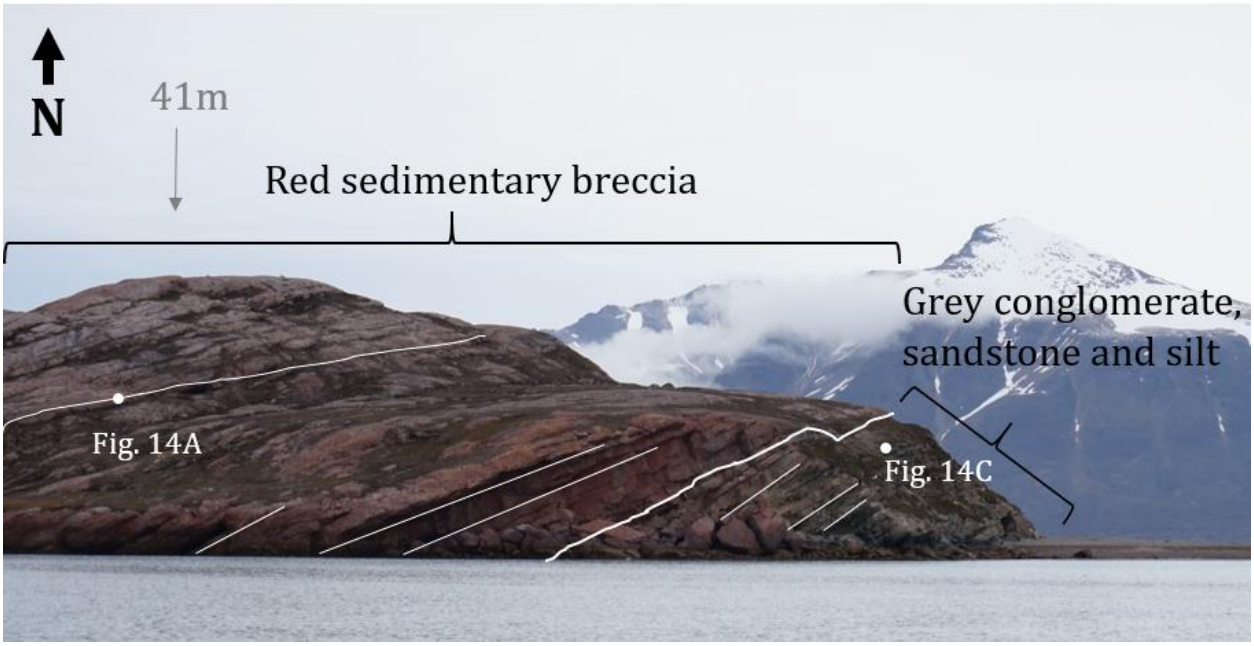

Figure 15: View looking from the north of Midtholmen towards the south of Observasjonsholmen. The base of the sedimentary rocks consists of grey conglomerate and the top consists of altering sedimentary breccia with thin sandy layers (<0.5m). White lines indicate bedding. Note the polished surface at the top and the rugged slopes at the side of the hill. Paleo-ice flow is from right to left.

Marbles

Marbles from the Generalfjella formation, dispersed throughout the study area, were described at several locations. However, the characteristics of the marbles differ significantly from each other. In the east, i.e. on Ossian Sarsfjellet and on Stemmeknausane, the marbles are predominantly composed of composite-banded marble with some calk-silicate inclusions, Figure 31A. At the Lovénøyane archipelago, i.e. on Sigridholmen and Juttaholmen, the marbles are mostly altered and brecciated and only partly composed of composite banded marbles, Figure 16A. These altered marbles have different bedrock characteristics such as a red stain brecciated with red matrix, and a laminated very fine grained green-greyish carbonate, Figure 16 (B, C and D, respectively). These characteristics are in accordance with descriptions of the Viggobreen formation by Thiedig & Manby (1992) and Piepjohn (2000).

The contact interfaces between the marbles and the red sedimentary rocks are characterized by fracture zones, which are well exposed on Juttaholmen. The compositional banding within the marbles strikes N-S and dips 40° towards the west on Sigridholmen, similar to the bedding of the red sedimentary rocks (Figure 13). On Ossian Sarsfjellet and on Stemmeknausane the marbles dip about 60° towards the east.

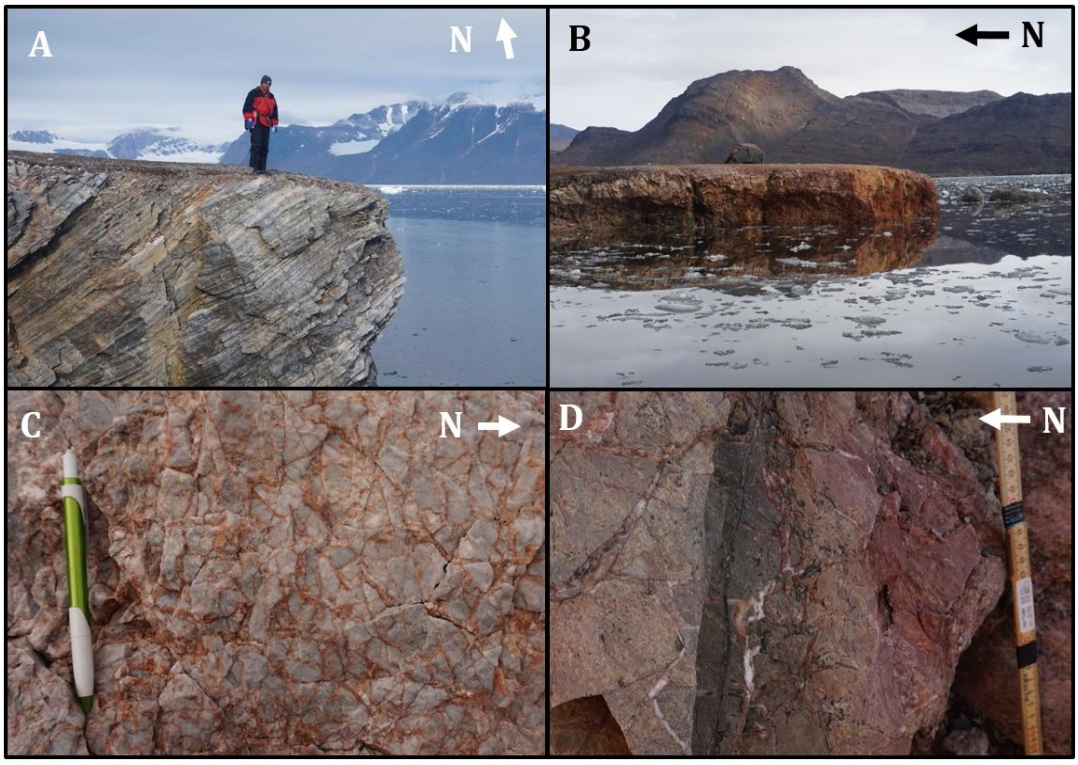

Figure 16: Different lithological occurrences of marble: (A) Compositional banding on Sigridholmen; (B) Red staining on Sigridholmen; (C) Brecciated marble on Juttaholmen; and (D) Grey-green, very fine grained, laminated carbonate, with calcite veins.

Quartz mica-schist, phyllite and quartzite

Quartz mica-schist, which alters with bands of phyllite and quartzite from the Signehamna formation, was described on Ossian Sarsfjellet. At Ossian Sarsfjellet quartz mica-schist occurs in two different forms: one weakly foliated, well-polished form interlayered with quartzite bands and phyllite (found at the western part of Ossian Sarsfjellet), and one densely foliated mylonite form (found at the eastern part of Ossian Sarsfjellet, close to the contact with the marble), Figure 17 (A and B). The composition of the mica-schist changes when moving between eastern and western direction. In the west, the mica-schist is dominated by muscovite and chlorite altering quartzite bands. In the east, the mica schist is dominated by biotite. In all outcrops quartzite lenses are found in the mica-schist, of up to 10cm in length. The foliation of the mica-schist is generally trending N-S and is dipping 60° towards the east. At some localities on the eastern part of Ossian Sarsfjellet, the mica-schist appeared to have a linear rather than planar fabric. The linear fabric plunges slightly towards the south. The quartz mica-schist occurred in bands altered by 5m wide foliated yellowish-brown quartzite. The foliation of the quartzite trends N-S, parallel to the quartz mica-schist

foliation, and has a foliation spacing of about 10cm, Figure 18. The tectonic lineations on the foliation planes are sub-horizontal.

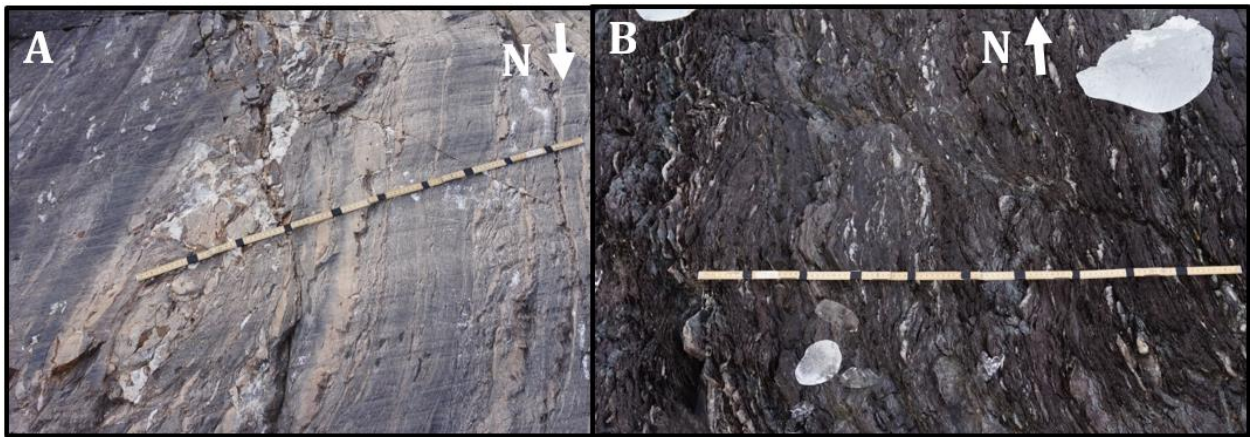

Figure 17: (A) Quartz mica-schist and phyllite at the western margin of Ossian Sarsfjellet with weak foliation. Note the polished and striated surface; (B) Strongly foliated quartz mica-schist close to the contact with the marble at the eastern end of Ossian Sarsfjellet. Note the absence of striations on the strongly foliated quartz mica-schist.

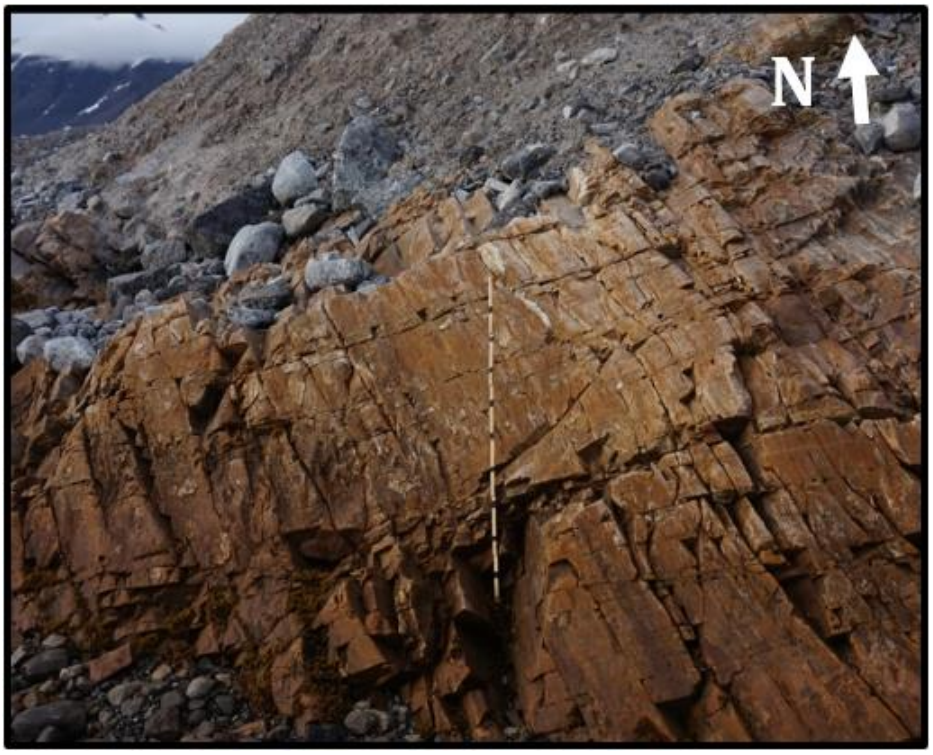

Figure 18: Quartzite at Ossian Sarsfjellet. Note the angular bedrock surface and foliation spacing of 10cm.

Migmatites

Migmatites from the Smeerenburgfjorden complex occur on Colletthøgda and Stemmeknausane, close to the present glacier margin, see Figure 11. At both localities, the migmatites are zoned in diatexite and metatexite. Diatexite is a variety of migmatites where all the pre-migmatization structures are destroyed, resulting in homogenization of the texture (the darker and lighter parts merge into one another). Metatexite describes a variety of migmatites containing structures that survived the partial melting. This, in its turn, resulted in discrete light-colored areas (leucosomes) and darker areas (melanosomes)(Fettes & Desmons, 2007). The diatexite migmatite are distributed close to the western section of the migmatite, near to the contact zone with the marbles, Figure 19A, and the metatexite migmatite are distributed towards the east, Figure 19B, about 200m distance from the contact. The contact itself, at both locations, is covered with subglacial debris. The diatexite migmatite has a biotite schistosity texture, Figure 19A, with muscovite grains on the foliation plains and includes tourmaline crystals in black melt pockets. The foliation is N-S oriented and dips around 60° towards the east. The mineral assemblage of the metatexite includes lecosomes consisting of quartz, plagioclase, K-feldspar, cordiorite and silliminite and melanosomes consisting of garnet, biotite schist with quartz lenses.

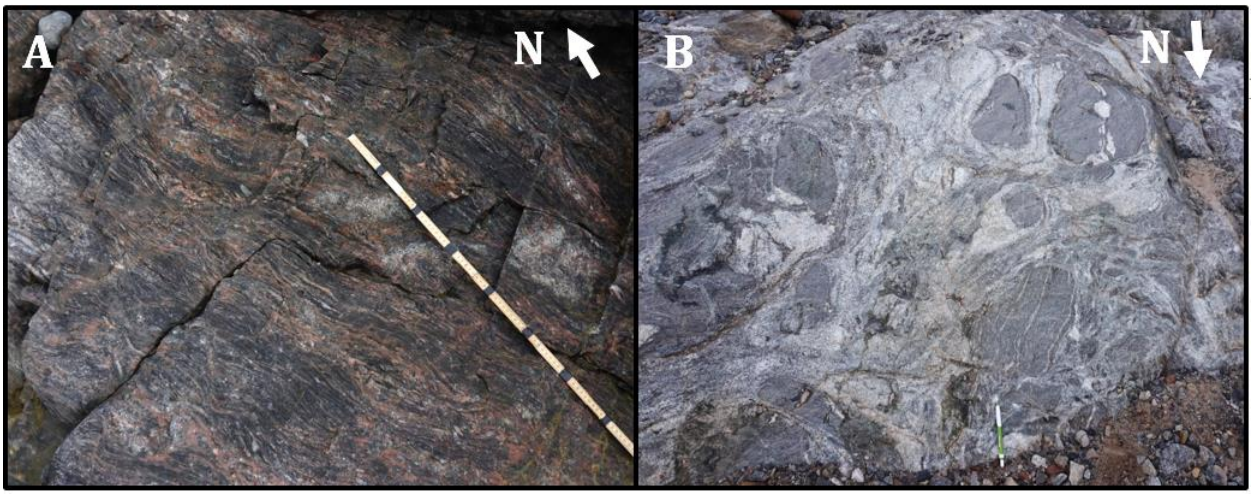

Figure 19: (A) Diatexite migmatite close to the contact zone with the marbles at Stemmeknausane. Note the N-S oriented foliation. (B) Metatexite migmatites including melanosomes and leucosomes found in further distance from the western contact of the migmatite at Colletthøgda. Note the polished surface and absence of joints and foliation.

5.1.2 Bedrock mechanical properties in Kongsfjorden

The bedrock mechanical properties of the different lithologies within the Kongsfjorden area are summarized in Table 2. The measured fracture spacing is plotted against Schmidt Hammer hardness (Q) in Figure 20. Figures used for deriving fracture spacing values for each lithology are shown in Figure 21.

The measured Schmidt Hammer hardness values, i.e. indicating the intact rock strength, range between 50 and 80Q. The rocks with highest intact rock strength are the 'massive' rocks without significant mechanical anisotropy, e.g. quartzites and migmatites. The rocks with the lowest intact rock strength – i.e. altered marbles, sedimentary breccias and mylonite quartz mica-schists – have a strong mechanical anisotropy (a large number of non-uniform discontinuities). This strong mechanical anisotropy can either be attributed to dense foliation in the quartz mica-schists or to the numerous of (minor) discontinuities within the sedimentary breccias and altered marbles.

The fracture spacing values, indicating rock mass strength, vary between 0.01 to 2.1m. The rocks with the lowest fracture spacing (between 0.01 and 0.1m) are predominantly situated close to fracture zones or structural contacts, such as mylonite quartz mica-schist on Ossian Sarsfjellet and brecciated marbles and sedimentary rocks on Lovénøyane. Rocks with the highest fracture spacing (> 0.1m) are situated at some distance from the fracture zones, examples of which are migmatites on Colletthøgda and marbles on Stemmeknausane. The wide range of intact rock strength and rock mass strength of the altered marble, found both on Sigridholmen and Juttaholmen, can be attributed to the fact that the Viggobreen marbles come in different altered forms with each their own mechanical properties.

Bedrock Properties

Lithology	Setting	Circle area: A (m^2)	Total length fractures: L (m)	Fracture Spacing: A/L (m)	Fracture density: L/A (m^{-1})	Hardness (Q)	Locality	GPS
Migmatite A	Background jointing	4.4	16.0	0.278	3.6	78.83 ± 0.83	085	78.910 N 12.650 E
Migmatite B	Background jointing	4.4	6.4	0.699	1.4	78.83 ± 0.83	085	78.910 N 12.650 E
Migmatite C	Background jointing	6.0	2.1	2.056	0.5	78.83 ± 0.83	085	78.910 N 12.650 E
Marble	Background jointing	0.9	3.8	0.225	4.4	67.37 ± 1.30	091	78.976 N 12.586 E
Quartz mica-schist	Background jointing	1.0	8.6	0.116	8.6	74.75 ± 0.65	026	78.969 N 12.464 E
Quartz mica-schist	Mylonite zone	0.4	59.2	0.007	149.0	59.77 ± 1.90	033	78.967 N 12.511 E
Quartzite	Background jointing	3.5	24.9	0.142	7.0	80.35 ± 0.88	027	78.969 N 12.465 E
Sedimentary breccia	Background jointing	5.2	26.1	0.201	5.0	52.42 ± 2.22	005	78.937 N 12.285 E
Tectonic breccia	Fracture zone	1.1	15.8	0.059 ± 0.013	16.9	47.1 ± 3.8	010	78.943 N 12.253 E
Marble	Altered and brecciated	1.0	21.7	0.035 ± 0.01	28.6	61.40 ± 2.35	007	78.943 N 12.250 E
Marble	Strongly altered	0.7	3.5	0.168 ± 0.039	6.0	23.0 ± 5.4	010	78.943 N 12.253 E

Table 2: Bedrock hardness, joint and fracture density data of lithologies visited in the field localities within the Kongsfjorden area.

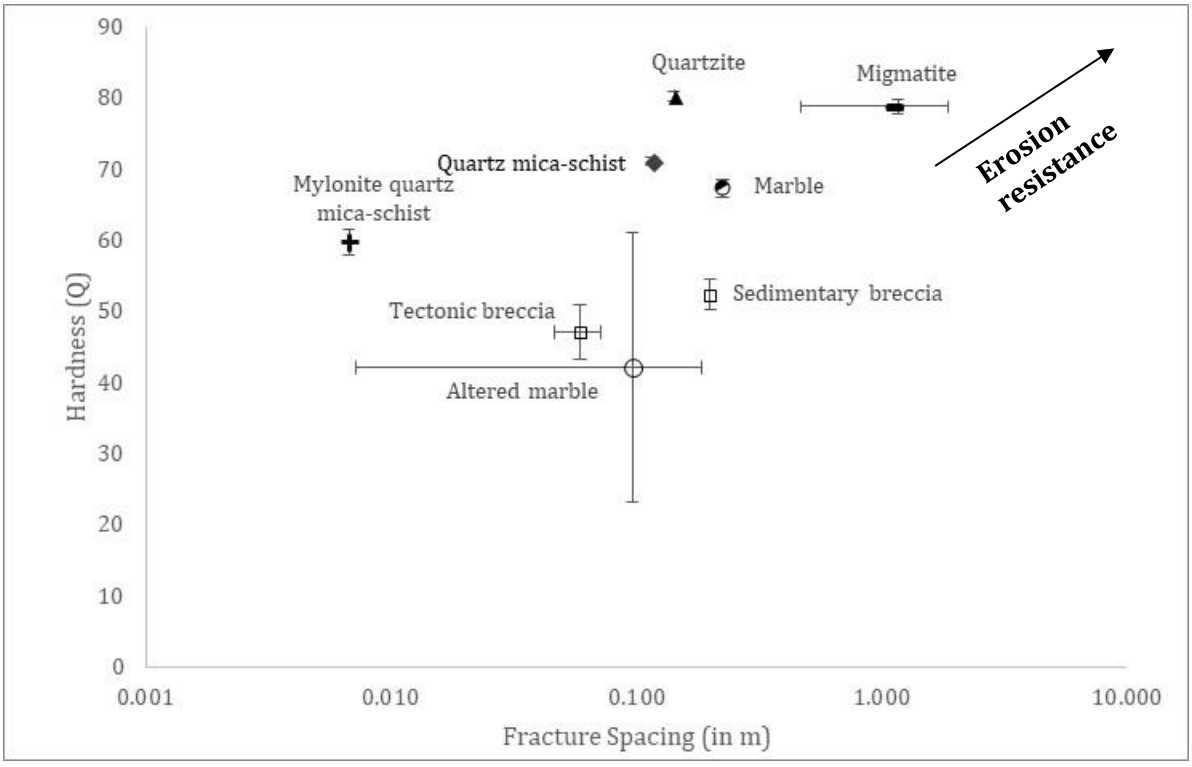

Figure 20: Bedrock mechanical properties of the different lithologies shown in Table 2. Rock hardness represents intact rock strength measured using the Schmidt Hammer. Fracture spacing represents rock mass strength determined by the 'circle inventory method' using field photographs of rock outcrops, Figure 21. The black markers are lithologies from the Northwest Basement Province situated in the east, while the white markers are lithologies distributed at Lovénøyane in the west, Figure 11 and Figure 13.

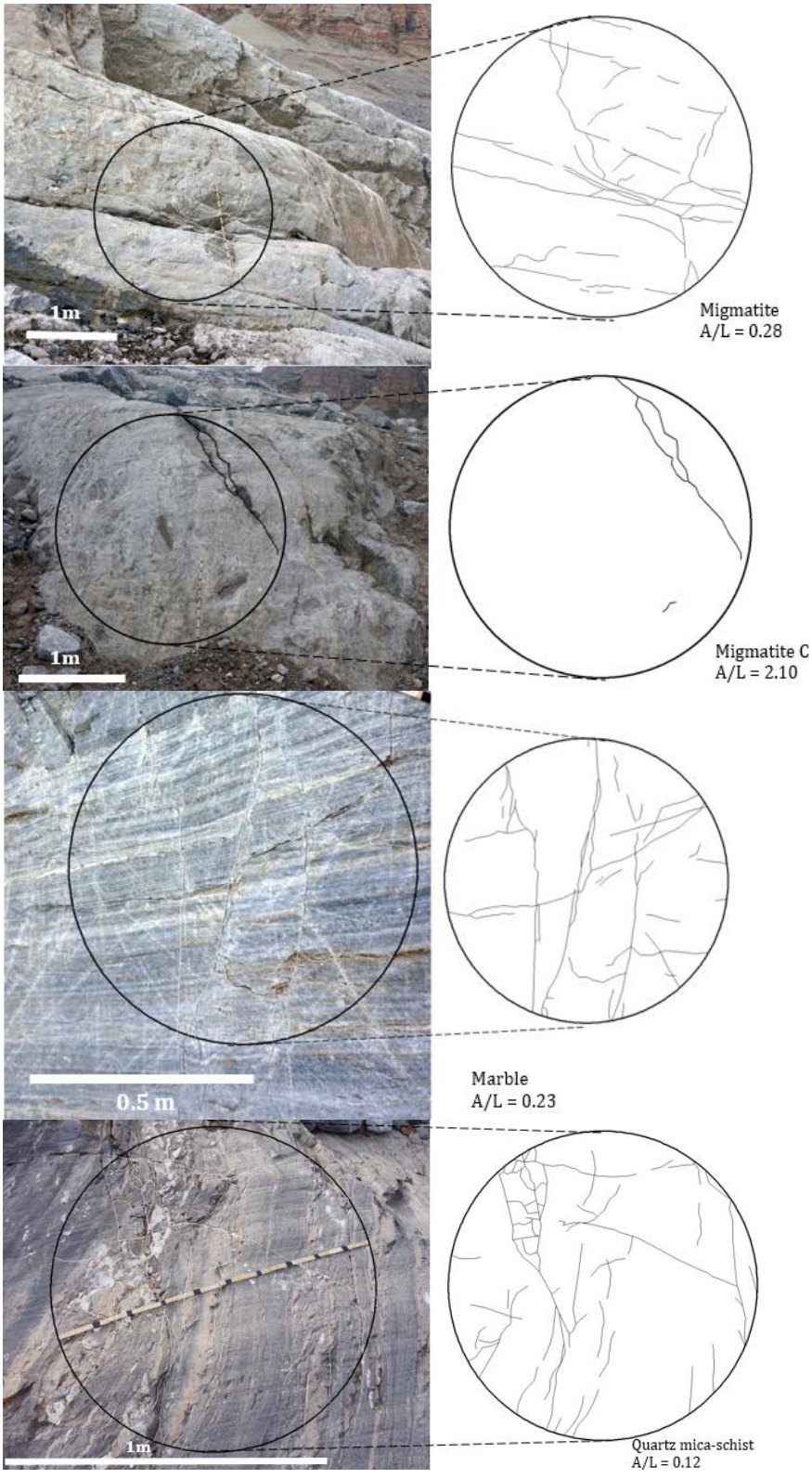
1m
Migmatite
A/L = 0.28
1m
Migmatite C
A/L = 2.10
0.5 m
Marble
A/L = 0.23
1m
Quartz mica-schist
A/L = 0.12

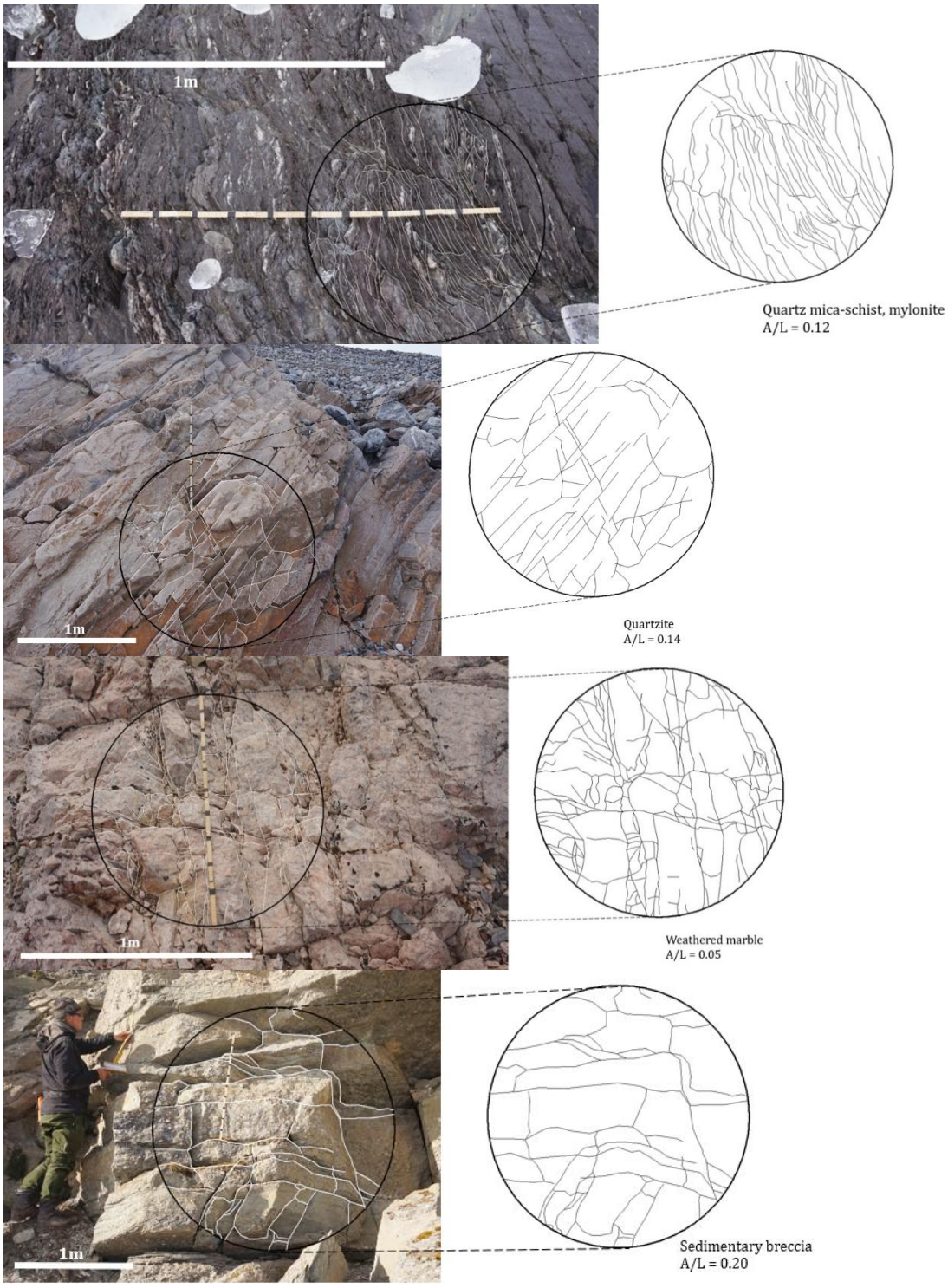

Figure 21: Photos of outcrops of various lithologies visited in the field within the Kongsfjorden area. Right of the photographs indicates the digitized fractures within the predefined area (black circle) for each lithology with the subsequent fracture spacing (A/L).

There is no clear difference in fracture spacing between basement rocks assessed at the nunataks in the east (black markers) and rocks assessed on the Lovénøyane archipelago (white markers). However, there is a difference in fracture spacing between lithologies distributed near to or at fault lines, and lithologies distributed at a distance from them. The tectonic breccia, for example, has a much lower fracture spacing (~0.06m) than sedimentary breccia (~ 0.2m). Furthermore, the basement rocks are predominantly plotted towards the upper right corner of the graph, reflecting a higher erosion resistance relative to the lithologies distributed at the Lovénøyane archipelago.

5.1.3 Fracture zones on Juttaholmen

On Juttaholmen, three different fracture zones were identified. On these, the marbles of the Generalfjella formation are juxtaposed against, and situated on top of, the sedimentary breccia of the Red Bay Group, Figure 22. Two of the fracture zones mark the contact between the two formations at the eastern and western edge of the island and both strike NNW - SSE. The eastern fracture zone is about 5m wide and is composed of unconsolidated grey to black schist with larger marble fragments. The faults are shallow and dip towards the west. The slickenside on the fault planes indicates predominant normal displacement. The western fracture zone is about 7m wide and dips nearly vertical. Slickensides on the fault planes of the western fracture zone indicate predominantly sinistral strike-slip displacement.

The central fracture zone cuts straight through the long axis at the center part of the island, Figure 13 and Figure 22. The central fracture zone is N-S oriented and about 20m wide. The fracture zone is well exposed and is therefore described in more detail. Within the central fracture zone five different units were recognized, Figure 23 (A and B). All units are bound by major fault planes and will be described separately below.

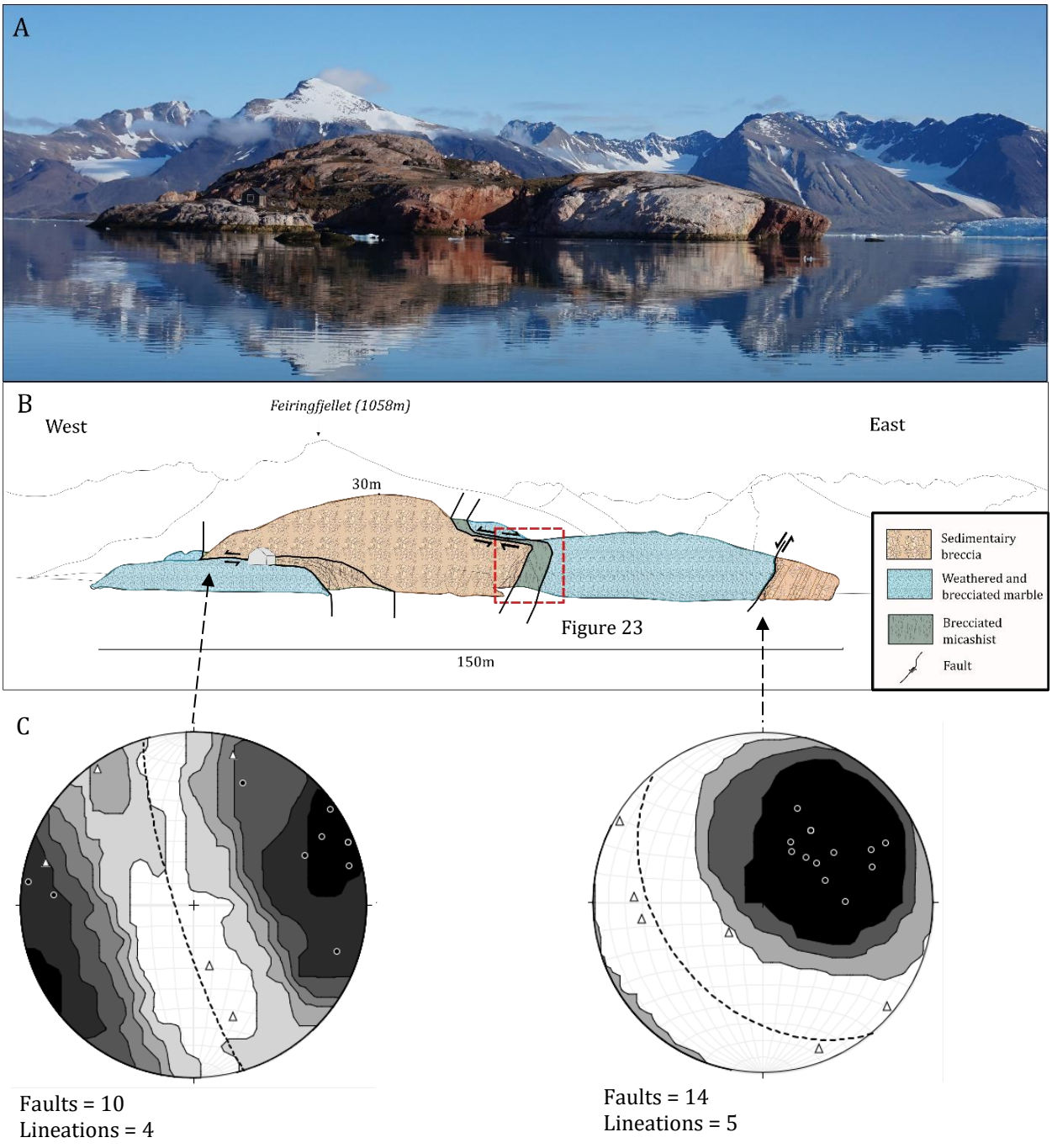

Figure 22: (A) Image of Juttaholmen, view towards the north. (B) Sketch on basis of the photograph showing the cross-sectional configuration of the interpreted fault movements. The red box indicates the location of Figure 23. (C) This graph indicates stereoplots of the western (left) and eastern (right) fracture zone, which show contour intervals of the poles to fault planes (black dots); the main fault orientation (dashed black line; and the lineations (white triangles). The western fracture zone is characterized by nearly vertical N-S oriented strike-slip faults. The eastern fracture zone, on its turn, is characterized by high angle normal and strike-slip displacement.

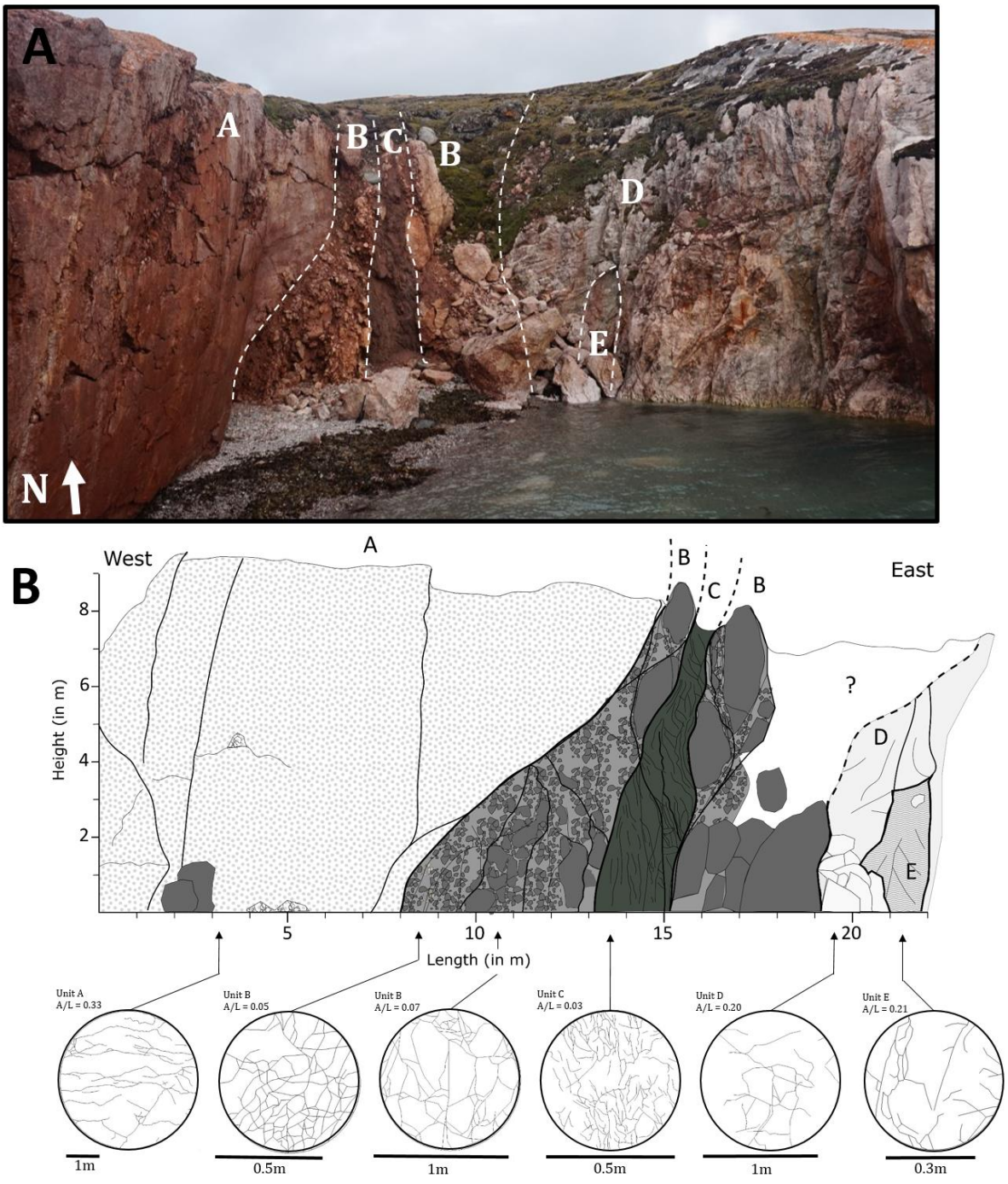

Figure 23: (A) Central fracture zone at Juttaholmen indicating the different units, cf. Figure 22 for geographical location. B) Sketch of the central fracture zone, including the major faults (black lines) and fracture spacing measurements of the different units. The bedrock properties of each unit are summarized in Table 3.

Unit A is about 8m thick at the base and 9m high. It is a clast-supported breccia with angular to rounded grey and white marble clasts, between 2mm and 5cm in length. The matrix is composed of reddish silt varying to very fine sand. The exposed surface of Unit A, shown in Figure 23A, represents a fault plane covered with numerous grooves and slickensides, Figure 24 (A and B). The slickensides indicate sinistral movement with two different plunge directions; one dipping 20 degrees towards the south and the other dipping 40 degrees towards the south, Figure 24A.

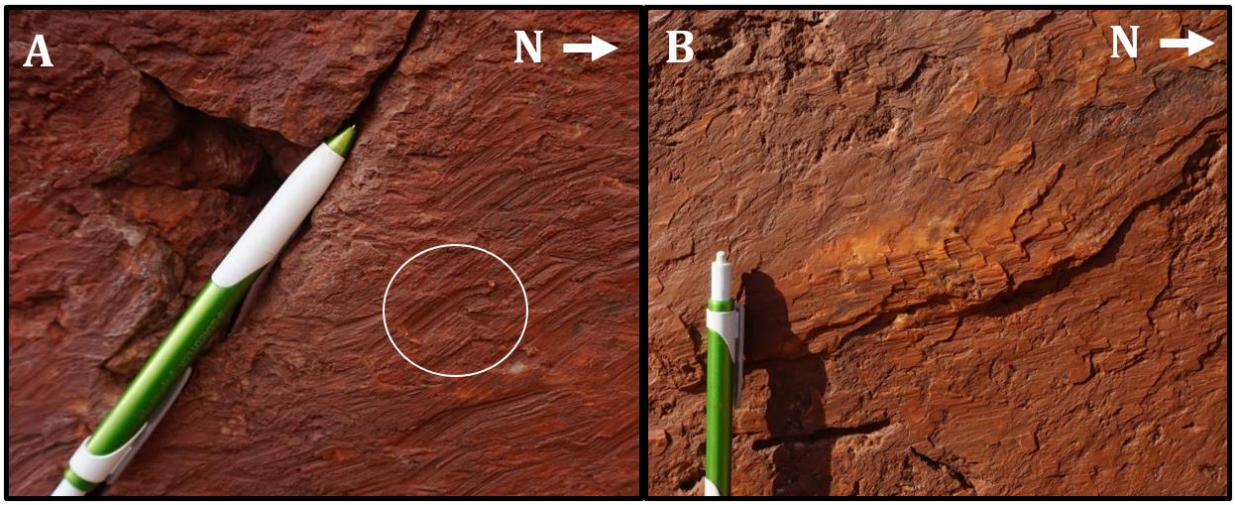

Figure 24: (A) Grooves with two different plunges with trailed grain (indicated by the white circle). (B) Indications of crystal fibers growth. Note that the kinematic indicators in both images indicate sinistral displacement.

Unit B is characterized as a more brecciated version of Unit A situated on either side of Unit C. The western section is well exposed and stretches about 5m wide at the base to only 1m at the top. The eastern section is about 4 m wide and is largely covered by unconsolidated debris or covered by soil. Unit B has a similar composition as Unit A, i.e. clast-supported breccia with red stained fine matrix. However, the variability in clast size is larger and the clasts are more angular. The size of the marble clasts within Unit B average between 5 to 30cm but can be up to 1m in length (Figure 25B). Most of the fractures within this unit seem to follow the grain boundary around the clasts. Calcite mineralization and slickensides are distributed on those grain boundaries as well. The slickensides indicate predominant sinistral displacement.

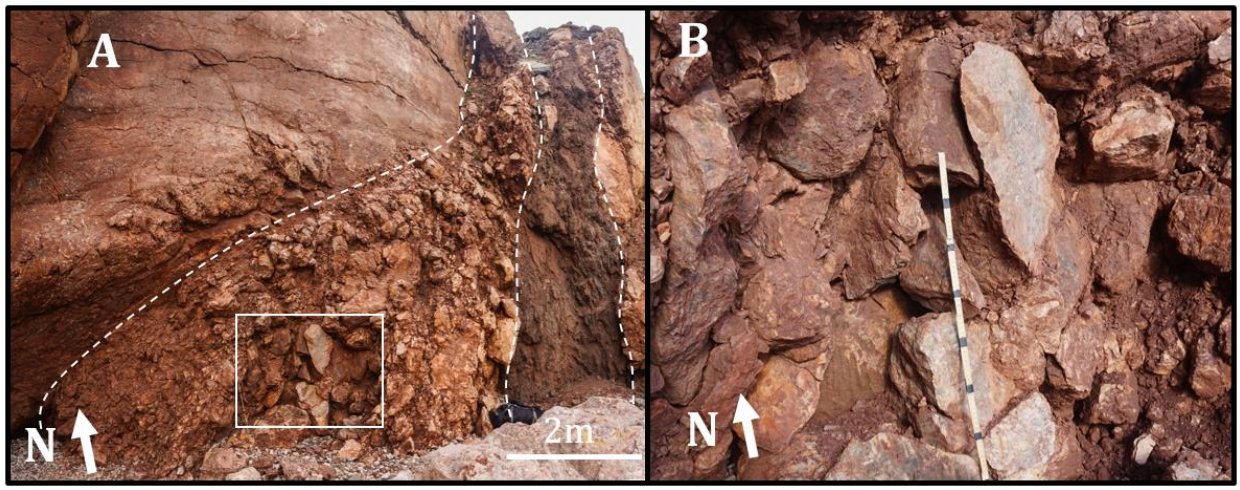

Figure 25: (A) Overview of Unit B showing the variability in clast size throughout the unit. (B) is a detail image of (A) indicated with the white box. (B) Detailed image of Unit C indicating very angular marble clasts and fractures following the grain boundary.

Unit C is a 2m thick dark section of brecciated material mostly composed of dark green, brown and black mica schist as well as some marble fragments. The average clasts size of the mica schist is about 0.5cm and does not exceed 2cm. This unit is heavily brecciated, Figure 26 (A and B). Most of the faults within Unit C strike into the exposed surface, which makes it difficult to measure the structural characteristics of each individual fault plane.

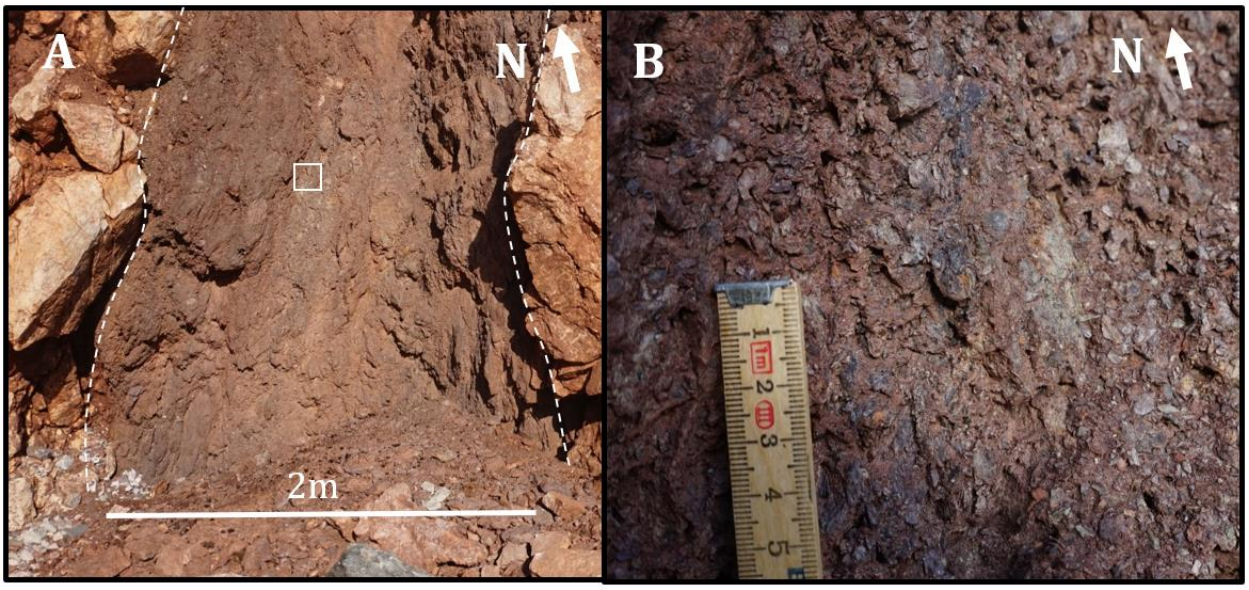

Figure 26: (A) Overview of Unit C. The white box marks the extent of B. Note that the majority of the fractures strike into the exposed surface. (B) Detail of Unit C indicating brecciated green-brown-black mica schist. Note the small size of the clasts.

Unit D marks the eastern boundary of the fracture zone and continues 30m towards the east in the direction of the eastern fracture zone in Juttaholmen (Figure 22A). Unit D is composed of altered marble which is characterized by consolidated white brecciated marbles in a red silty matrix, Figure 27A. Unit D has a more massive texture than both Unit B and Unit C.

Unit E is situated within Unit D and is about 1m wide and 4m high. The composition of the unit is characterized by very fine green and red laminated carbonates cut by cm scale calcite veins (Figure 27B). The contact between Unit D and Unit E is characterized by fault planes on all sides (Figure 27C). The concave direction of the crescent marks towards the north suggest dextral displacement according to Petit (1987), Figure 27C. The texture visible in both Unit E and Unit D can be interpreted as indications of altered marbles from the Viggobreen formation although they represent different alternation forms.

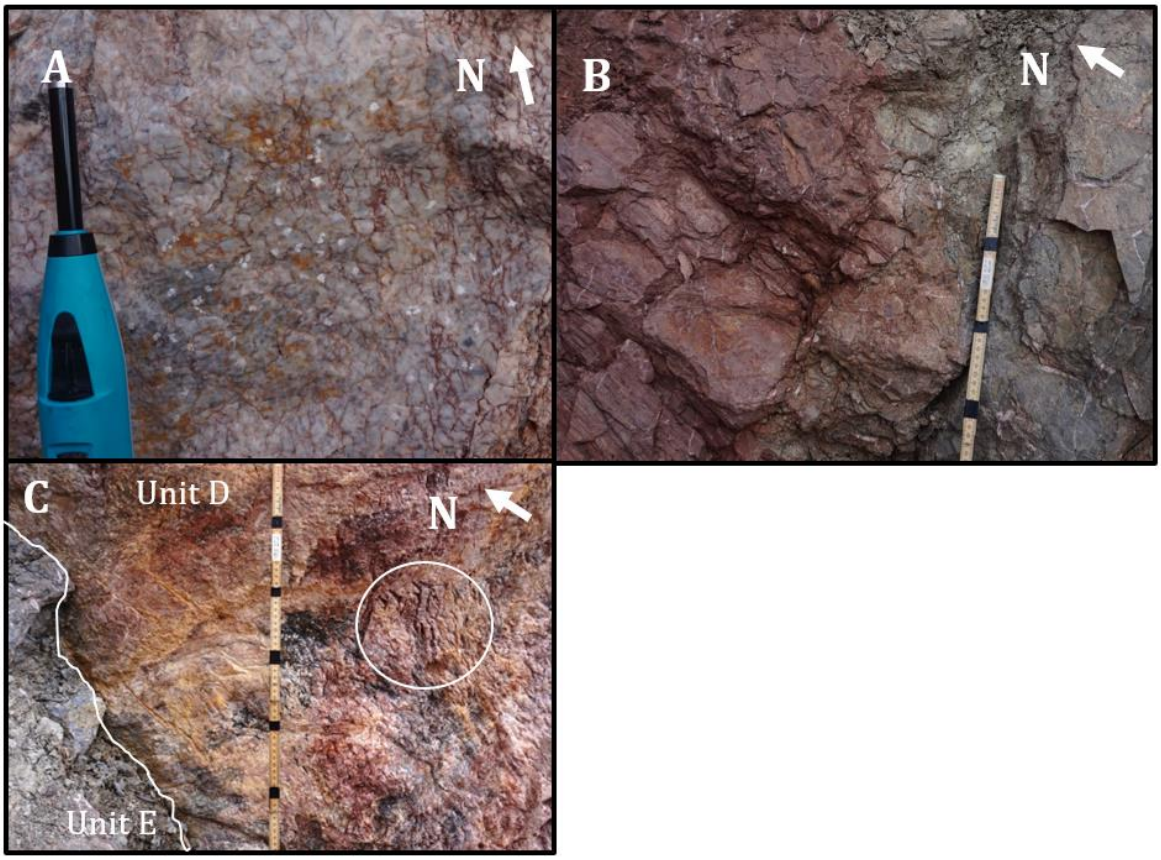

Figure 27: (A) Altered marble of Unit D with the Schmidt Hammer for scale (the piston is about 2cm wide). Note the white brecciated marble in red silty matrix. (B) Unit E composed of fine grained green-grey and red-laminated carbonate. Note calcite veins cutting the laminated carbonate rock. (C) The area of contact between Unit E and Unit D along a fault plane. Crescent marks are highlighted by the white circle, these suggest dextral displacement.

Bedrock mechanical properties of fracture zone

The mechanical properties of each unit are listed in Table 3 and plotted in Figure 28. The units with the highest erosion resistance – i.e. the rocks with the highest rock hardness (Q) and largest fracture spacing – are the units marking the eastern and western boundary of the fracture zone (unit D and unit A, respectively). Unit C has the lowest erosion resistance with an internal rock strength of 21 Q and a fracture spacing of 0.031m. Despite the fact that the variation of erosion resistance of the different units is quite substantial, the surface expression of the fault zone at the top of the island is hardly visible. The only topographical expression of the fault zone can be identified as the bay at the southern tip of Juttaholmen, Figure 8B.

Fracture zone Juttaholmen

78.943 °N 12.253 °E

Unit	Circle area: A (m^2)	Total length fractures: L (m)	Fracture spacing: A/L (m)	Fracture density L/A (m^{-1})	Hardness (Q)
A	11.9	35.9	0.266 ± 0.066	3.8	62.5 ± 3.1
B	1.1	15.8	0.059 ± 0.013	1.7	47.1 ± 3.8
C	0.3	9.6	0.031	32.3	21.8 ± 6.2
D	1.8	9.0	0.266 ± 0.068	0.4	67.5 ± 1.4
E	0.7	3.5	0.168 ± 0.039	6.0	23.0 ± 5.4

Table 3: Bedrock mechanical properties of the different units within the central fracture zone at Juttaholmen.

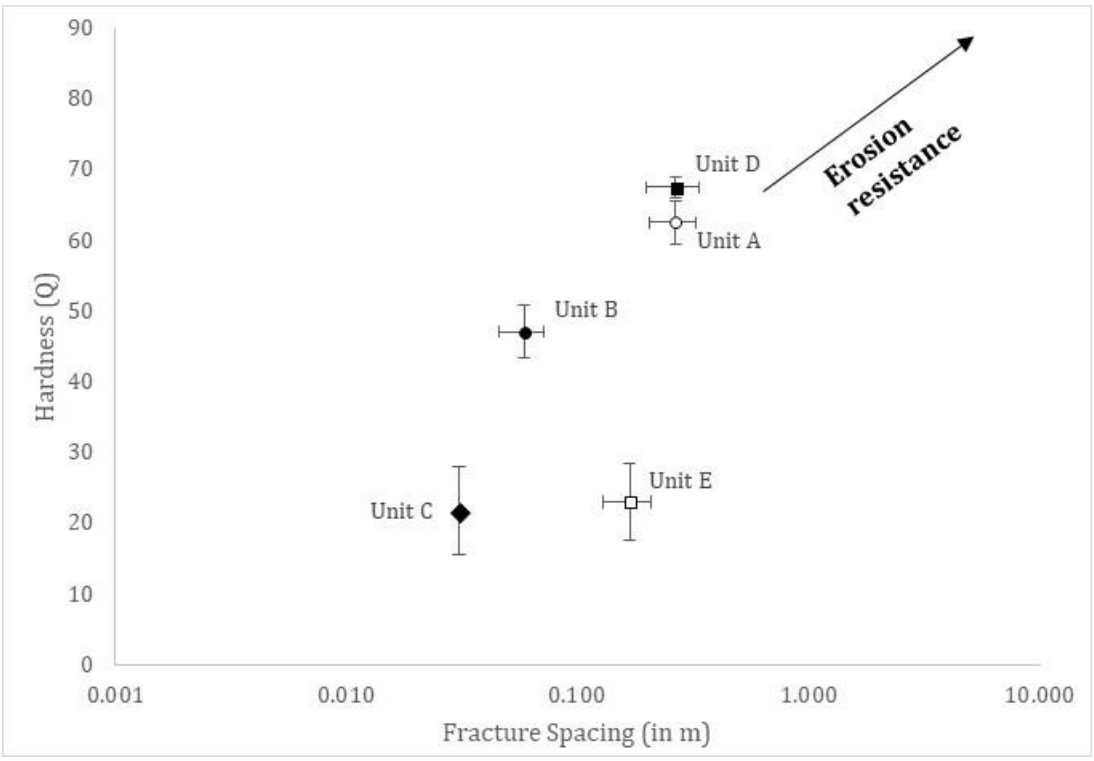

Figure 28: Bedrock mechanical properties of different units within the central fracture zone on Juttaholmen. Note that units at the center of the fracture zone have a lower erosion resistance than rocks located towards its margin.

Structural data of central fracture zone

All the measured fault planes of the fracture zone are plotted in Figure 29A. Four different clusters of fault planes can be recognized, based on the contour lines of the poles of the fault planes (black dots). The four clusters represent two different fault populations which are extracted and plotted in Figure 29 (B and C). The majority of the measured fault planes can be categorized into one of the two fault populations (139 out of 180). The faults of Figure 29B are near vertical and are predominantly striking NE-SW. The faults at Figure 29C are also near vertical, yet these are predominantly striking N-S.

All the measured striations on the fault planes are plotted in Figure 29D. Three different clusters can be recognized based on the contours of the plotted striations (hollow triangles). The three clusters represent three different fault populations which are extracted and plotted in Figure 29 (E, F and G). Nearly all of the measured striations can be categorized into one of the three fault populations (67 out of 75). The faults corresponding with the striations in Figure 29E comprise of nearly vertical faults striking NE-SW, similar to the faults plotted in Figure 29B. Nearly all of the striations in Figure 26E plunge towards the SW between 10° and 40°, suggesting strike-slip displacement with a slight dipping component. The kinematic indicators along these fault planes indicate predominantly sinistral displacement with some dextral displacement, Figure 24 (A and B) and Figure 27C. These faults are defined as fault population A. The faults corresponding with the striations plotted in Figure 29F include nearly vertical faults striking NNW-SSE, similar to what is represented in Figure 29C. The striations are slightly more spread out than the striations presented in Figure 29E, but the majority are shallowly plunging towards the north and towards the south, suggesting strike-slip displacement. The kinematic indicators along these fault planes indicate predominantly sinistral displacement. These faults are defined as fault population B. The faults related to the striations plotted in Figure 29G include nearly vertical faults striking E-W. All the striations plunge towards the east between 20° and 30°. The kinematic indicators suggest a predominantly dextral displacement. These faults are defined as fault population C.

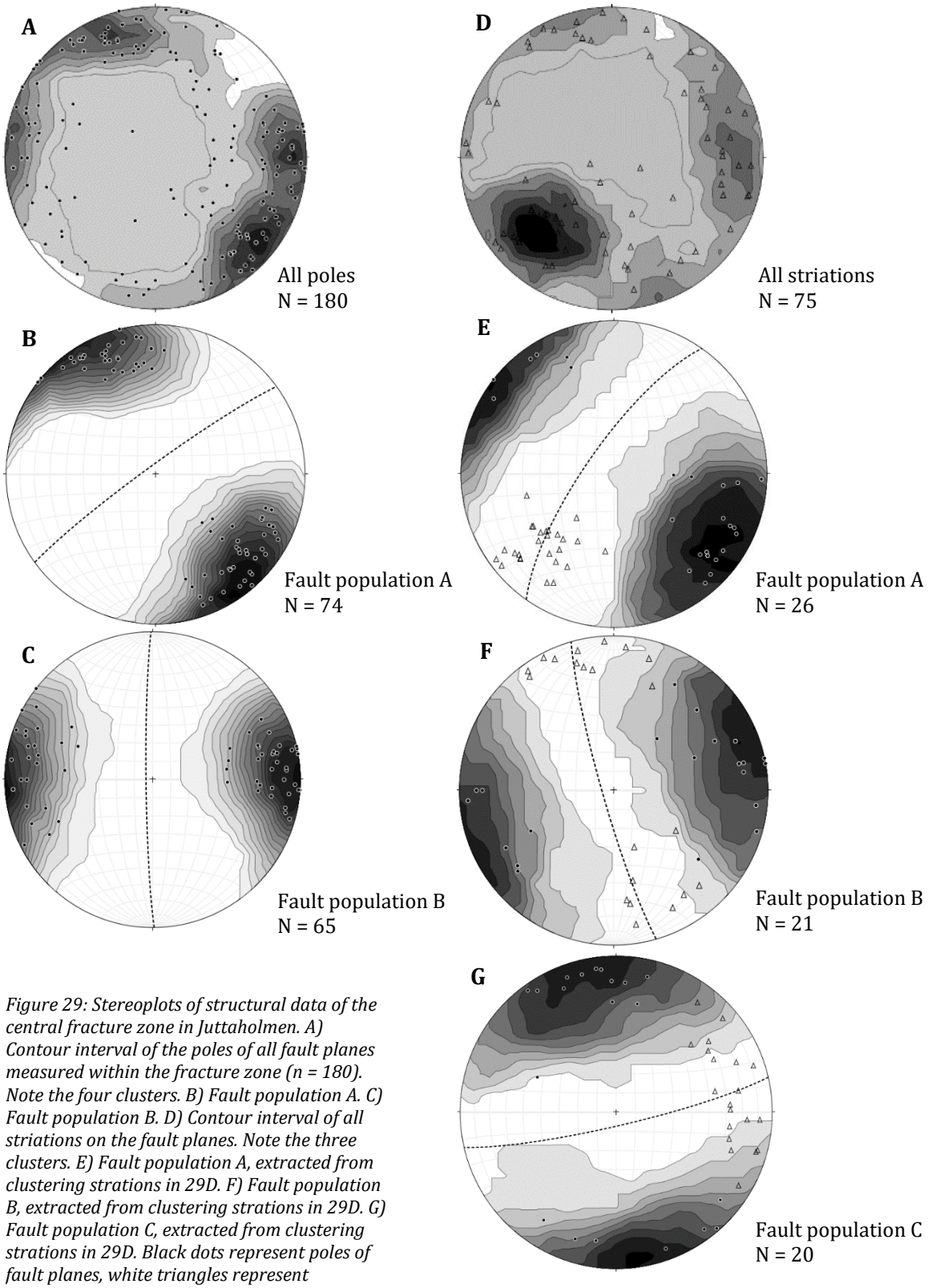

Figure 29: Stereoplots of structural data of the central fracture zone in Juttaholmen. A) Contour interval of the poles of all fault planes measured within the fracture zone (n = 180). Note the four clusters. B) Fault population A. C) Fault population B. D) Contour interval of all striations on the fault planes. Note the three clusters. E) Fault population A, extracted from clustering strations in 29D. F) Fault population B, extracted from clustering strations in 29D. G) Fault population C, extracted from clustering strations in 29D. Black dots represent poles of fault planes, white triangles represent striations and black dashed line represents main fault orientation.

5.2 The main geomorphological characteristics

The description of the main geomorphological characteristics provided below includes i) glacio-erosional landforms on outcrop scale; ii) elongation ratio of landforms on regional scale; and iii) transverse surface profiles of Kongsfjorden.

5.2.1 Glacio-erosional landforms for each lithology

Red Bay Group

The glacial-erosional landforms within the Red Bay Group include both polished and quarried surfaces. Striations are found only sporadically on top of abraded rocks. Remarkable is that only the marble clasts within the sedimentary breccia are striated, Figure 30B. Only the upper surface of rocks are polished, leaving the sides of the rock outcrops to be rather rough, Figure 30A. The polished upper surfaces are mostly distributed within the sedimentary breccia where distinct bedding is present. Close to faults, or at the fracture zones, the breccia is rather rough and does not have a polished upper surface. Moreover, the morphology of the islands within Lovénøyane at large appears to be smoother at the upper surface, whereas the sides tend to be a bit rougher with signs of rock falls along cliffs, Figure 15 and Figure 22A.

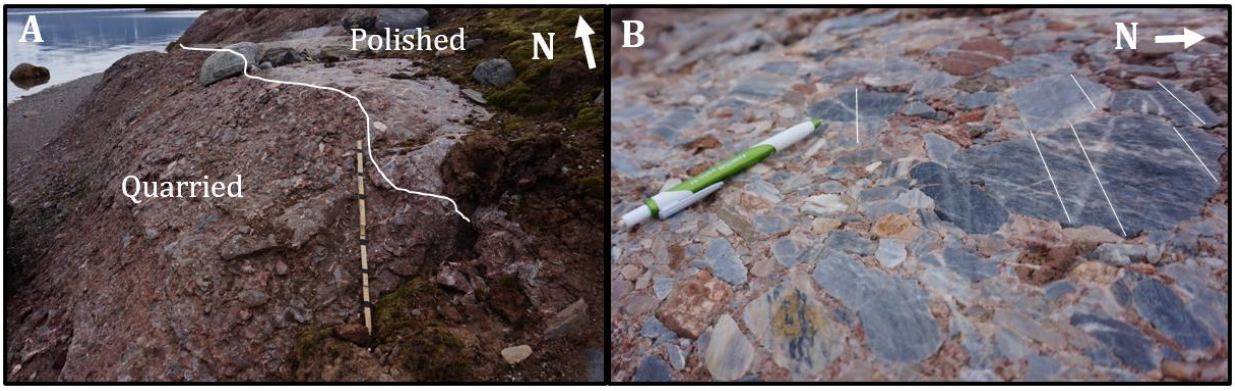

Figure 30: (A) Polished and quarried surfaces within the red sandstones. (B) Polished surface of the Red Bay Group; note that the striations (white lines) are only visible on the marble clasts.

Generalfjella formation

The glacio-erosional landforms within the Generalfjella formation vary throughout the area. The marbles at Lovénøyane are in most cases rough and quarried with some polished surfaces, Figure 31 (C and D). The overall surface morphology of the island is quite flat. Most of the surfaces were covered by post-glacial soil (Figure 16). The marbles observed on Ossian Sarsfjellet and Stemmeknausane were covered by glaciers during the Little Ice Age. These marbles have only recently been exposed to the surface which has resulted in a much higher preservation potential of glacio-erosional landforms. For this reason, the outcrops on Ossian Sarsfjellet and Stemmeknausane are heavily striated along with locally quarried faces, predominantly coinciding with joints, Figure 31B. Additional landforms within these freshly exposed marbles include micro crag-and-tails on Ossian Sarsfjellet. These micro crag-and-tails are about 1 m long and consist of a resistant calk-silicate nodule at the ice-proximal side protecting the marble at the lee-side.

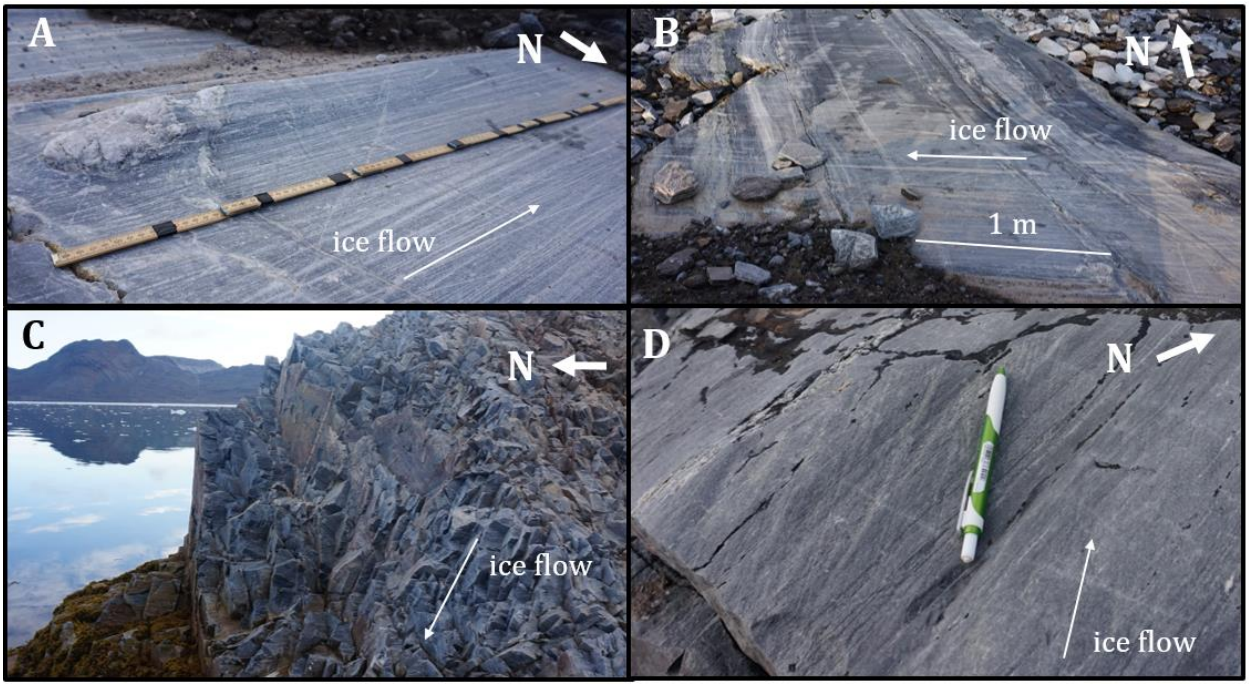

Figure 31: A) Micro crag-and-tail of about 1 m long at Ossian Sarsfjellet. The calk-silicate nodule on the left (proximal) end of the feature protects the marble on the right (distal) end of the feature. B) Polished marble on Ossian Sarsfjellet. C) Quarried rock surfaces at Sigridholmen, Lovénøyane. D) Polished surface including striations close to the shore at Sigridholmen.

Signehamna formation

The glacio-erosional landforms visible within the Signehamna formations vary with the lithology. The quartz mica-schist is dominated by polished surfaces, including some stoss-and-lee side landforms (Figure 32A) whereas the foliated quartzite has only quarried surfaces (Figure 18 and Figure 32B). Striations are present on the weakly foliated quartz mica-schist and on the quartzite, interlayered within the mica-schist (Figure 32B and 32D, respectively). There are no striations present on the strongly foliated quartz mica-schist (Figure 17B). Furthermore, stoss-and-lee side landforms, interpreted as roches moutonnées, are only present in the more weakly foliated quartz mica-schist at distance from the contact with the marbles. The quarried surfaces within the quartzite correspond with the foliation spacing, suggesting that the size of the blocks, quarried by the ice, did not exceed the foliation spacing (5-10cm).

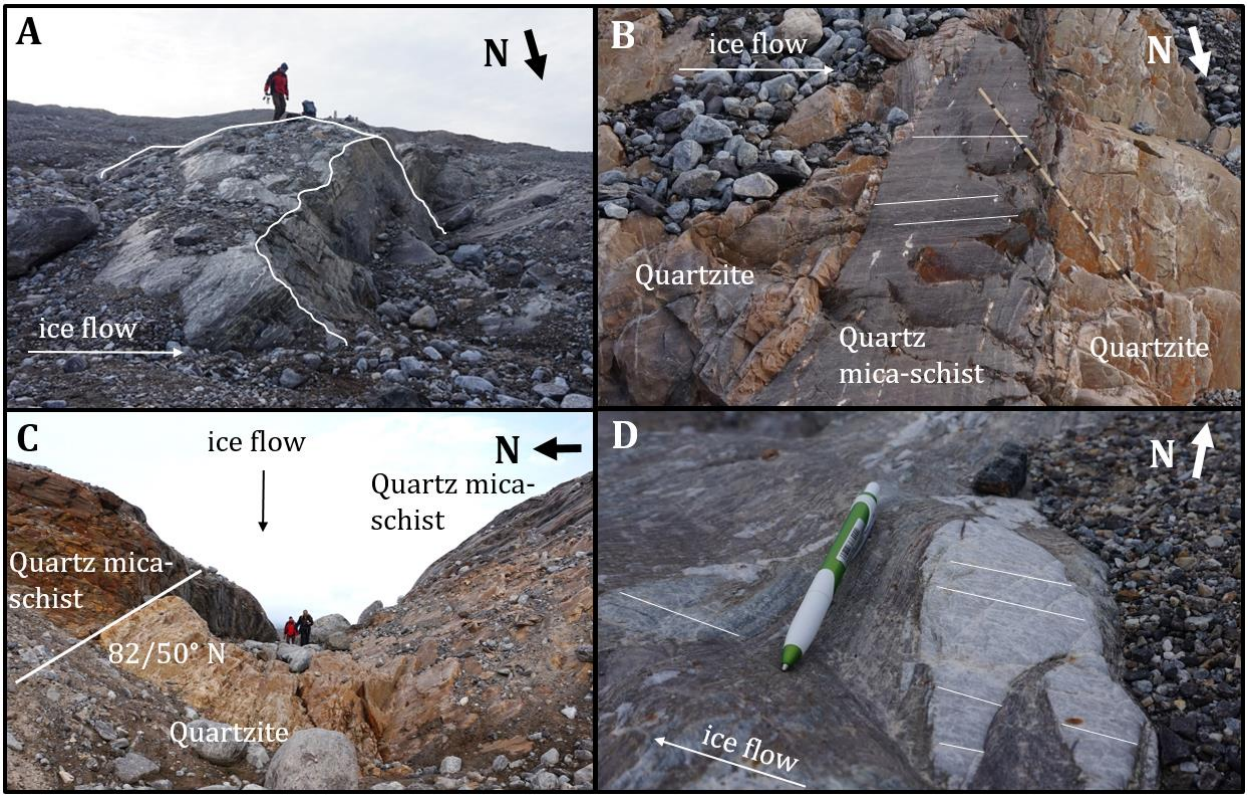

Figure 32: A) Roches moutonnée at the quartz mica-schist. B) Quarried quartzite surfaces and polished quartz mica-schist surfaces with striations (white lines). C) Linear valley parallel to ice flow. Note the fault at the left side dipping towards the north. D) Differential erosion between biotite mica-schist with no striations and the interlayered quartzite bands with striations (white lines). Note that the quartzite lens sticks out above the mica schist.

Smeerenburgfjorden complex

The glacio-erosional landforms within the migmatite of the Smeerenburgfjorden complex include polished and quarried surfaces. The migmatite outcrops are predominantly polished and striated. Many of the migmatite outcrops do have quarried lee-sides, but seem to be related to the background jointing (Figure 33).

Figure 33: Roches moutonnée of migmatite outcrop. Note the polished surface at the ice proximal side and the quarried surfaces along joints at the ice distal side.

5.2.2 Elongation ratio of landforms

In total, 204 landforms were mapped in the Kongsfjorden area, the majority of which was distributed within the fjord (Figure 34). Most of the mapped submarine landforms are tens of meters high. Howe et al. (2003) interpret the composition of the fjord floor to be bedrock dominated draped by a thin layer of sediments (<10m). It seems unlikely that the thin layer of sediments could generate submarine landforms rising tens of meters from the fjord floor. It is therefore likely that the majority of the mapped landforms are composed of a bedrock core.

The mapped landforms were subdivided into four different assemblage zones. These will be described separately below. A frequency plot of the elongation ration of the landforms for each assemblage zone is presented in Figure 34. The orientations of the long-axis of the landforms and the paleo-ice flow are plotted in rose diagrams, which are presented in Figure 35 as well. The orientation of the paleo-ice flow is measured to be NW-SE between 260 to 320°, at Lovénøyane, similar to the main trend of the fjord (Figure 35).

Assemblage Zone 1 is situated at the inner fjord towards the east and includes Blomstrandhalvøya and the area around the Lovénøyane archipelago. According to the frequency plot, most of the landforms within this assemblage zone have an elongation ratio below 1:1, which implies that the features are more rounded or elongated transverse to the paleo-ice flow. This is well illustrated by the rose diagrams which show that the majority of the landforms in Zone 1 are N-S oriented, between 350 and 30°, and nearly perpendicular to the paleo-ice flow.

Assemblage Zone 2 is situated southwest of Zone 1 and covers all the landforms constrained by the channel like feature, Figure 36C. The frequency of elongated landforms in Zone 2 (with elongation ratio values between 1:1 and 1:5.5) are higher than those in Zone 1 (with elongation ratio values below 1:1). Two singular landforms are very elongated, with elongation ratio values reaching 1:12. The main orientation of the long axis of the landforms in Zone 2 is at a slight angle to the paleo-ice flow measured in the field. However, locally the paleo-ice flow might be topographically controlled by the channel between Ny-Ålesund and Blomstrandhalvøya. Therefore, the landforms of Zone 2 are interpreted to be more streamlined than those found in Assemblage Zone 1.

Assemblage Zone 3 is situated northwest of Zone 2 and west of Blomstrandhalvøya. This zone is characterized by a slight change within the main orientation of the long axis of the landforms. Zone 2 has NW-SE orientation, whereas Zone 3 is more NNW-SSE oriented. The elongation ratios of

the landforms within Zone 3 range between 1:1 and 1:4. The majority of the landforms have an elongation ratio of 1:3.

Assemblage Zone 4 is located northwest of Zone 3 and marks the outermost zone of Kongsfjorden before it merges with Krossfjorden in the north. This zone is characterized by a high number of elongate landforms, with elongation ratios ranging between 1:1 and 1:7. Three singular landforms exceed the 1:7 ratio and reach elongation ratios up to 1:13. These are the highest elongation ratios measured within the study area. The majority of the landforms are NW-SE oriented, similar to directions of orientations in Zone 2.

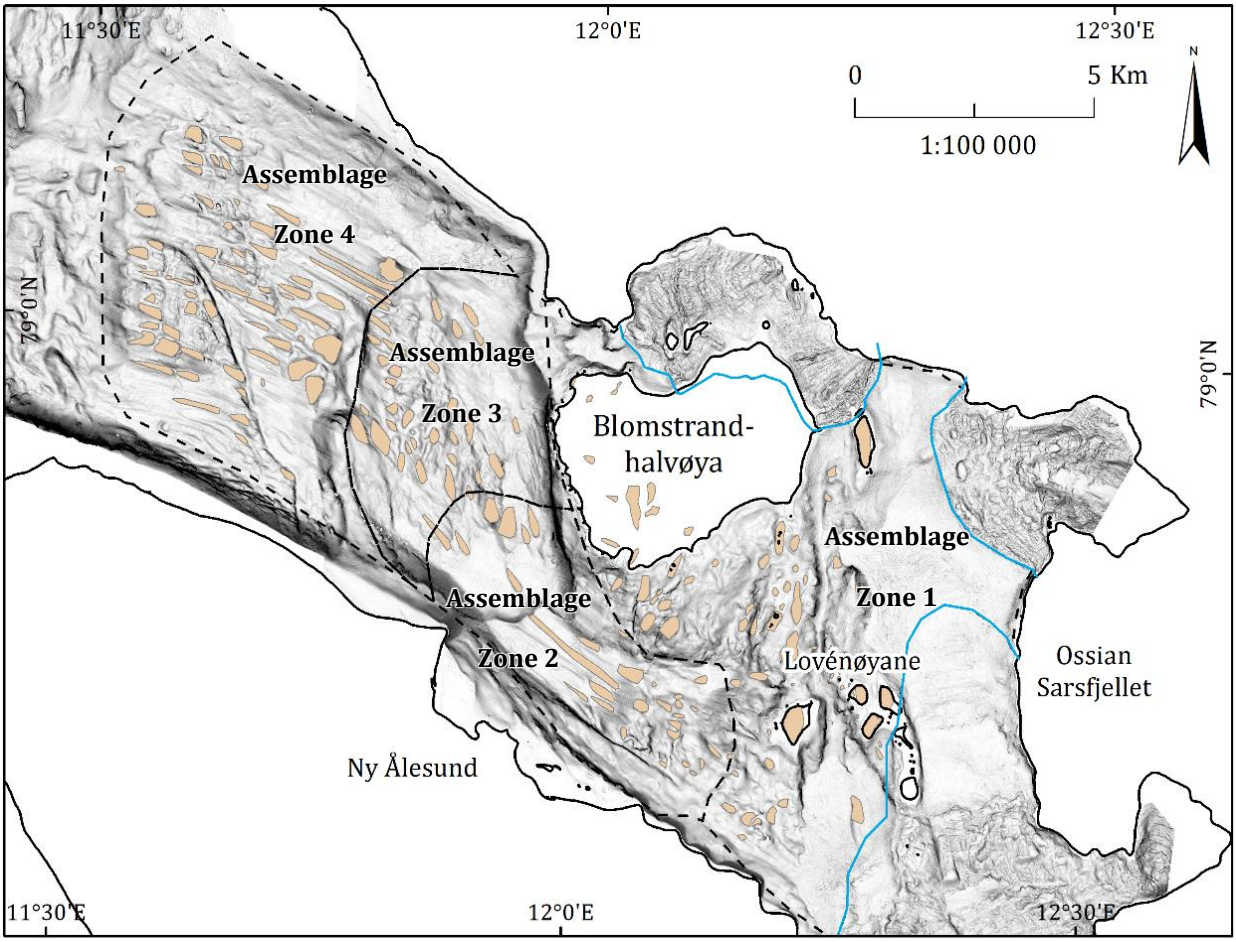

Figure 34: Landform distribution, including the four different assemblage zones separated by black dashed lines. Background map is a slope map of the bathymetrical DEM (courtesy of Norwegian Mapping Authority Hydrographic Service, 2014). Blue lines mark the LIA maximum extent after Liestøl (1988). Note the overdeepened section (channel) in Assemblage Zone 2.

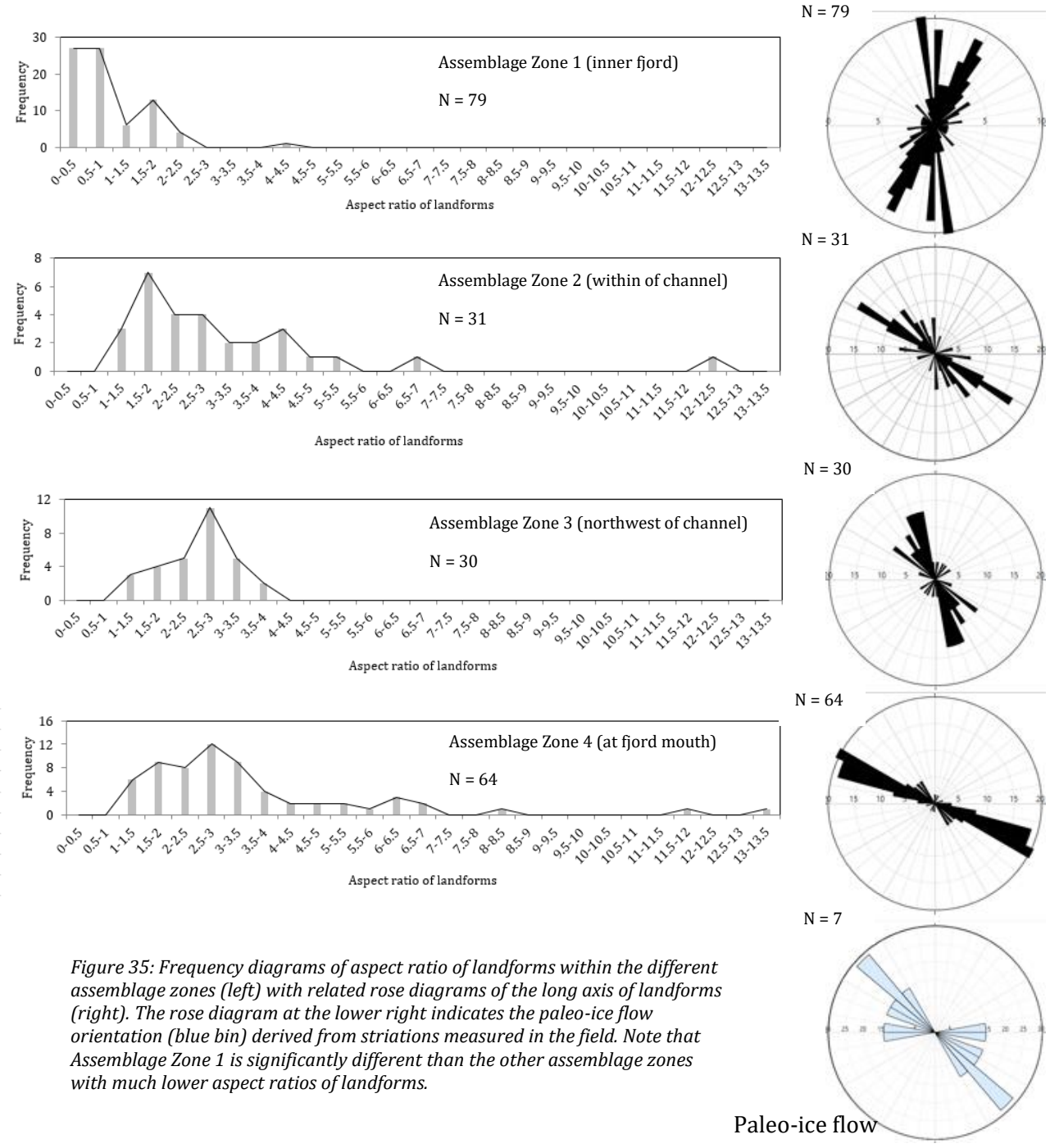

Figure 35: Frequency diagrams of aspect ratio of landforms within the different assemblage zones (left) with related rose diagrams of the long axis of landforms (right). The rose diagram at the lower right indicates the paleo-ice flow orientation (blue bin) derived from striations measured in the field. Note that Assemblage Zone 1 is significantly different than the other assemblage zones with much lower aspect ratios of landforms.

5.2.3 Surface profiles along Kongsfjorden

Four transverse surface profiles of the topography across Kongsfjorden are drawn and plotted in Figure 36. The landforms associated with Assemblage Zone 1 correspond to the transverse surface profile B-B' and the northern half of profile C-C', covering Blomstrandhalvøya. The mapped landforms of Assemblage Zone 1 are all distributed on land or located in relatively shallow water (at depths above 100m). The landforms associated with Assemblage Zone 2 correspond to the channel within the southern half of surface profile C-C'. The more elongate landforms are strictly located within the deeper parts of the channel (at depths below 100m) which is only about 2 km wide (Figure 36). The landforms associated with Assemblage Zones 3 and 4 are located in the section between the mouth of the channel and Kapp Guissez, where Kongsfjorden intersects with Krossfjorden into the open sea. The outer basin along this section is relatively deep (below 200m depth) and is about 4 to 6km wide (profile D-D' in Figure 36).

There is a clear distinction along the southern margin of Kongsfjorden between the eastern profiles (A-A' and B-B') and the western profiles (C-C' and D-D'). This southern margin is characterized by a lithological boundary between the WFSB, at Brøggerhalvøya, and the basement rocks, towards the north (cf. Figure 11). The topographic expression of this lithological boundary between the WFSB and the basement rocks can clearly be identified on profiles C-C' and D-D' by steep slopes and deep basins. This lithological boundary appears to be shallower and flat along profiles A-A' and B-B'.

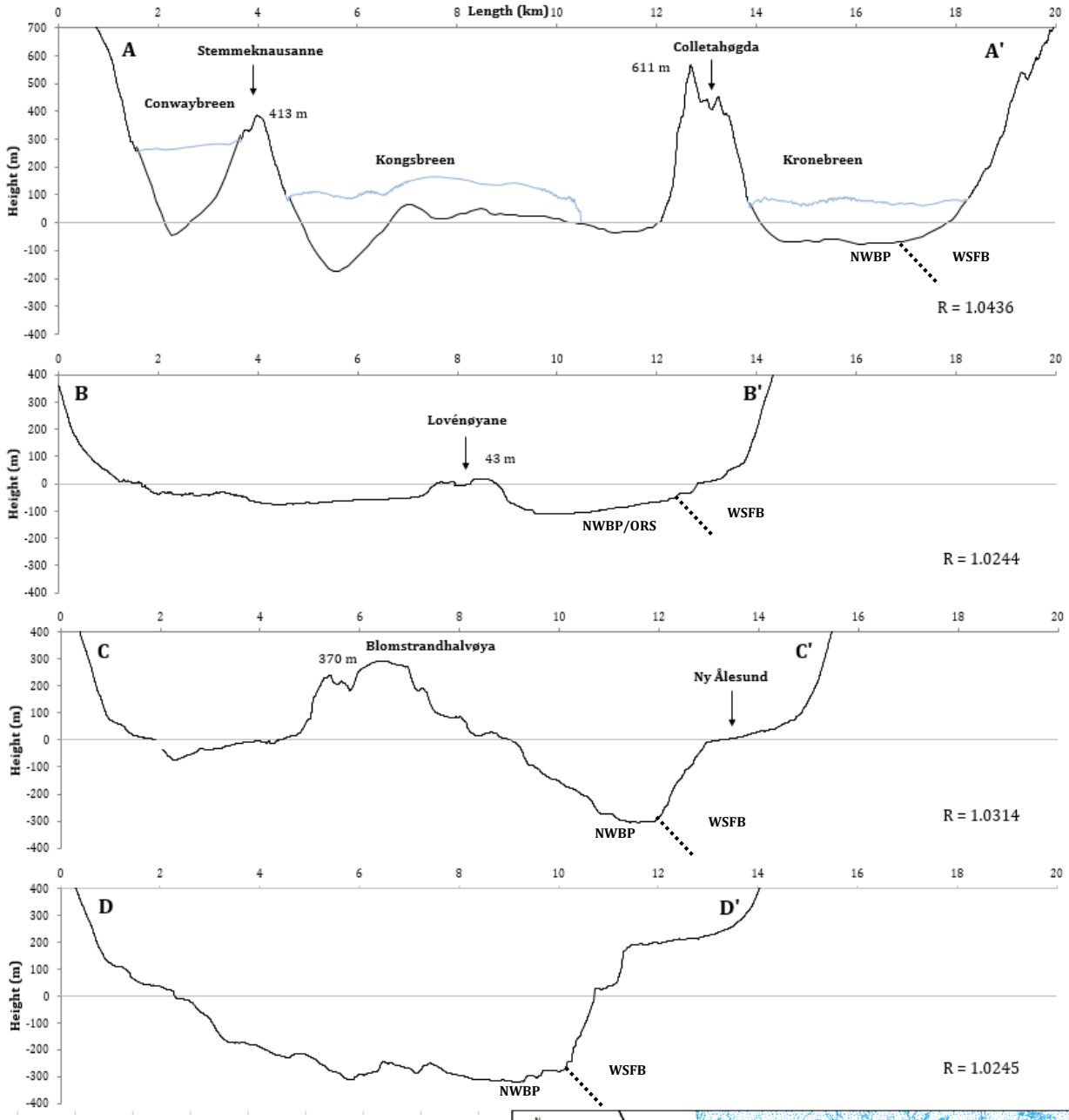

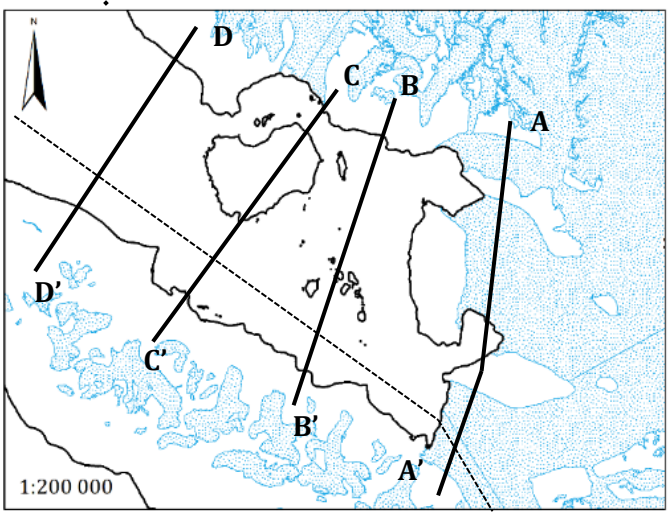

Figure 36: Transverse surface profiles of Kongsfjorden along four different transects. Locations of transects are indicated at the right hand side. R = surface roughness (surface distance/map distance). The approximate lithological boundary between the West Spitsbergen Fold-and-thrust Belt (WSFB), the Northwestern Basement Province (NWBP) and Old Red Sandstones (ORS) is indicated by the dashed lines. Note that the elevations are 5.5x vertically exaggerated.

5.3 Linear morphological features

In Figure 37A, the aspect map of slopes that are steeper than 30° is projected on top of a slope map of Kongsfjorden. A histogram indicating the dominant slope azimuth direction of the aspect map is presented in Figure 37B.

Most of the slopes at the shores of Brøggerhalvøya are NW-SE oriented and have their slope azimuth facing towards the north or northeast. This is indicated with the largest orange peak in the histogram situated around 40°. The strike of these slopes (around 130°) coincides well with the strike of the frontal thrust of the West Spitsbergen Fold-and-thrust Belt (WFSB), Figure 3. However, the majority of the slopes around the Lovénøyane ridge and Blomstrandhalvøya have a slope azimuth facing towards the east and the west. These slopes are represented by the small yellow peak at 90° and the large blue peak around 255° in Figure 37B. Remarkable is the narrow cyan peak at 180° representing the slopes facing towards the south. These slopes are only sporadically distributed along the northern shores of Kongsfjorden and along the northern face of the trough between Blomstandhalvøya and Ny-Ålesund.

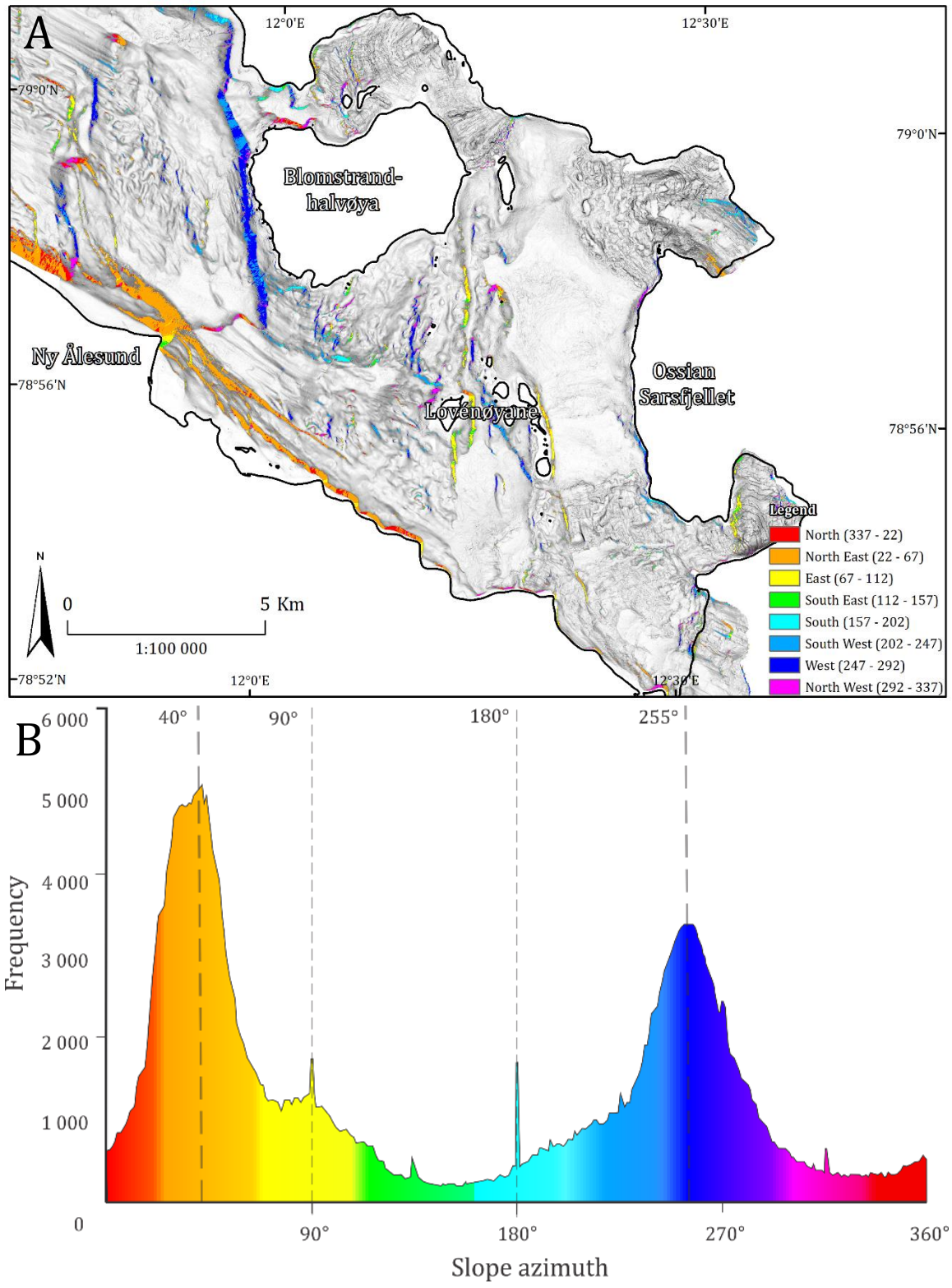

Figure 37: A) Aspect map of Kongsfjorden of slopes larger than 30°. Background image is a slope map of the bathymetrical DEM (Norwegian Mapping Authority Hydrographic Service, 2014). The shore line, courtesy of the Norwegian Polar Institute (2014b), is modified by a smoothening filter. B) Histogram showing aspect of slopes steeper than 30°. Dashed lines indicate peaks in slope azimuth direction described in the text. The histogram is created in ArcGIS and redrawn using CorelDRAW 2017.

The linear morphological features derived from the aspect map are drawn and presented in Figure 38. The orientations of the linear morphological features are plotted into a length-weighted rose diagram (Figure 38). The orientations of the linear features appear to be distributed into two dominant sets: set A, trending N-S oriented (between 340° to 10°), and set B, trending NW-SE (between 290° and 310°).

Set A represents the majority of the linear features and relates to the slopes facing towards the east and west, i.e. yellow and blue peaks in Figure 37B, respectively. These lineaments are mostly distributed across Blomstrandhalvøya and the Lovénøyane ridge.

Set B represents a lower number of linear features but tends to be much longer. These linear features relate with the slopes facing towards the northeast and south, i.e. orange and cyan peak in Figure 37B, respectively. The features of set B are distributed in two different areas: one group close to the northern shores of Brøggerhalvøya and another group distributed at the northern end of the channel between Blomstrandhalvøya and Ny-Ålesund. The latter group runs from the Lovenøyane ridge towards the northwest and ends abruptly at the widening of the channel (Figure 37A).

The linear morphological features are interpreted as relating to fracture zones occurring in two settings and are therefore referred to as geological lineaments.

Set A correlates well with Fault population B (Figure 29). Set A also is oriented parallel to structures observed in the basement rocks, including lithological boundaries and foliation (Figure 11). The group close to the shores of Brøggerhalvøya in Set B relates to the northeast facing slopes which on their turn are associated with the lithological boundary between the NWBP and the WSFB (Figure 3). However, the group at the northern end of the channel in Set B relates to the south facing slopes, indicated by the cyan color in Figure 34B. These south facing slopes correlate well with the main fault orientation measured on Midtholmen (Figure 13). These lineaments have not been described by other studies before.

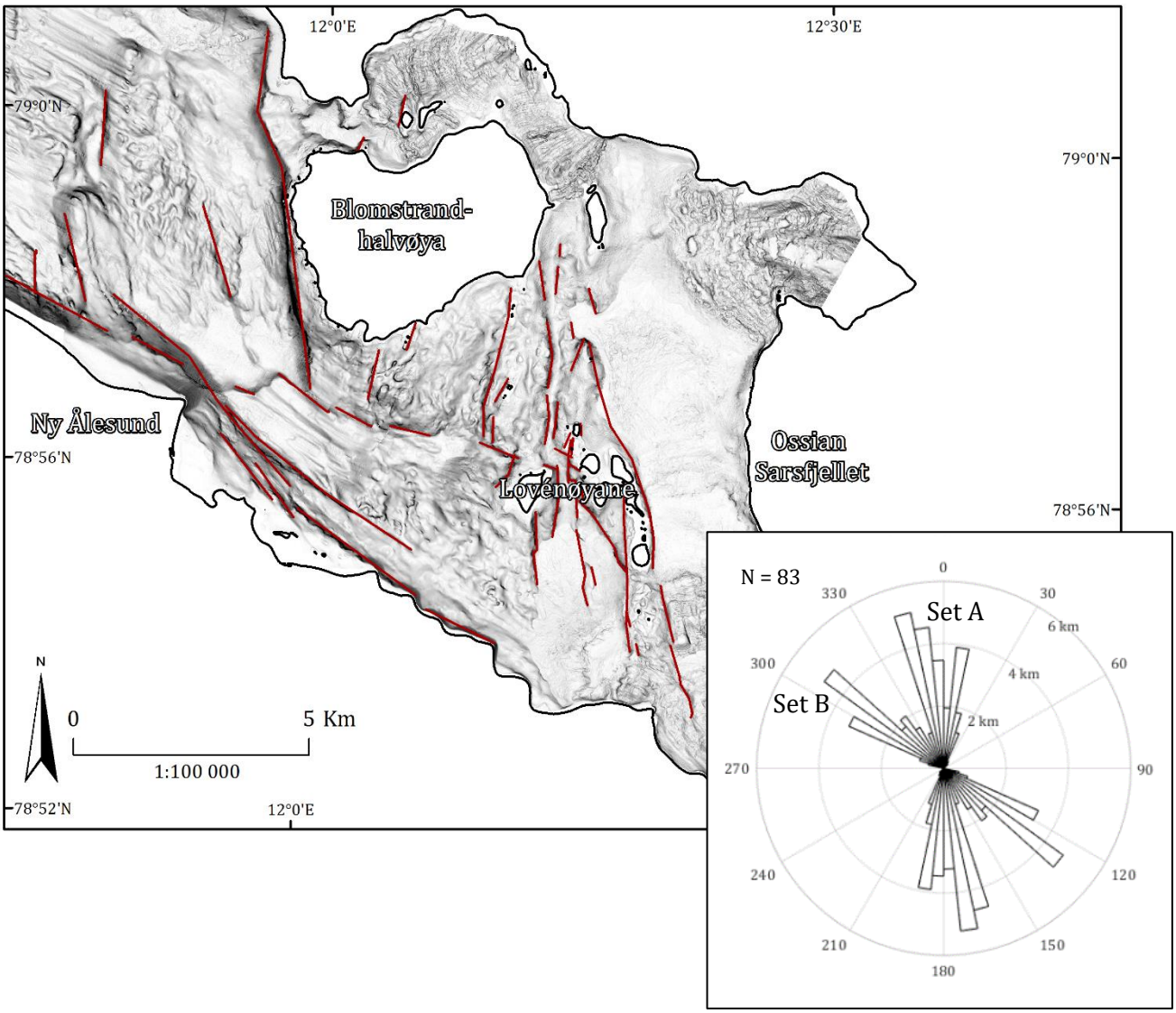

Figure 38: Lineament map based on aspect map. Background image is a slope map of the bathymetrical DEM (Norwegian Mapping Authority Hydrographic Service, 2014). The shore line, courtesy of the Norwegian Polar Institute (2014b), is modified by a smoothening filter. The graph at the right hand indicates the length weighted rose diagrams of all the linear features, created with a MATLAB script modified from Puszta (2017). The bin size is 5° and the radius represents the cumulative length of the lineaments.

6 Discussion

6.1 Uncertainties

In general, it can be said that there are typical challenges in identifying factors that control variable glacial modification. There are two main reasons for this.

1) Glacio-erosional landforms can relate to more than one erosional event. Areas may have repeatedly been glaciated over time, and thus several types of erosional processes might have contributed to the formation of the present morphology at hand.
   These different types of erosion events include:
   i. Repeated glaciations. Glacio-erosional landforms have acquired their present shapes by the impact of more than one individual glacial cycle. More specifically: present glacier activity may have overprinted or modified glacial-erosional landforms formed during the last glaciation.
   ii. Glacial dynamical flow behavior tends to vary over time. Roberts and Long (2005) suggest that during these deglaciation events, smoothened landforms such as whalebacks could have been subjected to quarrying due to lowering of ice overburden pressures.
   iii. Interglacial- and post-glacial erosion processes. Slope processes, glacial valley erosion and wave cut erosion are common erosion processes during interglacial periods and also these could modify the glacial erosional landforms (Benn & Evans, 2010; Ingólfsson, 2011).

2) It remains a challenge to differentiate soft sediment landforms from bedrock dominated landforms with a restricted usage of high resolution DEMs. It is important to distinguish between depositional and erosional processes in order to be able to interpret variability of glacial modification.

The first challenge in relating glacio-erosional landforms to the paleo-ice stream tributary activity proved to be minor in the case of Kongsfjorden for the following reasons:

i) In Kongsfjorden, modification of glacio-erosional landforms due to Holocene glacial activity seems modest. Glacial erosion rates for the drainage area of Kronebreen are estimated to be around 0.6mm/yr since the LIA (Elverhøi et al., 1980). Even though these erosion rates are estimates of recent glacial activity, it is likely that only the top layer may have been

stripped off due to recent glacial activity, and that the larger (meso-scale) glacio-erosional landforms thus were formed during earlier glaciations and have remained preserved.

ii) Additionally, in the case of Kongsfjorden, incidence of post-glacial rock falls, due to wave cut erosion, seems to be modest. Many of the visited outcrops on the Lovénøyane archipelago had retained their polished surfaces, as these were preserved in time from the last glaciation (including glacial striations). The post-glacial rock falls at Lovénøyane seem to have been most active at the margins of the islands close to fracture zones (cf. Figure 15 and Figure 22A).

The second challenge, of how to effectively distinguish soft sediment landforms from bedrock dominated landforms, is also less demanding in the specific case of Kongsfjorden. Sub-bottom profiling of outer Kongsfjorden has been performed by Howe et al. (2003) and by Maclachlan et al. (2010). Howe et al. (2003) interpret the fjord floor to be predominantly bedrock dominated, draped with a thin sedimentary cover (<10m). As most of the mapped landforms are elevated above 10m from the fjord floor, it seems likely that the landforms are composed of a bedrock core. However, Maclachlan et al. (2010) attribute glacial lineations (landforms with an elongation ratio >1:10) to the effects of soft sediment deformation.

6.2 Controlling factors on variable glacier modification

Comparison of the main bedrock and the geomorphological characteristics with the linear morphological features indicates that several factors control the variability of glacial modification of bedrock dominated areas in Kongsfjorden. Each of these controlling factors will be discussed separately below.

6.2.1 Bedrock characteristics

The bedrock control on the variability of glacial modification can be subdivided into either lithological control (due to changes in mechanical properties) *or* structural control due to fracturing and jointing of the bedrock.

6.2.1.1 Lithological control

The following features suggest a lithological control in variable glacier modification:

1) There is a clear difference in mechanical properties of basement rocks located at the nunataks in the east and sedimentary and altered marble rocks around the Lovénøyane archipelago (Figure 20). The erosion resistance is much higher among the rocks with low mechanical anisotropy and high fracture spacing, e.g. migmatite and quartzite. The erosion resistance is considerably lower in high mechanical anistropical rocks with dense fracture spacing, e.g. sedimentary breccia, altered marble and tectonic breccia, which are found predominantly on the Lovénøyane archipelago. Therefore, profound topography of narrow (deep) troughs and steep islands is to be expected in more resistant rocks (Swift et al., 2008), such as those found at Blomstrandhalvøya, Ossian Sarsfjellet and Stemmeknausane. This is supported by the high surface roughness of transverse profile (A-A'), Figure 36.
2) The altered marble, i.e. the Viggobreen formation, seems to exert a significant effect on the erosion resistance of marble. The plot in Figure 20 shows clear difference in mechanical properties of the altered marble, observed on Sigridholmen, compared to the more mechanically massive marble, observed on Stemmeknausane and Ossian Sarsfjellet.
3) The micro crag-and-tail highlights a variation of erosion resistance between lithologies, as the resistant calk-silicate nodule at the ice-proximal side protects the marble at the lee-side.

6.2.1.2 Structural control

The following features suggest a structural control in variable glacier modification:

1) Assessment along the central fracture zone in Juttaholmen showed a clear trend of more resistant rock at the side, e.g. in Units A and D, and weaker brecciated rock towards the center of the fracture zone, e.g. in Units B and C (Figure 28). The center part of the fracture zone appeared to be more brecciated and therefore accommodated large displacement. Significant changes in bedrock mechanical properties along the fracture zone suggest that bedrock material is more easily erodible along major fracture zones.
2) The islands within the Lovénøyane archipelago are fault-bound and have steep faces characterized with small post-glacial rock falls (Figure 13 and Figure 15). These steep faces can be interpreted as such that they have been formed by a combination of glacier erosion (including abrasion and quarrying) and a repeated sequence of slope collapse and rock falls during interglacial periods and subsequent removal of debris during glacial erosion. I interpret this as a formative process of the overdeepened linear valleys along the major fracture zones at the Lovénøyane ridge, similar to the process described by Krabbendam & Bradwell (2014).
3) A strong correlation has been established between linear features and fault populations measured in the field. Set A corresponds with Fault population B (Figure 39). The overdeepened linear valleys along the Lovénøyane ridge coincide with the linear features from Set A and this suggests that the overdeepened valleys are distributed along N-S trending strike-slip fracture zones. These overdeepened valleys may also have been subjected to drainage of subglacial meltwater, so a component of subglacial fluvial erosion seems plausible.

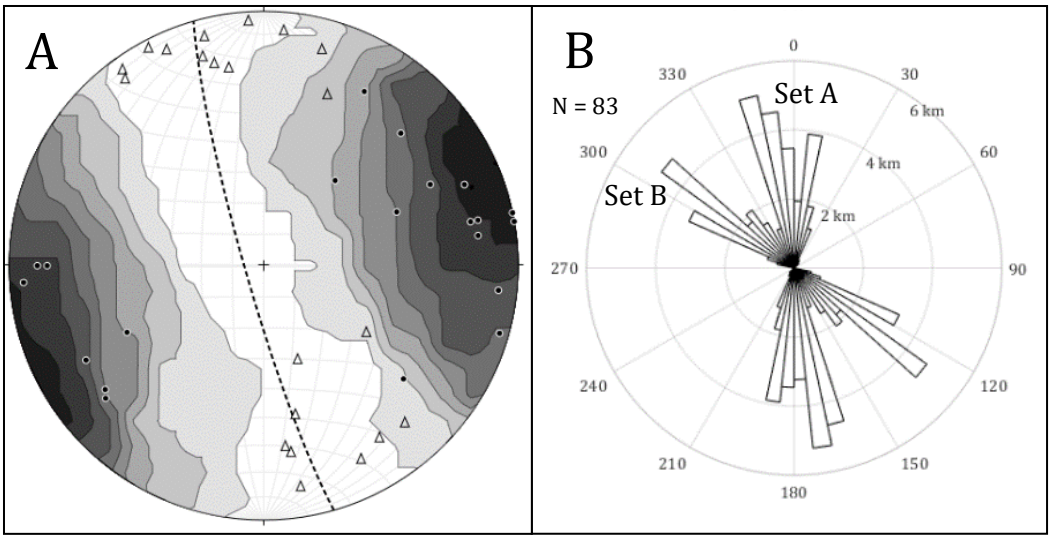

Fault population B Linear morphological features

Figure 39: A) Schmidt net of fault population B, measured at the central fracture zone at Juttaholmen, dashed line indicates the main fault orientation. B) Length weighted rose diagram of linear morphological features at the fjord bottom. Note that the similarity between the orientation of Set A and the strike of fault population B.

4) The N-S oriented fracture zones measured at Lovénøyane run parallel to the structures occurring at the basement rocks in the east, such as the foliation and lithological boundaries on Ossian Sarsfjellet and Stemmeknausane (Figure 11). These structures are oriented perpendicular to paleo-ice flow and have a profound topographic expression. At the southern side of Kongsfjorden, the majority of the structures are NW-SE oriented, parallel to paleo-ice flow. Here the topography is much smoother (Figure 7).

   Previous studies have reported on the significance of the orientation of structures relative to paleo-ice flow in relation to variable glacial modification, showing that structures perpendicular to ice flow have a higher erosion resistance compared to structures parallel to ice flow (Gordon, 1981; Glasser et al., 1998; Krabbendam & Bradwell, 2014). It therefore seems likely that the large-scale structures parallel to paleo-ice flow within Kongsfjorden generate smoother landscape relative to structures oriented perpendicular to paleo-ice flow.

It is remarkable that the main trend of Kongsfjorden follows the lithological boundary of the NWBP and the WSFB (Figure 11). Svendsen et al. (2002) suggest that the frontal thrust of the WSFB acts as a structural weak zone that was carved out by the glacier. This seems likely, as fracture zones paralleling ice flow enhance glacial erosion (Harbor, 1995; Johansson et al., 2001; Gonzales & Aydin, 2008). However, the surface expression of the frontal thrust appears to be significantly more

profound at the outer basin of Kongsfjorden (west of Lovénøyane) than at the inner basin (Figure 36). The fjord bottom along the frontal thrust at the inner basin is smoother and less deep than at the outer basin, which is characterized by the channel between Blomstrandhalvøya and Ny-Ålesund. The fjord floor along the frontal thrust drops from 100m depth to 350m in the down-ice direction of the Lovénøyane archipelago. This would suggest that the magnitude of glacial modification carving out the channel increases towards the down-ice section of the structural weak zone. An extensive variability of the mechanical properties along the frontal thrust seems unlikely as the same lithology of the WSFB occurs at the lithological boundary and there is no evidence that this frontal thrust experienced variable tectonics. Therefore, the mere presence of the lithological boundary marked by the frontal thrust of the West Spitsbergen Fold-and-thrust Belt cannot explain, in itself, the variation of the surface expression and the development of the trough. A component of increased glacial activity down-ice along the lithological boundary could explain the more profound surface expression of the structural weak zone at the channel towards the outer basin.

6.2.2 Glacio-erosional processes

Evidence from glacio-erosional landforms and the elongation ratio of landforms show that different glacio-erosional processes took place which, in turn, affected the variability of glacial modification throughout Kongsfjorden. The factors suggesting a variability of glacial modification are described separately below.

6.2.2.1 Glacio-erosional landforms

The variability of bedrock landforms between outcrops found on different localities suggests different glacio-erosional processes acting upon them. Here are some examples:

1) Striations found on the red sedimentary rock outcrops are only distributed on the marble clasts within the breccia (Figure 30B). The same observations were made on the quartz-mica schist where striations are only present on the weakly foliated quartz-mica schist and absent on the quartzite (Figure 32B).
2) A clear spatial difference between polished and quarried surfaces was observed on Sigridholmen. Outcrops with more mechanically massive marble are dominated by polished surfaces (including striations towards the center of the island), whereas plucked surfaces dominate at the weathered and brecciated marbles at the margins of the island, Figure 31 (C and D). Differences in erosional processes could be explained by variation in mechanical properties of the marbles. The high mechanical anisotropy of the weathered and brecciated marbles favor fracture propagation that could lead to separation of rock fragments (Iverson, 1991b). This study suggest that the quarried rock fragments might be relatively small (1-10cm^3) due to the dense fracture spacing of the weathered marble.
3) There is a clear difference in quarried faces between the outcrops. The quarried faces of the densely fractured outcrops – i.e. mylonite quartz mica-schist, altered marble and tectonic breccia – are distributed over the whole surface of the outcrop where the removed rock fragments are smaller than < 5cm^3 in size (Figure 17B, Figure 30A and Figure 31C). The quarried faces at weakly fractured outcrops, i.e. migmatite and quartzite, coincide with the background jointing and this circumstance suggests that rock fragments >10cm^3 in size were removed (Figure 18, Figure 20 and Figure 33). These findings further indicate that the size of the removed rock fragments is related to the degree of fracture spacing and that glacial modification by quarrying tend to dominate at densely fractured rocks.

6.2.2.2 Elongation ratio of landforms

The features of the elongation ratio of landforms presented below suggest a spatial variability in glacial modification.

The majority of the landforms from Assemblage Zone 1 have an elongation ratio of around 1:1 or less. Most of the landforms of this zone in general are oriented perpendicular to paleo-ice flow, and are oriented sub-parallel to Set A in the lineament map (Figure 35 and Figure 38). This is in marked contrast with landforms from Assemblage Zones 2 to 4 which are more streamlined with the paleo-ice flow and which reach much higher elongation ratios (of up to 1:13).

Phillips et al. (2010) and Bradwell (2013) suggest that the higher elongation ratios of landforms parallel to paleo-ice flow could be attributed to weaker underlying bedrock or higher glacial modification of fast flowing ice. There seems to be no clear correlation between the 'weak' mechanical properties of the Lovénøyane archipelago and the high elongation ratios. Therefore, a higher paleo-ice velocity is necessary to sustain the glacial modification to form the more streamlined landforms. Due to the fact that the average elongation ratio of each assemblage zone increases towards the outer fjord, moving from Zone 1 to 4, an acceleration of the paleo-ice flow velocity is interpreted to have taken place between the Assemblage Zones 1 and 2 (Figure 35).

The absence of elongated streamlined glacial landforms within Assemblage Zone 1 could also be ascribed to glacial modification during deglaciation, as suggested by Roberts & Long (2005). However, this attribution seems unlikely, as hints of similar modification would be expected in other assemblage zones as well, and this is not as far as our findings indicate.

In summary, several factors controlling the variability of glacial modification were identified, including changes in bedrock properties and glacio-erosional processes. These identified factors have implications for understanding the landscape development of Kongsfjorden and for interpreting the subglacial topography of modern ice sheets which will be discussed in more detail below.

6.3 Implications on the Lovénøyane archipelago

In light of the above, it can be stated that the Lovénøyane archipelago contains many controls favoring strong glacial modification, including 'weak' mechanical bedrock properties and high density of fracture zones. Moreover, the Lovénøyane archipelago is distributed near to the centerline of the fjord where the highest glacial modification is to be expected.

In spite of this it seems likely that the degree of glacial modification of the bedrock at the Lovénøyane ridge was relatively modest, due to the following reasons:

1) The 'weak' mechanical rocks, i.e. the tectonic breccia and the weathered marbles of the Viggobreen formation, are still preserved and stand out above sea level (Figure 20);
2) The absence of till cover, a circumstance which suggests limited generation of basal debris;
3) The relative high roughness of the Lovénøyane ridge, which suggests that the smoothening of the landscape was inefficient (Figure 7);
4) The absence of elongated streamline landforms (Assemblage Zone 1 in Figure 35).
5) The absence of any surface expression at the lithological boundary between the NWBP and the WSFB.

The suggestion that the Lovénøyane archipelago experienced only modest levels of glacial modification relative to modifications in Assemblage Zone 2 could be explained by the presence of less dynamic ice. The high roughness of the Lovénøyane ridge paleo-ice flow velocities could exhibit the paleo-ice stream tributary to reach ice streaming velocities. An alternative suggestion would be that effective glacial modification is confined in the larger fracture zones by substantial strain. The high contrast in bedrock mechanical properties along the central fracture zone at Juttaholmen (Figure 28) supports the suggestion of differential erosion of the brecciated rocks with the highest strain along fracture zones. Over repeated glaciations this could then have led to an increase of the vertical component of the linear valleys resulting in a higher surface roughness.

On basis of the findings of this study it could be stated that it is likely that both processes mentioned above took place. Due to the occurrence of structures perpendicular to paleo-ice flow and higher roughness, the Lovénøyane ridge could have acted as a topographic threshold hampering the paleo-ice stream tributary in reaching ice streaming velocities. The landforms of Assemblage Zone 2, downstream of the Lovénøyane ridge, contain more elongate landforms and this suggests the presence of more dynamically active ice during the last glaciations (Phillips et al., 2010). The transition between Assemblage Zones 1 and 2 may represent a zone of acceleration of paleo-ice flow which could have been controlled by the topographic drawdown of ice into the

overdeepened channel, between Ny-Ålesund and Blomstrandhalvøya. This acceleration might represent a topographically controlled onset zone of the Kongsfjorden paleo-ice stream tributary, similar to the topographically controlled onset zone in NW Scotland as described by Bradwell (2013).

In short, the reason that the Lovénøyane ridge experienced relative modest erosion could conceivably be attributed to structures oriented perpendicular to paleo-ice flow and to a lower ice dynamical behavior relative to the narrow corridor between Ny-Ålesund and Blomstrandhalvøya. Evidence pointing in this direction is the absence of elongated streamlined landforms and the preservation of 'weak' mechanical rocks standing out above sea level. The findings of this study suggest that the ice accelerated after it would overcome the Lovénøyane ridge by a topographic drawdown into the overdeepend channel between Ny-Ålesund and Blomstrandhalvøya (Figure 40).

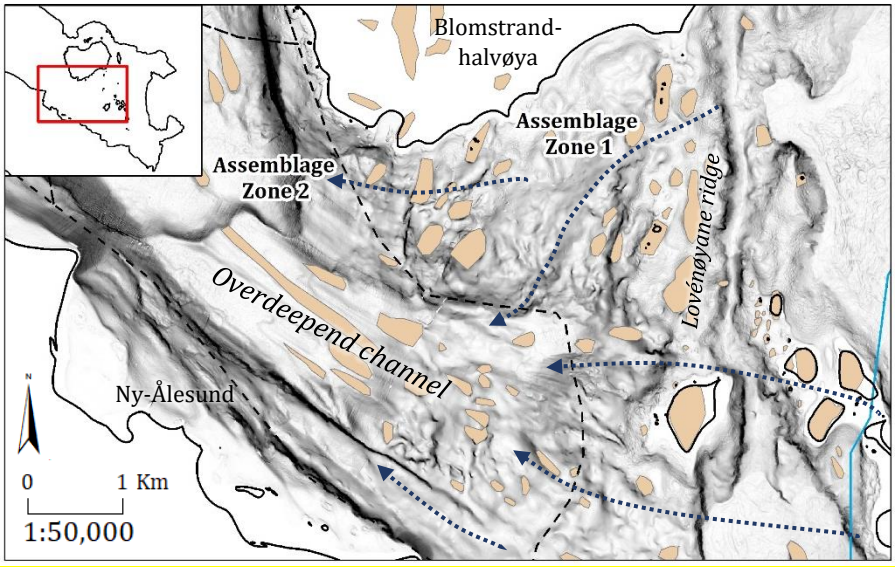

Figure 40: Interpreted paleo-ice flow (blue dashed arrows) between the Lovénøyane ridge and the topographic drawdown of ice into the overdeepend channel. The assemblage zones are separated with black dashed lines. Background map is a slope map of the bathymetrical DEM (courtesy of Norwegian Mapping Authority Hydrographic Service, 2014). The shore line, courtesy of the Norwegian Polar Institute (2014b), is modified by a smoothening filter. Note that the more elongate and streamlined landforms are distributed within the overdeepend channel.

6.5 Implications of morphological features under modern ice sheets

In this study, detailed outcrop observations were related with regional patterns within the Kongsfjorden paleo-ice stream tributary, an approach that was suggested by previous studies (e.g. those of Glasser et al., 1998; Glasser & Bennett, 2004; Roberts & Long, 2005; Glasser & Ghiglione, 2009; Phillips et al., 2010; Krabbendam & Bradwell, 2011, 2014; and Bradwell, 2013). The identified controlling factors on the variability of glacial modification in this study highlight the importance of collecting field data to enable a thorough interpretation of glacial modification. This study suggests that the collected field data should include the bedrock and geomorphological characteristics on various scales (mico to macro scale) of the area. Relying on data provided by remote sensing techniques alone would therefore make it difficult to interpret the intensity of glacial modification on morphological features.

The widespread occurrence of major fault lines coinciding with glacial troughs and across overdeepened structures at the bed of deglaciated fjords (as identified e.g. by England, 1987; Gonzales & Aydin, 2008; Glasser & Ghiglione, 2009; Krabbendam & Bradwell, 2014) suggests that major fracture zones are distributed along present-day overdeepened structures at the bed of ice sheets and/or glacial valleys. These structures may provide an approximate indication about relative erosion resistance of the bed, and could be a basis for further improvement of geological maps. They help to identify lineaments under present glaciated areas using DEMs. Eventually, a better understanding of subglacial geology could be invaluable when the aim is to develop more accurate models of predicting and possibly constraining glacio-erosional processes and dynamic ice flow behavior.

7 Conclusions

This thesis has identified several controls on the variability of glacial modification based on analysis of the bedrock characteristics, geomorphological characteristics, and linear morphological features in the Kongsfjorden area. On basis of this, the following conclusions are drawn.

1. The Kongsfjorden area exhibits a varied bedrock configuration, including a number of fracture zones and lithologies with distinct mechanical properties. More resistant lithologies are located at the innermost part of Kongsfjorden. Fracture zones and lithological boundaries are predominantly N-S and NW-SE orientated. This circumstance, together with the occurrence of N-S orientated structures perpendicular to the paleo-ice flow, could explain the high surface roughness and the profound topography of Ossian Sarsfjellet and Stemmeknausane. Structures oriented parallel to paleo-ice flow, such as the lithological boundary between the NWBP and the WSFB, generate a smoother landscape.
2. Most of the fractures within the Lovénøyane archipelago are characterized by N-S sinistral strike-slip faulting. The fracture zones at Lovénøyane are characterized by weak brecciated rocks towards the center part of the fracture zone, accompanied by more resistant rock towards the sides of the fracture zones. The N-S sinistral strike-slip fault zones are associated with the N-S oriented linear features along the Lovénøyane ridge. The major fracture zones within the Lovénøyane ridge are overdeepened by subsequent glacial erosion, resulting in an increase of the vertical component of the surface topography.
3. The Kongsfjorden area consists of a varied hard-bed landform assemblage, including distinct glacio-erosional landforms for the different bedrock lithologies. Various glacio-erosional processes have acted upon the bedrock between the different lithologies, resulting in variable glacial modification of the bedrock.
4. The elongated landform distribution ranges from near circular to highly elongated landforms. Near circular landforms perpendicular to paleo-ice flow were identified at Assemblage Zone 1 (towards the inner fjord), whereas highly elongated streamlined landforms were found mostly at Assemblage Zones 2-4 (towards the outer fjord). The study suggests that the more elongated streamlined landforms could be the result of more intense glacial modification beneath a more dynamically active paleo-ice stream tributary.

5. Lovénøyane archipelago experienced relatively modest erosion which, on basis of the analysis put forward in this study, could be attributed to structures oriented perpendicular to paleo-ice flow and a lower ice dynamical behavior relative to the down-ice channel between Ny-Ålesund and Blomstrandhalvøya.

The factors that control the variability of glacial modification within the Kongsfjorden area suggest that glacial erosion did not occur with the same intensity at all locations along the fjord, and this resulted in dissimilar morphological features in the landscape. Knowledge of this variability in glacial modification can be applied to identify morphological features below present-day ice sheets. These could then be related with geological structures, provided that sufficient field data are available to support such an undertaking.

8 Points of further study

There are still significant local variations in the morphological expressions found in different lithological boundaries. For example, the surface expression of the contact between the migmatites and marbles at Stemmeknausane is much less profound than the fracture zones at Lovénøyane. Therefore, there is a need for a better understanding of the relation between the occurrence of different types of structural weak zones and overdeepened linear valleys. Such an understanding could be acquired by identifying bedrock properties of different fault types from different tectonic settings and through classifying these into different types of structural weak zone characteristics. Such a classification could then be used to relate the different types of structural weak zones with differential glacial erosion. More knowledge of such relationships would allow for a more accurate interpretation of morphological features by means of high resolution remote sensing techniques.

Studies have shown a clear correlation between width of fracture zones and strain of faults (Mitchell & Faulkner, 2009; Faulkner et al., 2011). Wider fracture zones have larger surface areas of 'weak' mechanical rock properties, susceptible to glacial modification and this tends to produce wider linear valleys. Therefore, the width of linear valleys might approximate the strain of the fracture zone. This, however, should be further substantiated through collecting additional data, such as mapping the dimensions of fracture zones by seismic interpretations or assessing the damage zone of different fracture zones to enable adequate comparison.

The suggested factors that control variable glacial modification that this study identified could be studied separately to quantify the relative effectiveness of each such factor. Studying fjord settings with low tectonic geologic activity would enable further assessment of the lithological control and glacio-erosional processes. This type of fjords settings could include fjords located in sedimentary basins such as in northern Greenland (Piepjohn et al., 2015), or in Isfjorden, Svalbard (Dallmann, 2015). Studying fjords with similar lithology could, on its turn, allow for further assessment of the controlling factors of structural weak zones and changes in glacio-erosional processes. Suitable locations for performing such future research could encompass fjords within granitoid plutons covering large areas such as in the basement provinces of Svalbard (Dallmann, 2015), in mainland Norway or in southeast Greenland, where large granite bodies cover a whole fjord area (Geological Survey of Greenland, 2015; Geological Survey of Norway, 2015).

9 References

Aliani, S., Sciascia, R., Conese, I., D'Angelo, A., Del Bianco, F., Giglio, F., Langone, L., Miserocchi, S., 2016. *Characterization of seawater properties and ocean heat content in Kongsfjorden, Svalbard Archipelago*. Rend. Lincei. 27, 155–162.

Augustinus, P.C., 1992. *The influence of rock mass strength on glacial valley cross-profile morphometry: A case study from the Southern Alps, New Zealand*. Earth Surf. Process. Landforms. 17, 39–51.

Augustinus, P.C., 1995. *Glacial valley cross-profile development: the influence of in situ rock stress and rock mass strength, with examples from the Southern Alps, New Zealand*. Geomorphology. 14, 87–97.

Aydin, A., Basu, A., 2005. *The Schmidt hammer in rock material characterization*. Eng. Geol. 81, 1–14.

Benn, D.I., Evans, D.J.A., 2010. *Glaciers and Glaciation*. John Wiley and Sons, New York.

Bergh, S.G., Maher, H.D., Braathen, A., 2000. *Tertiary divergent thrust directions from partitioned transpression, Broggerhalvoya, Spitsbergen*. Nor. Geol. Tidsskr. 80, 63–81.

Boulton, G., 1974. *Processes and Patterns of Glacial Erosion*. 41–87.

Boulton, G., 1979. *Processes of Glacier Erosion on Different Substrata*. J. Glaciol. 23, 15–38.

Braathen, A., Osmundsen, P.T., Maher, H., Ganerød, M., 2017. *The Keisarhjelmen detachment records Silurian-Devonian extensional collapse in Northern Svalbard*. Terra Nov. 0–2.

Bradwell, T., 2013. *Identifying palaeo-ice-stream tributaries on hard beds: Mapping glacial bedforms and erosion zones in NW Scotland*. Geomorphology. 201, 397–414.

Brook, M.S., Brock, B.W., Kirkbride, M.P., 2003. *Glacial outlet valley size-ice drainage area relationships: Some considerations*. Earth Surf. Process. Landforms. 28, 645–653.

Brook, M.S., Kirkbride, M.P., Brock, B.W., 2004. *Rock strength and development of glacial valley morphology in the Scottish Highlands and northwest Iceland*. Geogr. Ann. Ser. A Phys. Geogr. 86, 225–234.

Cisek, M., Makuch, P., Petelski, T., 2017. *Comparison of meteorological conditions in Svalbard fjords: Hornsund and Kongsfjorden*. Oceanologia. 59, 413–421.

Cohen, D., Hooyer, T.S., Iverson, N.R., Thomason, J.F., Jackson, M., 2006. *Role of transient water pressure in quarrying: A subglacial experiment using acoustic emissions*. J. Geophys. Res. Earth Surf. 111, 1–13.

Cook, S.J., Swift, D.A., 2012. *Subglacial basins: Their origin and importance in glacial systems and landscapes*. Earth-Science Rev. 115, 332–372.

Dallmann, W.K., 2012. *Geological map Svalbard 1:100.000, Tre Kroner*. Nor. Polarinstitutt Temakart. 49.

Dallmann, W.K., 2015. *Geoscience Atlas of Svalbard*. Norwegian Polar Institute, Tromsø.

Dallmann, W.K., Gjelberg, J.G., Harland, W.B., Johannessen, E.P., Keilen, H.B., Lønøy, A., Nilsson, I., Worsley, D., 1999. *Upper Palaeozoic lithostratigraphy*. Lithostratigr. Lex. Svalbard. Nor. Polarinstitutt, Tromsø. 25–126.

Dallmann, W.K., Sirkotkin, A.N., Ohta, Y., Piepjohn, K., 2006. *Geological map Svalbard 1:100.000, Eidsvollfjellet*. Nor. Polarinstitutt Temakart. 39, 100.

Davis, G.H., Raynolds, S.J., 1996. *Structural Geology of Rocks and Regions*. John Wiley and Sons.

Dühnforth, M., Anderson, R.S., Ward, D., Stock, G.M., 2010. *Bedrock fracture control of glacial erosion processes and rates*. Geology. 38, 423–426.

Egholm, D.L., Jansen, J.D., Brædstrup, C.F., Pedersen, V.K., Andersen, J.L., Ugelvig, S. V., Larsen, N.K., Knudsen, M.F., 2017. *Formation of plateau landscapes on glaciated continental margins*. Nat. Geosci. 10, 592–597.

Elverhøi, A., Liestøl, O., Nagy, J., 1980. *Glacial erosion, sedimentation and microfauna in the inner part of Kongsfjorden, Spitsbergen*. Geol. Geophys. Res. Svalbard Jan Mayen. 184.

England, J., 1987. *Glaciation and the evolution of the Canadian high arctic landscape*. Geology. 15, 419–424.

Evans, I.S., 1996. *Abraded rock landforms (whalebacks) developed under ice streams in mountain areas*. Ann. Glaciol. 22, 9–16.

Farnsworth, W.R., Ingólfsson, Ó., Retelle, M., Schomacker, A., 2016. *Over 400 previously undocumented Svalbard surge-type glaciers identified*. Geomorphology. 264, 52–60.

Faulkner, D.R., Mitchell, T.M., Jensen, E., Cembrano, J., 2011. *Scaling of fault damage zones with displacement and the implications for fault growth processes*. J. Geophys. Res. Solid Earth. 116, 1–11.

Fettes, D., Desmons, J., 2007. *Metamorphic Rocks: A Classification and Glossary of Terms*. Cambridge University Press.

Forwick, M., Dowdeswell, J.A., Laberg, J.S., Ottesen, D., 2016. *Glacial landform assemblages in Spitsbergen fjords from the last full-glacial, deglaciation and the late Holocene*. Geol. Soc. London, Mem. 46, 147–150.

Fossen, H., 2010. *Structural Geology*. Cambridge University Press, Cambridge.

Friend, P.F., 1961. *the Devonian Stratigraphy of North and Central Vestspitsbergen*. Proc. Yorksh. Geol. Soc. 33, 77–118.

Friend, P.F., Harland, W.B., Rogers, D.A., Snape, I., Thornley, R.S.W., 1997. *Late Silurian and Early Devonian stratigraphy and probable strike-slip tectonics in northwestern Spitsbergen*. Geol. Mag. 134, 459–479.

Gee, D.G., Tebenkov, A.M., 2004. *Svalbard: a fragment of the Laurentian margin*. Geol. Soc. London, Mem. 30, 191–206.

Geological Survey of Greenland, 2015. *Bedrock 500K*, GEUS http://data.geus.dk/arcgis/rest/services/GtW/S064_G500_Geology_map/MapServer/tile/%7Bz%7D/%7By%7D/%7Bx%7D.

Geological Survey of Norway, 2015. *Bedrock N250*, NGU http://geo.ngu.no/kart/berggrunn_mobil/?lang=eng.

Gjelsvik, T., 1974. *A new occurrence of Devonian rocks in Spitsbergen*. Nor. Polarinstitutt Årb. 1972. 23–28.

Gjermundsen, E.F., Briner, J.P., Akçar, N., Foros, J., Kubik, P.W., Salvigsen, O., Hormes, A., 2015. *Minimal erosion of Arctic alpine topography during late Quaternary glaciation*. Nat. Geosci. 8, 789–792.

Gjermundsen, E.F., Briner, J.P., Akçar, N., Salvigsen, O., Kubik, P., Gantert, N., Hormes, A., 2013. *Late Weichselian local ice dome configuration and chronology in Northwestern Svalbard: Early thinning, late retreat*. Quat. Sci. Rev. 72, 112–127.

Glasser, N.F., Bennett, M.R., 2004. *Glacial erosional landforms: origins and significance for palaeoglaciology*. Prog. Phys. Geogr. 28, 43–75.

Glasser, N.F., Crawford, K.R., Hambrey, M.J., Bennett, M.R., Huddart, D., 1998. *Lithological and Structural Controls on the Surface Wear Characteristics of Glaciated Metamorphic Bedrock Surfaces: Ossian Sarsfjellet, Svalbard*. J. Geol. 106, 319–330.

Glasser, N.F., Ghiglione, M.C., 2009. *Structural, tectonic and glaciological controls on the evolution of fjord landscapes*. Geomorphology. 105, 291–302.

Gonzales, J., Aydin, A., 2008. *The origin of oriented lakes in the Andean foreland, Parque Nacional Torres del Paine (Chilean Patagonia)*. Geomorphology. 97, 502–515.

Gordon, J.E., 1981. *Ice-Scoured Topography and Its Relationships to Bedrock Structure and Ice Movement in Parts of Northern Scotland and West Greenland*. Geogr. Ann. Ser. A Phys. Geogr. 63, 55–65.

Grant, O.R., 2016. *The deglaciation of Kongsfjorden, Svalbard—based on surface exposure dating of glacial erratics and Quaternary geological mapping of Blomstrandhalvøya*. Master's thesis. The University of Bergen.

Gupta, V., Sharma, R., Sah, M.P., 2009. *An evaluation of surface hardness of natural and modified rocks using schmidt hammer: Study from northwestern Himalaya, India*. Geogr. Ann. Ser. A Phys. Geogr. 91, 179–188.

Hack, R., Huisman, M., 2002. *Estimating the intact rock strength of a rock mass by simple means*. Eng. Geol. Dev. Ctries. 1971–1977.

Hallet, B., 1979. *A theoretical model of glacier abrasion*. J. Glaciol. 23, 39–50.

Hallet, B., 1996. *Glacial quarrying: a simple theoretical model*. Ann. Glaciol. 22, 1–8.

Harbor, J.M., 1995. *Development of glacial-valley cross sections under conditions of spatially variable resistance to erosion*. Geomorphology. 14, 99–107.

Henriksen, M., Alexanderson, H., Landvik, J.Y., Linge, H., Peterson, G., 2014. *Dynamics and retreat of the Late Weichselian Kongsfjorden ice stream, NW Svalbard*. Quat. Sci. Rev. 92, 235–245.

Hirano, M., Aniya, M., 1989. *A rational explanation of cross???profile morphology for glacial valleys and of glacial valley development: A further note*. Earth Surf. Process. Landforms. 14, 173–174.

Hjelle, A., 1993. *Geology of Svalbard*. Norwegian Polar Institute, Oslo.

Hjelle, A., Piepjohn, K., Saalmann, K., Ohta, Y., Salvigsen, O., Thiedig, F., Dallmann, W.K., 1999. *Geological map Svalbard 1:100.000, Kongsfjorden*. Nor. Polarinstitutt Temakart. 30.

Hooyer, T.S., Cohen, D., Iverson, N.R., 2012. *Control of glacial quarrying by bedrock joints*. Geomorphology. 153, 91–101.

Hormes, A., Akçar, N., Kubik, P.W., 2011. *Cosmogenic radionuclide dating indicates ice-sheet configuration during MIS 2 on Nordaustlandet, Svalbard*. Boreas. 40, 636–649.

Hormes, A., Gjermundsen, E.F., Rasmussen, T.L., 2013. *From mountain top to the deep sea - Deglaciation in 4D of the northwestern Barents Sea ice sheet*. Quat. Sci. Rev. 75, 78–99.

Houmark-Nielsen, M., Funder, S., 1999. *Pleistocene stratigraphy of Kongsfjordhallet, Spitsbergen, Svalbard*. Polar Res. 18, 39–50.

Howe, J.A., Moreton, S.G., Morri, C., Morris, P., 2003. *Multibeam bathymetry and the depositional environments of Kongsfjorden and Krossjorden, western Spitzbergen, Svalbard*. Polar Res. 22, 301–316.

Ingólfsson, Ó., 2011. *Fingerprints of Quaternary glaciations on Svalbard*. Geol. Soc. London, Spec. Publ. 354, 15–31.

Ingólfsson, Ó., Landvik, J.Y., 2013. *The Svalbard-Barents Sea ice-sheet-Historical, current and future perspectives*. Quat. Sci. Rev. 64, 33–60.

Iverson, N.R., 1991a. *Morphology of glacial striae: Implications for abrasion of glacier beds and fault surfaces*. Geol. Soc. Am. Bull. 103, 1308–1316.

Iverson, N.R., 1991b. *Potential Effects of Subglacial Water-Pressure Fluctuations on Quarrying*. J. Glaciol. 37, 27–36.

Jessen, S.P., Rasmussen, T.L., Nielsen, T., Solheim, A., 2010. *A new Late Weichselian and Holocene marine chronology for the western Svalbard slope 30,000-0 cal years BP*. Quat. Sci. Rev. 29, 1301–1312.

Johansson, M., Migon, P., Olvmo, M., 2001. *Development of joint-controlled rock basins in Bohus granite, SW Sweden*. Geomorphology. 40, 145–161.

Kirkbride, M., Matthews, D., 1997. *The role of fluvial and glacial erosion in landscape evolution: The Ben Ohau Range, New Zealand*. Earth Surf. Process. Landforms. 22, 317–327.

Knies, J., Matthiessen, J., Vogt, C., Laberg, J.S., Hjelstuen, B.O., Smelror, M., Larsen, E., Andreassen, K., Eidvin, T., Vorren, T.O., 2009. *The Plio-Pleistocene glaciation of the Barents Sea-Svalbard region: a new model based on revised chronostratigraphy*. Quat. Sci. Rev. 28, 812–829.

Krabbendam, M., Bradwell, T., 2011. *Lateral plucking as a mechanism for elongate erosional glacial bedforms: Explaining megagrooves in Britain and Canada*. Earth Surf. Process. Landforms. 36, 1335–1349.

Krabbendam, M., Bradwell, T., 2014. *Quaternary evolution of glaciated gneiss terrains: Pre-glacial weathering vs. glacial erosion*. Quat. Sci. Rev. 95, 20–42.

Krabbendam, M., Eyles, N., Putkinen, N., Bradwell, T., Arbelaez-Moreno, L., 2016. *Streamlined hard beds formed by palaeo-ice streams: A review*. Sediment. Geol. 338, 24–50.

Krabbendam, M., Glasser, N., 2011. *Bedrock properties and glacial erosion : hardness and joint spacing , abrasion and plucking*. Geomorphology. 13, 2537–2537.

Landvik, J.Y., Alexanderson, H., Henriksen, M., Ingólfsson, Ó., 2014. *Landscape imprints of changing glacial regimes during ice-sheet build-up and decay: A conceptual model from Svalbard*. Quat. Sci. Rev. 92, 258–268.

Landvik, J.Y., Brook, E.J., Gualtieri, L., Linge, H., Raisbeck, G., Salvigsen, O., Yiou, F., 2013. *10Be exposure age constraints on the Late Weichselian ice-sheet geometry and dynamics in inter-ice-stream areas, western Svalbard*. Boreas. 42, 43–56.

Landvik, J.Y., Ingólfsson, Ó., Mienert, J., Lehman, S.J., Solheim, A., Elverhøi, A., Ottesen, D., 2005. *Rethinking Late Weichselian ice-sheet dynamics in coastal NW Svalbard*. Boreas. 34, 7–24.

Lehman, S.J., Forman, S.L., 1992. *Late Weichselian glacier retreat in Kongsfjorden, west Spitsbergen, Svalbard*. Quat. Res. 37, 139–154.

Liestøl, O., 1988. *The glaciers in the Kongsfjorden area, Spitsbergen*. Nor. Geogr. Tidsskr. . 42, 231–238.

Lindbäck, K., Kohler, J., Pettersson, R., Nuth, C., Langley, K., Vallot, D., Matsuoka, K., Brandt, O., in review, 2018. *Subglacial topography, ice thickness, and bathymetry of Kongsfjorden, northwestern Svalbard* 163, 1–19.

Livingstone, S.J., Cofaigh, C.Ó., Stokes, C.R., Hillenbrand, C.D., Vieli, A., Jamieson, S.S.R., 2013. *Glacial geomorphology of Marguerite Bay Palaeo-Ice stream, western Antarctic Peninsula*. J. Maps. 9, 558–572.

Maclachlan, S.E., Howe, J.A., Vardy, M.E., 2010. *Morphodynamic evolution of Kongsfjorden-Krossfjorden, Svalbard, during the Late Weichselian and Holocene*. Geol. Soc. London, Spec. Publ. 344, 195–205.

Margold, M., Stokes, C.R., Clark, C.D., 2015. *Ice streams in the Laurentide Ice Sheet: Identification, characteristics and comparison to modern ice sheets*. Earth-Science Rev. 143, 117–146.

McCann, A.J., 2000. *Deformation of the Old Red Sandstone of NW Spitsbergen; links to the Ellesmerian and Caledonian orogenies*. In: Friend, P.F., Williams, B.P.J. (Eds.), New Perspectives on the Old Red Sandstone. Geological Society of London, pp. 567–584.

McCann, A.J., Dallmann, W.K., 1996. *Reactivation history of the long-lived Billefjorden Fault Zone in north central Spitsbergen, Svalbard*. Geol. Mag. 133, 63.

Miccadei, E., Piacentini, T., Berti, C., 2016. *Geomorphological features of the Kongsfjorden area: Ny-Ålesund, Blomstrandøya (NW Svalbard, Norway)*. Rend. Lincei. 27, 217–228.

Miller, G.H., 1982. *Quaternary Depositional Episodes , Western Spitsbergen , Norway : Aminostratigraphy and Glacial History*. Arct. Alp. Res. 14, 321–340.

Mitchell, T.M., Faulkner, D.R., 2009. *The nature and origin of off-fault damage surrounding strike-slip fault zones with a wide range of displacements: A field study from the Atacama fault system, northern Chile*. J. Struct. Geol. 31, 802–816.

Myhre, P.I., Corfu, F., Andresen, A., 2009. *Caledonian anatexis of grenvillian crust: A U/Pb study of Albert I Land, NW Svalbard*. Nor. Geol. Tidsskr. 89, 173–191.

Nesje, A., Whillans, I.M., 1994. *Erosion of Sognefjord, Norway*. Geomorphology. 9, 33–45.

Noorian Bidgoli, M., Jing, L., 2014. *Anisotropy of strength and deformability of fractured rocks*. J. Rock Mech. Geotech. Eng. 6, 156–164.

Norwegian Mapping Authority Hydrographic Service, 2014. *5m Bathymetry DEM Kongsfjorden*.

Norwegian Polar Institute, 2014a&b. *Terrengmodell Svalbard (S0 Terrengmodell) [Data set]*. https://doi.org/10.21334/npolar.2014.dce53a47.

Norwegian Polar Institute, 2014c. *Kartdata Svalbard 1:100 000 (S100 Kartdata) / Map Data [Data set]*.

Ohta, Y., Piepjohn, K., Dallmann, W.K., Elvevold, S., 2008a. *Geological map Svalbard 1:100.000, Krossfjorden*. Nor. Polarinstitutt Temakart. 42.

Ohta, Y., Piepjohn, K., Dallmann, W.K., Elvevold, S., 2008b. *Geological map Svalbard 1:100.000, Krossfjorden*. Nor. Polarinstitutt Temakart. 42.

Ottesen, D., Dowdeswell, J.A., Landvik, J.Y., Mienert, J., 2007. *Dynamics of the Late Weichselian ice sheet on Svalbard inferred from high-resolution sea-floor morphology*. Boreas. 36, 286–306.

Ottesen, D., Dowdeswell, J.A., Rise, L., 2005. *Submarine landforms and the reconstruction of fast-flowing ice streams within a large Quaternary ice sheet: The 2500-km-long Norwegian-Svalbard margin (57°-80°N)*. Bull. Geol. Soc. Am. 117, 1033–1050.

Patton, H., Andreassen, K., Bjarnadóttir, L.R., Dowdeswell, J.A., Winsborrow, M.C.M., Noormets, R., Polyak, L., Auriac, A., Hubbard, A., 2015. *Geophysical constraints on the dynamics and retreat of the Barents Sea Ice Sheet as a palaeo-benchmark for models of marine ice-sheet deglaciation*. Rev. Geophys. 53, 1051–1098.

Petit, J., 1987. *Criteria for the sense of movement on fault surfaces in brittle rocks*. J. Struct. Geol. 9, 597–608.

Peulvast, J.-P., Bonow, J.M., Japsen, P., Wilson, R.W., McCaffrey, K.J.W., 2011. *Morphostructural patterns and landform generations in a glaciated passive margin: the Kobberminebugt-Qaqortoq region of South Greenland*. Geodin. Acta. 24, 1–19.

Phillips, E., Everest, J., Diaz-Doce, D., 2010. *Bedrock controls on subglacial landform distribution and geomorphological processes: Evidence from the Late Devensian Irish Sea Ice Stream*. Sediment. Geol. 232, 98–118.

Piepjohn, K., 1997. *Erläuterung zur Geologischen Karte 1:150.000 des Woodfjorden-Gebietes (Haakon VII Land, Andrée Land), NW-Spitzbergen, Svalbard*. Münster. Forsch. Geol. Paläont. 82, 15–37.

Piepjohn, K., 2000. *The Svalbardian-Ellesmerian deformation of the Old Red Sandstone and the pre-Devonian basement in NW Spitsbergen (Svalbard)*. Geol. Soc. London, Spec. Publ. 180, 585–601.

Piepjohn, K., von Gosen, W., Läufer, A., McClelland, W.C., Estrada, S., 2013. *Ellesmerian and Eurekan fault tectonics at the northern margin of Ellesmere Island (Canadian High Arctic) [Ellesmerische und Eurekan-Störungstektonik am Nordrand von Ellesmere Island (kanadische Hocharktis)]*. Zeitschrift der Dtsch. Gesellschaft für Geowissenschaften. 164, 81–105.

Piepjohn, K., von Gosen, W., Tessensohn, F., Reinhardt, L., McClelland, W.C., Dallmann, W.K., Gaedicke, C., Harrison, J.C., 2015. *Tectonic map of the Ellesmerian and Eurekan deformation belts on Svalbard, North Greenland, and the Queen Elizabeth Islands (Canadian Arctic)*. Arktos. 1, 12.

Puszta, A., 2017. *Weighted rose plot*. MATLAB Central File Exchange. https://www.mathworks.com/matlabcentral/fileexchange/6c5009-weighted-rose.

Rebesco, M., Laberg, J.S., Pedrosa, M.T., Camerlenghi, A., Lucchi, R.G., Zgur, F., Wardell, N., 2014. *Onset and growth of Trough-Mouth Fans on the North-Western Barents Sea margin - implications for the evolution of the Barents Sea/Svalbard Ice Sheet*. Quat. Sci. Rev. 92, 227–234.

Rignot, E., Mouginot, J., Scheuchl, B., 2011. *Ice flow of the Antarctic Ice Sheet*. Science. 333, 1427–1431.

Roberts, D.H., Long, A.J., 2005. *Streamlined bedrock terrain and fast ice flow, Jakobshavns Isbrae, West Greenland: Implications for ice stream and ice sheet dynamics*. Boreas. 34, 25–42.

Sachpazis, C.I., 1990. *Correlating schmidt hardness with compressive strength and young's modulus of carbonate rocks*. Bull. Int. Assoc. Eng. Geol. 42, 75–83.

Sejrup, H.P., Hjelstuen, B.O., Dahlgren, K.I.T., Haflidason, H., Kuijpers, A., Nygård, A., Praeg, D., Stoker, M.S., Vorren, T.O., 2005. *Pleistocene glacial history of the NW European continental margin*. Mar. Pet. Geol. 22, 1111–1129.

Shoemaker, E.M., 1986. *The formation of fjord thresholds*. J. Glaciol. 32, 65–71.

Sklar, D.W.E., 2001. *Sediment and rock strength controls on river incision into bedrock*. Geology. 29, 1087–1090. Arktos. 1, 14.

Streuff, K., 2013*. Landform Assemblages in Inner Kongsfjorden, Svalbard: Evidence of Recent Glacial (Surge) Activity.* Master's thesis. The Arctic University of Norway UiT.

Streuff, K., Forwick, M., Szczuciński, W., Andreassen, K., Ó Cofaigh, C., 2015. *Submarine landform assemblages and sedimentary processes related to glacier surging in Kongsfjorden, Svalbard*.

Sugden, D.E., 1974. *Landscapes of glacial erosion in Greenland and their relationship to ice, topographic and bedrock conditions*. Inst. Br. Geogr. Spec. Publ. 7, 177–195.

Sugden, D.E., 1978. *Glacial erosion by the Laurentide Ice Sheet*. J. Glaciol. 20, 367–390.

Svendsen, H., Beszczynska-Møller, A., Hagen, J.O., Lefauconnier, B., Tverberg, V., Gerland, S., Ørbæk, J.B., Bischof, K., Papucci, C., Zajaczkowski, M., Azzolini, R., Bruland, O., Wiencke, C., Winther, J.-G., Dallmann, W., 2002. *The physical environment of Kongsfjorden – Krossfjorden, an Arctic fjord system in Svalbard*. Polar Res. 21, 133–166.

Swift, D.A., Persano, C., Stuart, F.M., Gallagher, K., Whitham, A., 2008. *A reassessment of the role of ice sheet glaciation in the long-term evolution of the East Greenland fjord region*. Geomorphology. 97, 109–125.

Thiedig, F., Manby, G.M., 1992. *Origins and deformation of post-Caledonian sediments on Blomstrandhalvøya and Lovénøyane, northwest Spitsbergen*. Nor. Geol. Tidsskr. 72, 23–33.

Viles, H., Goudie, A., Grab, S., Lalley, J., 2011. *The use of the Schmidt Hammer and Equotip for rock hardness assessment in geomorphology and heritage science: A comparative analysis*. Earth Surf. Process. Landforms. 36, 320–333.